THE STATIC AND DYNAMIC FRACTURE OF BRITTLE MATERIALS

B. W. Payne

A thesis presented to fulfil the requirements for the degree of Doctor of Philosophy, University of Cape Town

1977

SYNOPSIS

Experiments on the behaviour of brittle materials, particularly quartz, during the initial period of loading, at the onset of fracture and during the stage of rapid crack propagation, have been performed in order to gain an insight into some of the fundamental processes of brittle fracture which might prove useful in the solution of practical problems in mining and process operations. Studies have also been conducted into the nature of the damage produced by a diamond stylus sliding on a quartz surface. The results of these studies have been correlated with ancilliary experiments in which the effects of the deformation produced by a sharp indenter and sliding diamond polishing particles on quartz were examined.

The geometry of cracks in glass and quartz during the loading stage has been observed by scanning electron microscopy and was found to be approximately elliptical. By making some simple assumptions, an equation has been derived that enables the fracture surface energy to be deduced from shape of the crack and the loading conditions.

The brittleness of a material is indicated by the difference between the fracture surface energy and the thermodynamic surface energy of the material. In a perfectly brittle body they are equal. In order to make an accurate comparison with the true surface energy in quartz as calculated from atomic bond energy data,

anisotropic elastic theory was used in the evaluation of the fracture surface energy. The fracture surface energy of the $(1\bar{1}00)$ crystal plane in α-quartz, experimentally obtained by tensile fracture, was found to have the value 3.0 ± 1.0 Jm^{-2}, and the true surface energy was calculated to be 3.0 Jm^{-2}.

A theory has been developed for the determination of crack velocities on planes of elastic symmetry in anisotropic materials by the use of Wallner lines. This theory has been used in conjunction with electrical resistance grid methods to measure crack velocities along the $(1\bar{2}10)$ fracture plane in α-quartz. These results indicate that, if bifurcation of the crack is suppressed, the terminal velocity of the crack is close to the Rayleigh surface wave velocity in the direction of crack propagation on the fracture plane.

At high velocities, cracks in quartz were observed to attempt to branch by oscillating about the fracture plane on low energy rhombohedral planes, and when branching did occur, it was found that the equivalent static stress intensity factor at the branching point was a constant for the material. A criterion for crack branching in brittle materials was obtained by requiring that the ratio of the dynamic stress intensity factor to the static critical stress intensity factor be a constant. The validity of this criterion was established for a number of materials with differing degrees of brittleness.

Indentation experiments with a Vickers hardness indenter were performed in order to observe the behaviour of quartz when subjected to large hydrostatic and shear stresses. The results of observations of thin sections in the transmission electron microscope have revealed that little of the deformation was produced or accompanied by the motion or generation of dislocations or twins. Tracks produced by diamond polishing particles on quartz did, however, generate dislocations.

A study of the behaviour of quartz under the action of a diamond stylus sliding on its surface was made in order to understand the mechanisms of hard rock cutting. The resulting crack pattern can be explained in terms of Hertzian cracking and the presence of an inelastic zone beneath the scratched surface. The effect of environments in which the zeta potential is near zero has been examined and the size of the damage zone beneath the scratch surface has been found to increase as the zeta potential approaches zero.

C O N T E N T S

1. INTRODUCTION

1.1 General introduction

One of the earliest skills acquired by man was that of flintknapping viz. the control of the fracture of stone for making useful implements. Man in time learnt to control the fracture of larger masses of material and the monuments and tombs of the early Egyptians are evidence of their ability to quarry and shape huge slabs of stone from rock. For example, they devised clever splitting techniques by making shallow slots in the rock and then driving wooden wedges into these slots. These wedges would be soaked with water and the subsequent expansion would propagate cracks from the bases of the slots. Scientific investigation of fracture coincided with the Renaissance and the rise of modern science and technology, but it appears that the formation of a satisfactory theory and predictive relationships such as those describing elastic behaviour, was a difficult task. No doubt because fracture, unlike elastic behaviour is sensitive to microstructure and the state of internal and surface perfection. For instance, Galileo (1638) made the suggestion that the high resistance bodies have to fracture occurs because 'nature abhors a vacuum' and therefore force was required to fracture bodies.

> Salviati : A little while ago, I expressed the hope that your good angel might assist you. I now find myself in the same straits. Experiment leaves no doubt that the reason why two plates cannot be separated, except with violent effort, is that they are held together by the resistance of the vacuum; and the same can be said of two large pieces of a marble or bronze column. This being so, I do not see why this same cause may not explain the coherence of smaller parts and indeed of the very smallest particles of these materials. Now, since each effect must have one true and sufficient cause and since I find no other cement, am I not justified in trying to discover whether the vacuum is not a sufficient cause?
>
> Galileo (1638)

The study of the behaviour of materials which were necessary for the engineering developments of the Industrial Revolution, led to the realisation that hard metals such as glass and cast iron were not very strong when tested in tension and also that they fractured suddenly without warning. A rational explanation for the behaviour of these hard materials was provided relatively late in the studies of materials by Griffith in 1920. He proposed a theory based upon the existence of microscopic flaws on the surface of brittle materials. On application of a tensile force to these materials there would be a

magnification of stress at the tips of the flaws which would cause local failure of the material and eventual propagation through the body. Using a thermodynamic approach and the then recently calculated stress field around an elliptic notch (Inglis, 1913), he derived an equation which enabled him to predict the load at which a brittle body would fail in tension. Experimental verification of this theory is well established and it stands as the basis for present day fracture mechanics.

Today, our understanding of fracture of brittle materials has advanced greatly, but the sudden catastrophic failure of pressure vessels and structures still occur and is of concern to the engineer. It is apparent that there are still many areas, both pure and applied, which require explanation if use is to be made of the high bond strength and chemical stability of brittle materials and conversely if efficient mining and comminution is to be achieved.

This thesis aims to advance the general theory and understanding of brittle fracture and the role played by external variables such as loading conditions and environment, in order that the knowledge obtained may in future be utilised and extended to the practical problems encountered in mining and process operations. With this aim in view materials were chosen which would most closely approximate ideal brittle behaviour, be obtainable in experimental dimensions and be a large constituent of mineral bearing rocks. Quartz alone

satisfies the above conditions, but because some experiments required an isotropic material, soda-lime glass was also studied.

Experiments were performed in order to investigate both the static and dynamic regimes of fracture under simple uniaxial loading conditions and also under triaxial loading conditions. Specimens were subjected to tensile, bending, abrasive and indentation deformation in controlled environments, and measurements of factors such as crack geometry, fracture velocity, effective surface energy, surface fractography and plastic deformation were made. The following section serves as an introduction to the basic concepts and definitions used in this thesis, while each chapter concerning a particular experiment contains an introduction and a review of pertinent work in the literature.

1.2 Basic concepts and definitions

In this section Griffith's theory and its extension by Orowan (1955) and Irwin (1958) is critically examined and the range of application of these theories is assessed. The concepts involved in these theories are then used to classify the brittleness of materials and finally some basic definitions of fracture mechanics are presented.

Griffith considered a slit crack of length 2c

in an infinite elastic plate of unit thickness with tensile stresses σ applied remotely from the crack. He found that the presence of the crack altered the strain energy in the body by an amount $V = \pi c^2\sigma^2/2E$ for plane stress conditions, where E is Young's modulus. As a result of the introduction of the crack the tensile loads would do an amount of work U. It has been shown that the quantity U - V is equal to V whether the tensile loads are allowed to do work when the crack is introduced or whether the ends of the body are fixed and no work is done. If the crack were to extend a unit amount, then the energy available for crack extension (U - V) will change by an amount $\pi c\sigma^2/E$. This change in strain energy per unit advance of the crack has subsequently been called the 'strain energy release rate' G. In terms of G, fracture will occur when the external loads are such that G is greater than the energy required to create two new surfaces. In the case of the Griffith criterion, the energy required to create a new surface per unit area is equal to the thermodynamic surface energy γ. This criterion is based on reversible thermodynamics and consequently, the point defined by $G = 2\gamma$ represents an equilibrium situation, such that if the external loads are altered so that G decreases, then the crack will close up and if G increases then the crack will propagate. A 'Griffith crack' is defined in this work, as a crack which obeys the equation $G = 2\gamma$. Thus in the original Griffith case $\pi c\sigma^2/E = 2\gamma$ and we define the 'Griffith stress' σ_g as the solution to this equation,

$$\text{i.e.} \qquad \sigma_g = \sqrt{\frac{2E\gamma}{\pi c}} \qquad (1)$$

Unfortunately, this thermodynamic approach is incomplete, as surface tension effects also occur because of the nature of surface energy and these effects can modify the elastic stress field at the crack tip. However, Rajapakse (1975) has shown that for crack tips with radii of atomic dimensions, the modification of the tensile stress at the crack tip is negligible. There are two other difficulties which further complicate the analysis. Firstly, finite strains occur at the crack tip and hence the infinitesimal theory is not applicable in this region (Goodier, 1968). Secondly, for any externally applied load the continuum elastic theory predicts that infinite stresses will occur at the crack tip which no physical body can withstand. Fortunately, neither of these effects presents any difficulty in the calculation of G.

In real bodies the high stresses at the crack tip may be relieved by plastic flow before fracture occurs and the amount of relaxation will determine the brittleness of the body. If a small and localised amount of plastic flow occurs around the crack tip, then it is possible to extend the Griffith criterion to obtain a new criterion for fracture given by $G = 2\gamma_f$ where γ_f is called the fracture surface energy and is a constant of the material and is greater than

the true surface energy. On this basis, the following characterisation will be made regarding 'brittle' materials. A 'perfectly brittle' solid is defined as one which will fracture when G is greater than 2γ (eg. diamond and mica when fractured along the cleavage plane).

A range of classifications from 'highly brittle' to 'semi-brittle' can be made on the basis of the equation $G = 2\gamma_f$. 'Highly brittle' materials will have a value of γ_f greater than γ of the material but only slightly greater, whereas 'semi-brittle' materials will have a value of γ_f greater than an order of magnitude above γ of the material.

In the Griffith case, the crack was assumed to be initially infinitely sharp. As this will not be the case in real materials we must establish what sharpness of crack is obtainable in a physical body which will correspond to Griffith's idealised crack. Orowan (1949) has obtained this result by calculating the energy required to separate atoms in a solid. Using the result of Inglis (1913) for the stress concentration at the tip of an elliptic notch, he found that the remotely applied stress required to cause fracture was the same as that predicted by Griffith's equation, provided that the initial radius of curvature of the crack was of the order of atomic dimensions. It is therefore seen that if the crack

in a material is not atomically sharp, a larger stress will be required to propagate this crack than that predicted by the Irwin-Orowan equation $G = 2\gamma_f$. Hence, in order to apply this theory successfully it is necessary to introduce cracks which are as sharp as possible.

There are many different loading conditions which will cause cracks to propagate, but as the displacement of the crack faces with respect to each other may be resolved into three orthogonal components, three basic modes of fracture are recognised and defined as shown in fig. 1.

It is found that for mode 1 conditions the stresses σ_{ij} a small distance r from the crack tip are of the form

$$\sigma_{ij} = \frac{K_1}{(2\pi r)^{\frac{1}{2}}} f_{ij}(\theta)$$

where $f_{ij}(\theta)$ is a function of the angle θ, where the stress is calculated, to the crack axis and K_1 is a constant for the given loading conditions. This equation is used as a definition of the stress intensity factor for mode 1 conditons as

$$K_1 = \lim_{r \to 0} (2\pi r)^{\frac{1}{2}} \sigma_{yy}(\theta=0) \qquad (2)$$

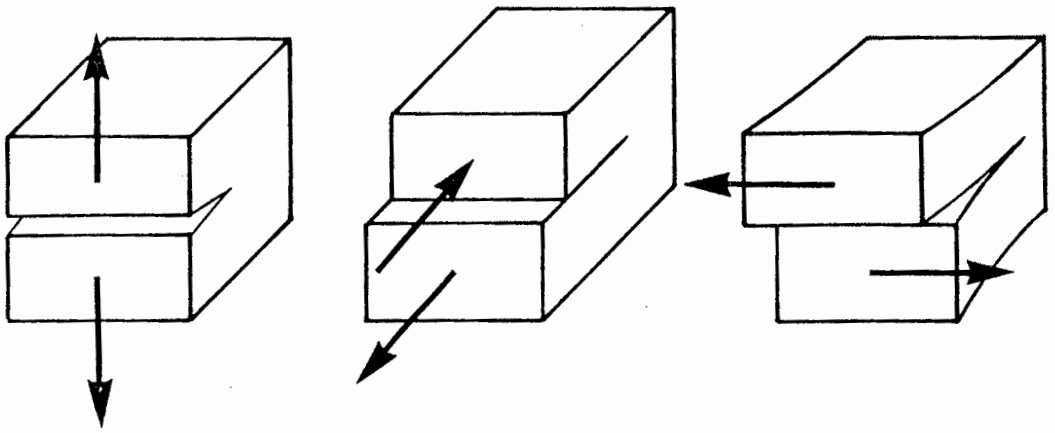

Figure 1

The three modes of crack propagation.

where σ_{yy} is the tensile stress perpendicular to the crack plane and $f_{yy}(\theta=0) = 1$. In terms of this concept, when a critical load occurs the material will fracture and the stress intensity factor will attain a critical value K_{1c}. It can be shown that this criterion for fracture is the same as the Irwin-Orowan formulation and it is found that $G = \pi K_{1c}^2/E$.

2. THE GEOMETRY OF CRACKS

2.1 Introduction

Crack propagation in brittle materials occurs by the rupturing of atomic bonds at the crack tip. A knowledge of the shape of the crack will enable the stress in the immediate vicinity of the crack tip to be calculated and the conditions necessary for onset of crack propagation to be predicted (Orowan, 1949). The mechanism of stress corrosion in various active environments has been explained by proposing that the molecules in the environment diffuse to the crack tip. The geometry of the crack will determine the diffusion rate and whether the mode of diffusion will be gaseous, surface or even bulk diffusion.

The actual measurement of the contour of a crack tip is very difficult to make, but in this experiment the shape of the rest of the crack was determined by scanning electron microscopy and these results were extrapolated to give some idea of the geometry near the crack tip.

Linear elastic methods have been used to calculate the geometry of the whole length of the crack, under specific loading conditions (Griffith 1920, Wigglesworth 1957, Keer and Freedman 1973) and have also been used to predict a parabolic shape for the crack tip under arbitrary loading conditions (Sih and Liebowitz, 1968). Hybrid models composed of continuum and atomistic regions have also been used to calculate the shape of the crack tip (Goodier and Kanninen 1966, Sinclair and Lawn 1972).

The experimental results reported here can be compared to these models.

2.2 Experimental methods

The first experiment to be described has been carried out in order to determine the geometry of cracks in glass and quartz and from one of these results the fracture surface energy of glass has been evaluated. A second experiment has also been performed in order to compare this value of fracture surface energy with that obtained by standard fracture mechanics techniques.

2.2.1 Crack shape and load displacement curve

Single crystals of quartz were cut into slices 45mm x 4mm x 0.5mm along the X, Z and Y crystal axes respectively, and glass slides were cut into slices with dimensions of 45mm x 4mm x 0.9mm. This particular orientation of the quartz crystal was chosen because of the ease of cutting the specimens to the required dimensions. These specimens had sharp cracks approximately 2mm long introduced into them by the method described in Appendix A, but the initial saw notches were removed by grinding the notched edge of the specimen down with a 320 grit silicon carbide slurry.

The samples were coated with approximately 10nm

of carbon by vacuum evaporation in order to prevent charging when they were examined in the three point bending module of a Cambridge Stereoscan 180 scanning electron microscope (S.E.M.) operating at a pressure of 10^{-5} Torr. The bending module was calibrated and the relationship between the depression of the loading arms and the angular rotation of the control lever was found to be linear.

The geometry of sharp cracks intersecting the upper specimen surface and placed centrally (see fig.2) was measured from photographs and the specimens were tilted in the microscope in such a way that the observed crack widths suffered no geometric distortion. However, the foreshortening of the length of the crack was corrected for by measuring the width of the specimen from a micrograph and comparing it to the actual width of the specimen. The crack opening displacement at the edge of the specimen was also measured as a function of the depression of the loading arms.

2.2.2 Fracture surface energy of glass (direct tension)

Glass slides of dimensions 76mm x 12mm x 0.9mm had sharp cracks of varying lengths introduced in the centre of the longest dimension and perpendicular to the long edge by the method described in Appendix A, and were fractured in tension in an Instron testing machine at a strain rate of about $7 \times 10^{-5} s^{-1}$. The experiment

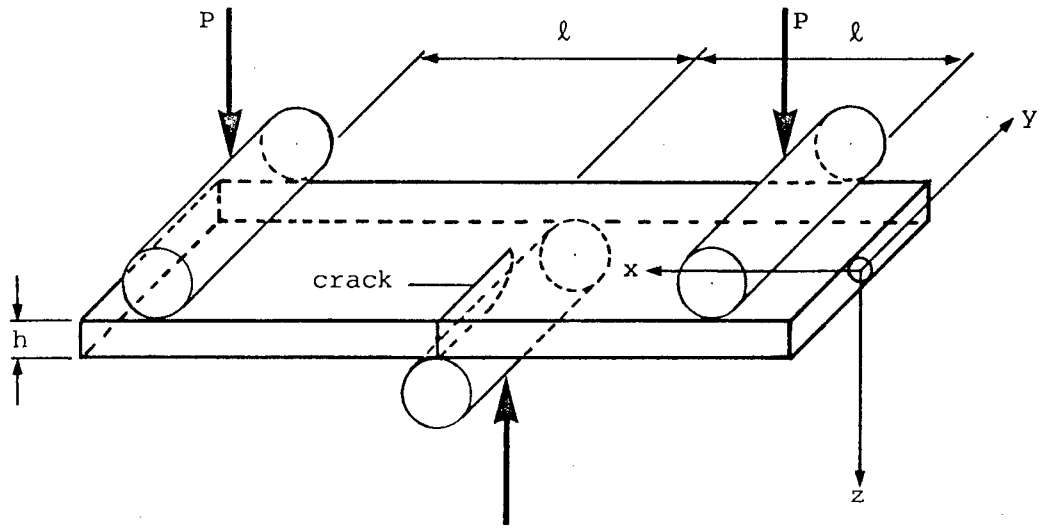

Figure 2

Three point bend specimen for S.E.M.

was performed in liquid nitrogen in order to eliminate the influence of a chemically active species in the environment and this should give results similar to those obtained in a good vacuum (Linger and Holloway, 1968). Small steel plates were glued to the ends of the samples with "Eastman's 910" adhesive and in order to ensure conditions of pure tension, these plates were then mounted in freely rotating gimbals which were attached to the testing machine by spherical bearings as shown in plate 46.

Young's modulus was found at the temperature of liquid nitrogen and also at room temperature by measuring the velocity of longitudinal waves at ultrasonic frequencies in a bar of the material.

2.3 Experimental results

2.3.1 Crack shape and load displacement curve

A photograph of a crack which has been opened on the surface of a glass specimen is shown in plate 1. The photograph was obtained by electronically altering the grey scale and differentiating the signal from the detector of the S.E.M. so that the best definition of the edges of the crack could be obtained. The photograph shows that the carbon film did not always break away cleanly from the edges and this together with the flaring that occurs at the edges of the crack give rise

to an error in the measurement of the crack opening displacement, especially for small crack opening displacements.

In the case of the glass samples it was always possible to have the crack inserted perpendicular to the edge of the specimen, but in the case of the quartz specimens, the cracks started perpendicular to the edge of the specimen but then veered off at an angle of approximately 30^0. Detailed examination in the S.E.M. of the initial straight regions of the cracks in quartz revealed that they tended to oscillate between two $\{11\bar{2}2\}$ second order trigonal pyramid cleavage planes as shown in plate 2.

The crack opening displacement of a crack in glass at about half the breaking stress is shown in fig.3 as a function of the distance from the edge of the specimen. Included in the diagram are three theoretical curves : the ellipse is the proposed configuration of a crack in an infinite medium under the action of remote tensile stresses (Griffith, 1920), the second curve is for an edge crack in a semi-infinite medium subjected to remotely applied tensile stresses (Wigglesworth, 1957) (see Appendix B) and the third curve is for an edge crack in a finite width specimen (Keer and Freedman, 1973). Because the data indicates that the crack shape is approximately elliptical, $(2u)^2$ is plotted against y^2, where $2u$ is the crack opening displacement and y is the distance from the edge of the specimen, so that

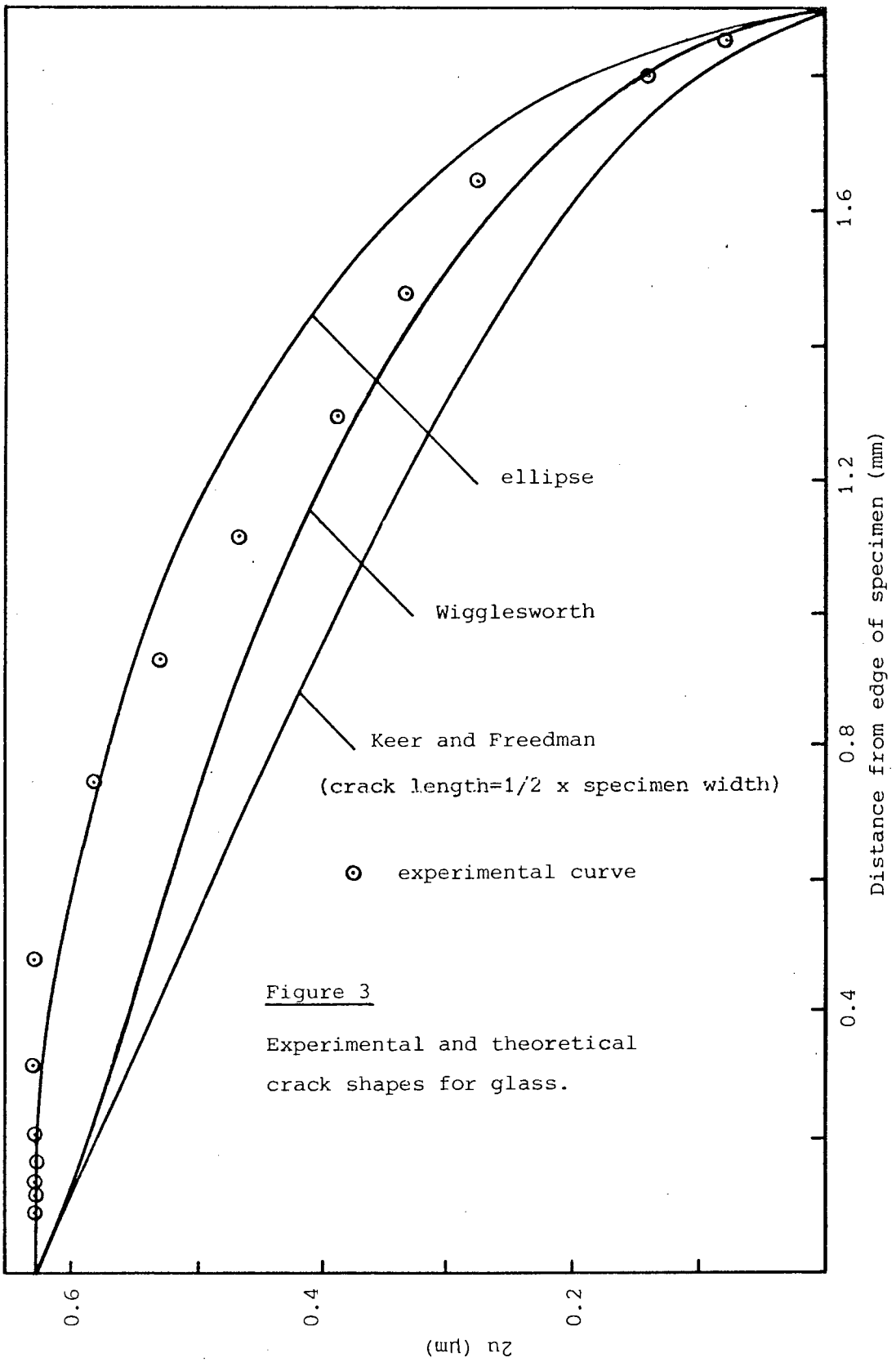

Figure 3

Experimental and theoretical crack shapes for glass.

if the plot is a straight line then the crack shape is elliptical. Fig.4 shows the results for three different glass samples and one quartz sample.

The crack opening displacement at the edge of the sample was measured as a function of the displacement of the loading arms. Results for a glass and a quartz sample are shown in fig.5. The initial curvature of these lines is assumed to be caused by an initial slackness in the system being taken up at low loads and only the steep straight line region of the curve was used in the calculations mentioned in the discussion on this experiment. The crack shape was determined at a number of different displacements of the loading arm and within experimental error the shapes of the cracks are linearly related to each other (i.e. the shapes are identical except for a scale factor). This is shown for a glass specimen in fig.6 where the scale factor (defined as u_2/u_1, where u_1, u_2 is half the crack opening displacement corresponding to a displacement of the loading arm d_1, d_2) is plotted against the distance from the edge of the specimen.

2.3.2 Fracture surface energy of glass as determined by direct tension tests

The fracture surface energy was calculated from the Irwin-Orowan formula $\sigma_f = \sqrt{2E\gamma_f/Yc}$, where σ_f is the measured fracture stress, E is Young's modulus, γ_f is

Figure 4

Comparison of experimental crack shapes for three different glass specimens and one quartz specimen. The loading conditions are different for each specimen and only shapes are being compared.

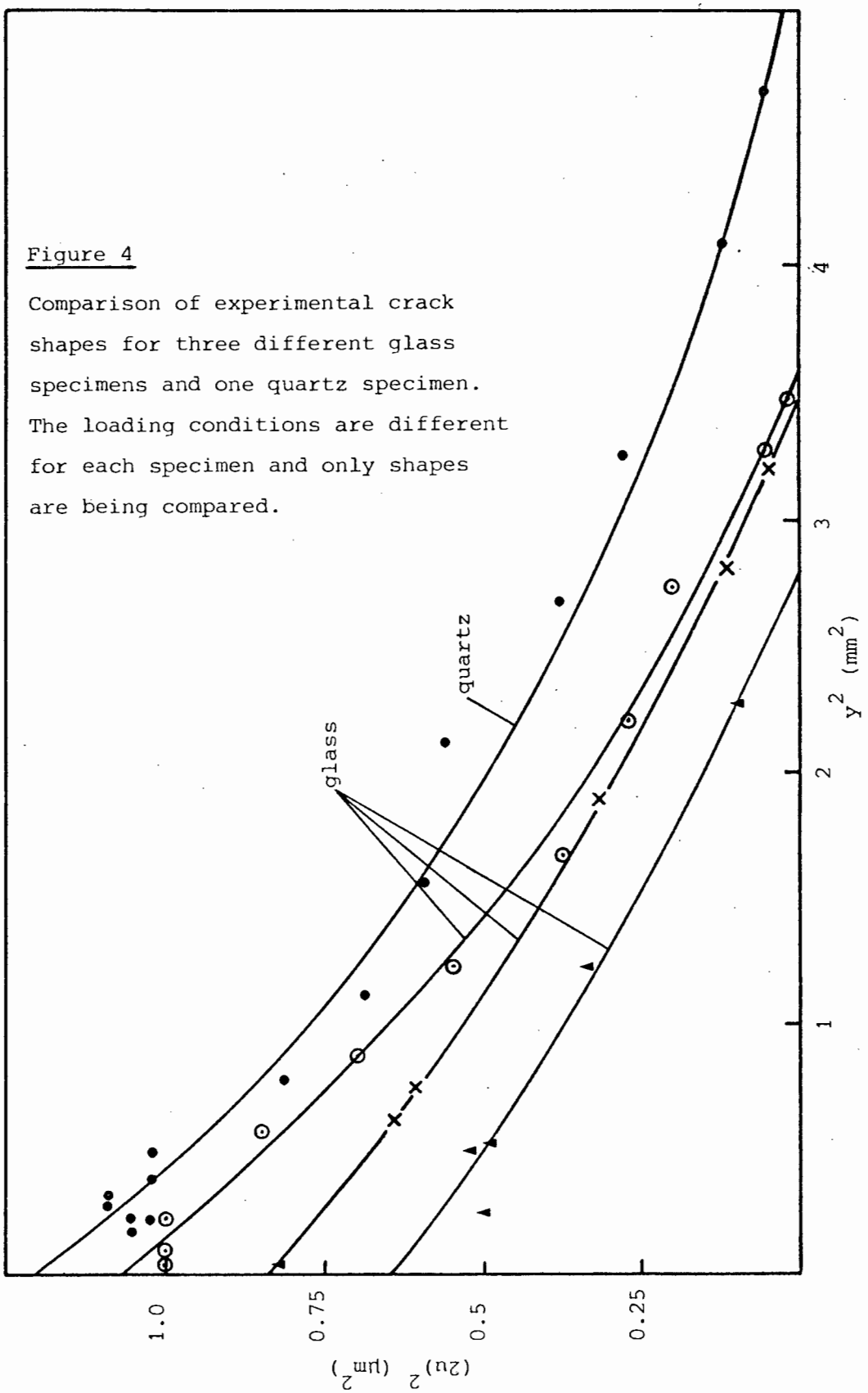

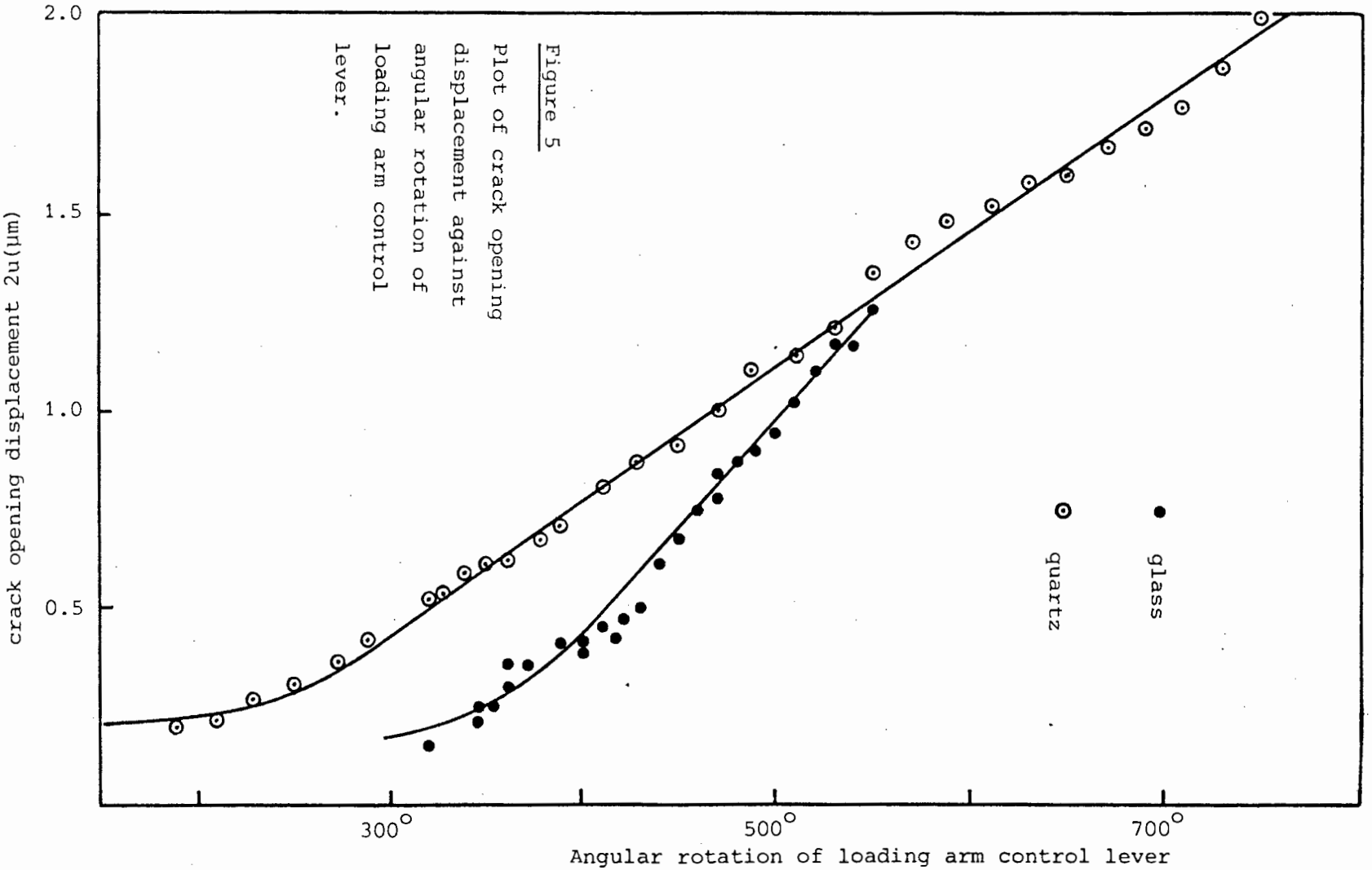

Figure 5

Plot of crack opening displacement against angular rotation of loading arm control lever.

Figure 6

Comparison of shapes of the same crack at two different loads.

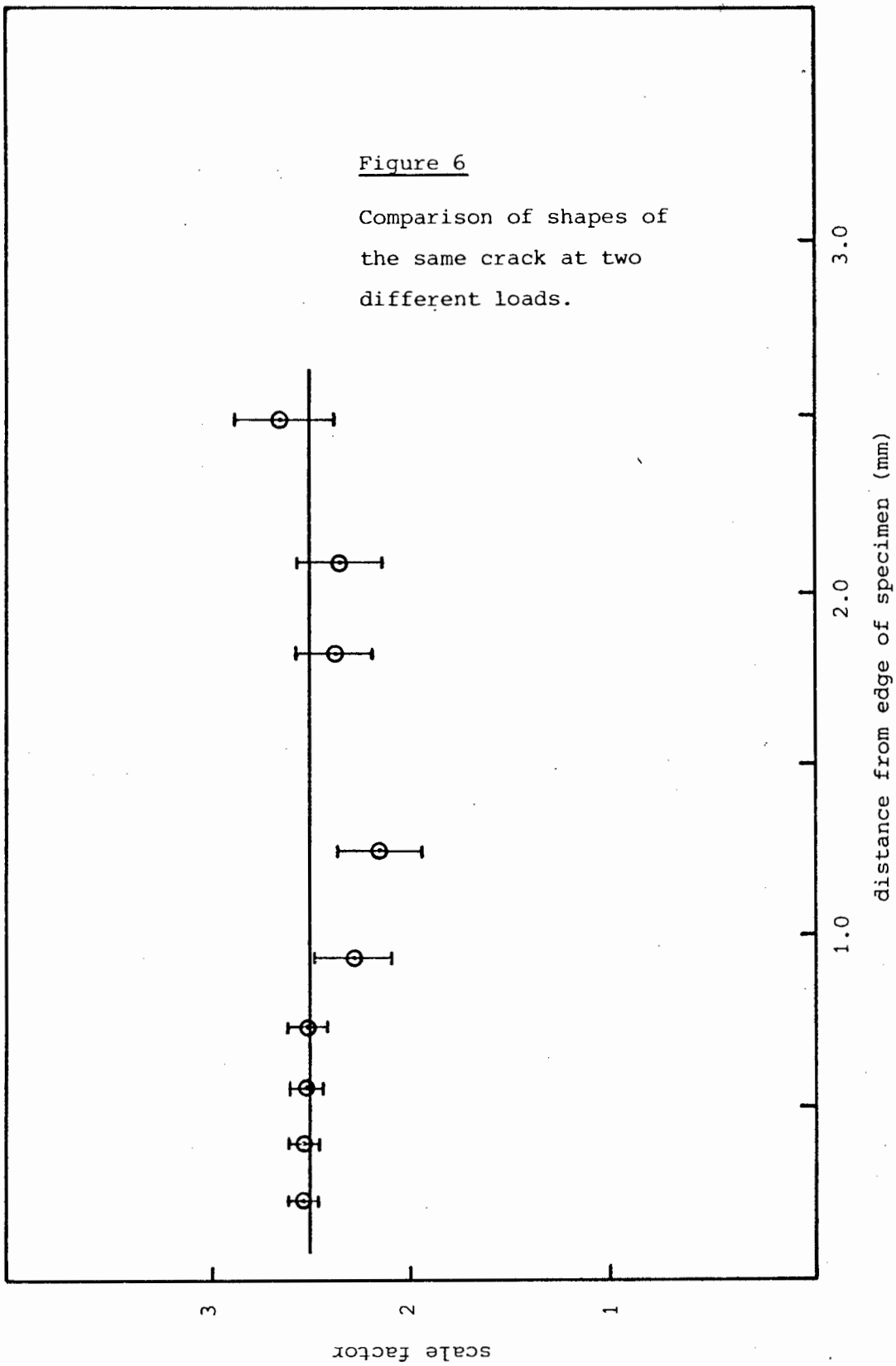

the fracture surface energy, c is the crack length and Y is a geometric parameter given by Brown and Srawley (1966) as

$$Y = 1.99-0.41(c/w)+18.7(c/w)^2-38.48(c/w)^3+53.85(c/w)^4 \quad (3)$$

where w is the width of the specimen - 12mm in this case. Young's modulus was determined to be $7.5\pm0.4 \times 10^{10}\ Nm^{-2}$ at both room temperature and at the temperature of liquid nitrogen. The average fracture surface energy for eleven specimens tested in liquid nitrogen was $4.3\pm1.3\ Jm^{-2}$.

2.4 Discussion

2.4.1 Stress distribution in loaded rectangular bar

Consider an elastically anisotropic cantilever of uniform section of length ℓ loaded with load P as shown in fig.7, where O is taken at the centre of area. The elastic displacements and stresses are given by Lekhnitskii (1963) and the tensile stress in the x direction is given as $\sigma_{xx} = -\frac{P}{I}zx$ where $I=I_{xx}$ is the second moment of area with respect to the principal axis of the cross-section. The deflection of the end of the beam at the centre of area is $d = \frac{P\ell^3}{3IE}$ where $E=E_{xx}$ in Young's modulus along the x axis.

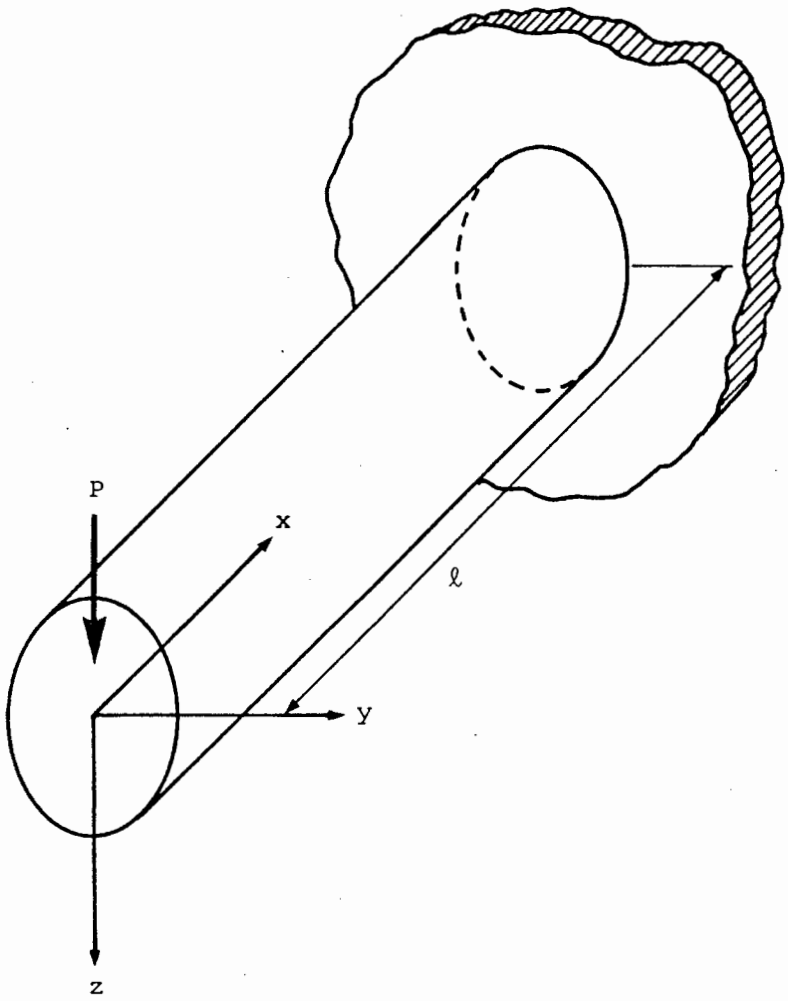

Figure 7

Cantilever with arbitrary cross section.

The microscope specimen may now be considered to be two joined cantilevers as shown in fig.2. Hence the tensile stress at the centre on the upper surface of the specimen shown in the diagram, before the crack is introduced, is given by

$$\sigma_{xx}\big|_{\text{centre}} = \sigma = \frac{3hdE}{2\ell^2} \qquad (4)$$

where we may take d to be the deflection of the upper surface of the specimen at the position where the load is applied.

2.4.2 Crack shape

It is shown in fig.4 that the cross sectional shape of the cracks in both glass and quartz are not truly elliptical but are only slightly flatter than ellipses. Because the experimental bending problem is three dimensional, an accurate comparison of the results with the two dimensional elastic theories outlined in the introduction cannot be made. However, the result (eqn.(4)) above shows that before the crack is introduced, the tensile stress on the upper surface at the centre of the specimen is uniform accross the specimen width and the state of stress is thus similar to the case of a specimen with an edge crack pulled in direct tension. However, it can be seen from fig.3 that if it is accepted that the crack is placed in a

uniform tensile field, then the crack does not seem to be aware that it is at an edge but behaves as though it was centrally placed. It can also be seen in fig.3 that near the crack tip the shape of the theoretical and experimental curves all take up the same shape. The atomistic analysis of Sinclair and Lawn (1972) has shown that the linear elastic solution is almost the same as the atomistic solution a few atoms away from the crack tip. Hence it would seem reasonable to assume that the observed crack shape can be extrapolated to near atomic dimensions. For instance, Sinclair and Lawn obtain a radius of curvature (ρ) of the crack tip at fracture to be $\rho \simeq 0.15$nm for silica for a crack in a uniform tensile field, whereas in the glass specimens presently studied ρ was determined to be $\simeq 0.25$nm at fracture, where the crack shape was taken as being elliptical and ρ is therefore given as $\rho = u^2/y$.

Even though the cracks in quartz deviated from a straight line, the tensile stresses opening the cracks were approximately the same as for a straight crack and so the crack shape should be approximately the same - this result is verified in fig. 4.

2.4.3 Calculation of the fracture surface energy from the shape of the crack

If we make the simplifying assumption that we need only consider a small thickness of material beneath the upper surface of the specimen, because the crack is longest and the tensile stress is greatest at the top

surface, then we may apply the Irwin-Orowan criterion for the onset of fracture. In order to calculate the work done to open the slit crack we can envisage the material as initially containing no crack so that the tensile stress on the upper surface given by eqn. (4) will be found at the centre of the upper surface of the specimen. If the crack is now inserted, this stress will relax to zero as the crack opens, and if the system is linear, it will decrease linearly. Let $u(\sigma,y,c)$ be the displacement of the crack in the x direction when the crack of length c has been opened under the action of the tensile stress σ as shown in the diagram below.

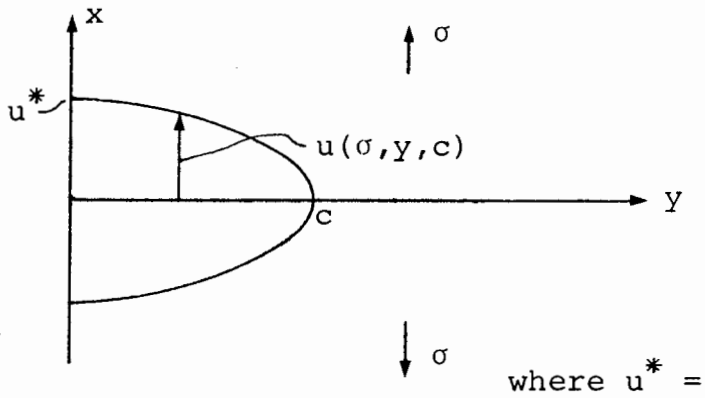

If we consider only a very small thickness of material beneath the upper surface of the specimen then the tensile stress σ will be uniform through this thickness, and as the system is linear, the work done to open the crack per unit thickness is equal to

$$W = 2\int_0^c \tfrac{1}{2}\sigma u\,dy$$

The Irwin-Orowan criterion requires that $dW/dc = 2\gamma_f$ (Goodier, 1968).

i.e. $$\frac{d}{dc}\left(\sigma \int_o^c u\,dy\right) = 2\gamma_f \qquad (5)$$

In the case of the crack described by Griffith (1920) the crack displacement changes in direct proportion to the crack length for constant stress. If we make the assumption that this is also true in the present case, then, as shown in Appendix C, we obtain the result that

$$\frac{d}{dc}\left(\int_o^c u\,dy\right) = \frac{2}{c}\int_o^c u\,dy$$

combining this result with eqns. (4) and (5) we obtain

$$\gamma_f = \frac{3hdE}{2\ell^2 c}\int_o^c u\,dy$$

If we approximate the crack shapes to ellipses, then

$$\int_o^c u\,dy = \frac{\pi}{4}u^* c$$

As the system is linear $u^* = kd$ (k a constant)

so that $$\gamma_f = \frac{3\pi(u^*)^2 hE}{8\ k\ \ell^2}$$

where u^* is evaluated at fracture. The fracture surface energy for three glass specimens calculated on this basis gave values of 8.1, 7.9 and 11.0 Jm^{-2}. Comparing these results to those obtained by the direct

tension experiments, and allowing for the fact that γ_f can be about 25 per cent higher for vacuo than for a liquid nitrogen environment (Linger and Holloway, 1968), these results are higher than the direct tension results and the discrepancy is thought to arise because of the simplifications and assumptions made in the above analysis. Because the cracks in quartz deviated from a straight line, the above analysis was not applied to them, as they fractured under mixed fracture mode conditions of shear as well as tension.

2.5 Conclusion

The shape of an edge crack in an approximately tensile stress field has been found to be almost elliptical in quartz and in soda-lime glass. A value of 0.25nm for the radius of the crack tip in glass at fracture was deduced from the shape of the rest of the crack. This value is in good agreement with the value of 0.15nm predicted by Sinclair and Lawn. Using an energy analysis based on crack shape and by applying the Irwin-Orowan criterion to this result, a value of the fracture surface energy of the glass specimens was determined to be about $8Jm^{-2}$. If this value is compared to a value of about $4Jm^{-2}$ for the fracture surface energy for the same glass in liquid nitrogen, found by standard methods, then it is seen that within the accuracy of the assumptions made, the agreement is very reasonable.

3. FRACTURE SURFACE ENERGIES IN QUARTZ

3.1 Introduction

A knowledge of the fracture surface energies in quartz will enable a calculation of the energy required for cutting and particle size reduction to be made. This amount of energy can then be compared to the actual amount expended in practice and the efficiency of cutting and comminuting assessed. A comparison of the fracture surface energy to the true surface energy will also give an indication of the extent of plastic blunting at the crack tip. In this connection, it is known that certain environments influence plastic flow and they can therefore be used to alter the brittleness of materials so that less energy is dissipated by plastic flow during fracture. Previous evidence (Ball and Payne, 1976) suggests that quartz may be perfectly brittle when fractured in tension and consequently a more accurate determination of the fracture surface energy has been undertaken. Because quartz is anisotropic with regard to its elastic properties and its surface energies, an accurate measurement of the fracture surface energy requires that anisotropic elastic theory be used to calculate the strain energy release rate. The results of Sih et al (1965) may be used for this calculation, but it is required that the crack extend in its own direction along a plane of elastic symmetry.

The $(1\bar{1}00)$ plane of α-quartz satisfies both of these requirements and was used for the determination of the fracture surface energy (i.e. orientation D, see section 5.2).

There are however, two experimental difficulties which may give rise to spurious values of the fracture surface energy even if the material is perfectly brittle, viz.

(i) stress corrosion at the crack tip may cause a change in crack geometry and also cause the crack to increase in length before rapid fracture occurs, and

(ii) the initial notch may be blunt and an overstress may be required for its propagation.

These difficulties have been obviated in the present work by the use of an inactive environment and a technique of introducing sharp cracks into the specimen.

3.2 Experimental Methods

Single crystals of quartz of dimensions 60mm x 12mm x 0.5mm parallel to the Y,Z and X axes respectively had sharp cracks of varying lengths (but always less than $\frac{1}{3}$ of the width of the specimen) introduced at the centre of the Y axis by the method described in Appendix A. It was found that the cracks tended to deviate slightly from a line perpendicular to the edge of the crystal, but only those specimens with cracks within 10^0 of the perpendicular line were tested.

Because of the known influence of water on the fracture of silica glass in tension (Charles 1958, Schoening 1960, Wiederhorn and Bolz 1970) and of quartz in compression (Scholz and Martin, 1971), the tests were carried out in toluene (which has a very low residual water content) to which freshly cleaved sodium was added. The tests were performed by applying direct tension parallel to the Y axis of the crystal at a strain rate of about $7 \times 10^{-5} s^{-1}$. The specimens were attached to the testing machine in the same manner as described in section 2.2.2.

The lengths of the initiating cracks were measured by reflected light microscopy by bending the crystals sufficiently to open the crack to its full

length. These values were correlated with the distances to the mark left on the fracture surface at the extremity of the initiating crack.

3.3 Experimental Results

Sih et al (1965) have successfully extended the Griffith theory to anisotropic materials and their results are applied to the present situation. However, their theory for a thin plate in plane stress (which is the one of interest here) is restricted to the case where there is a plane of elastic symmetry parallel to the surface of the plate and no load is applied perpendicularly to the surface of the plate. The $(11\bar{2}0)$ plane of α-quartz is one of elastic symmetry as it is perpendicular to a two fold axis of rotation (Lekhnitskii, 1963) and hence we may apply Sih's theory to a thin X cut quartz plate as used in this experiment.

We begin by writing the generalised equations for Hooke's Law in any material which is in a state of generalised plane stress where the inplane strains only depend on the inplane stresses and there is a plane of symmetry perpendicular to the Z axis.

i.e.
$$\left.\begin{aligned} \varepsilon_{xx} &= s_{11}\sigma_{xx} + s_{12}\sigma_{yy} + s_{16}\sigma_{xy} \\ \varepsilon_{yy} &= s_{12}\sigma_{xx} + s_{22}\sigma_{yy} + s_{26}\sigma_{xy} \\ \varepsilon_{xy} &= s_{16}\sigma_{xx} + s_{26}\sigma_{yy} + s_{66}\sigma_{xy} \end{aligned}\right\} \qquad (6)$$

The characteristic equation below is obtained from these equations which has roots that will determine the stresses and displacements.

$$s_{11}\mu^4-2s_{16}\mu^3+(2s_{12}+s_{66})\mu^2-2s_{26}\mu+s_{22} = 0$$

The roots of this equation are either complex or purely imaginary and cannot be real. If we assume unequal roots then we can set $s_1=\mu_1=\alpha_1+i\beta_1$, $s_2=\mu_2=\alpha_2+i\beta_2$, $\mu_3=\bar{\mu}_1$, and $\mu_4=\bar{\mu}_2$;

where α_i,β_i , i=1, 2 are real constants and β_1, $\beta_2>0$.

The energy release rate for a crack lying parallel to the X axis and extending in this direction when tensile stresses are applied along the Y axis is given by :

$$G_1 = \frac{\pi K_1^2}{2}\, s_{22}\, \mathrm{Re}\left\{\frac{i(s_1+s_2)}{s_1 s_2}\right\}$$

where K_1 is the anisotropic stress intensity factor. Fortunately, in the case of self balancing loads on the crack surface (as in the experimental situation), K_1 is the same as the isotropically evaluated stress intensity factor.

In the present case, where the crack lies in the $(1\bar{1}00)$ plane in α- quartz and a tensile stress σ is applied parallel to the Y axis, equations (6) become :

$$\varepsilon_{zz} = s_{33}\sigma_{zz} + s_{13}\sigma_{yy}$$

$$\varepsilon_{yy} = s_{13}\sigma_{zz} + s_{11}\sigma_{yy} - s_{14}\sigma_{yz}$$

$$\varepsilon_{yz} = -s_{14}\sigma_{yy} + s_{44}\sigma_{yz}$$

The characteristic equation is then given by

$$s_{33}\mu^4+(2s_{13}+s_{44})\mu^2+2s_{14}\mu+s_{11} = 0$$

The values of the elastic constants have been taken from Cady (1946) as $s_{11}=1.26\times10^{-11}Nm^{-2}$, $s_{13}=-0.15\times10^{-11}Nm^{-2}$, $s_{14}=-0.43\times10^{-11}Nm^{-2}$, $s_{44}=2.00\times10^{-11}Nm^{-2}$, $s_{33}=0.97\times10^{-11}Nm^{-2}$, and the roots of the above equation with positive imaginary parts have the values

$$s_1 = 0.432+i0.742 \text{ and } s_2 = -0.432+i1.255$$

The energy release rate is given by

$$G_1 = \frac{\pi K_1^{\,2} s'}{2}$$

where $$s' = s_{11}\mathrm{Re}\left\{\frac{i(s_1+s_2)}{s_1 s_2}\right\}$$

and has the value $2.162\times10^{-11}m^2N^{-1}$. The elastic constants given above have an accuracy of about one per cent and consequently s' will have a similar accuracy.

The fracture criterion is then determined by setting G_1 equal to $2\gamma_f$. The stress intensity factor is the same as that used in section 2.3.2 and hence we obtain the equation

$$\sigma^2 = \frac{4\gamma_f}{s'cY^2} \qquad (7)$$

where c is the length of the crack and Y is given by equation (3). If the experimental values of σ^2 are plotted against $1/cY^2$, a straight line of slope $4\gamma_f/s'$ should occur. This result is shown in fig.8 and the value of γ_f derived from the slope is $3.0 \pm 1.0\ Jm^{-2}$. It should be noted that if a quasi-isotropic method had been used by substituting Young's modulus parallel to the tension axis instead of 2/s' in equation (7), then γ_f would have been equal to $3.5 \pm 1.2\ Jm^{-2}$.

It was thought that because of the difficulty of introducing straight cracks (compared to glass), fracture might occur on a plane inclined to the tensile axis or bifurcation would occur easily. However, in all cases the crack propogated straight across the specimen and no branching occured.

3.4 Discussion

Before comparing the above result for γ_f with the value of γ obtained from the theoretical estimate from

Figure 8

Graph for the deduction of the fracture surface energy of the $(1\bar{1}00)$ plane in quartz

bond energy data as described in Appendix D, it is important to establish that the value of γ_f measured is indeed free from the two complicating factors mentioned in the introduction. The claim that the cracks introduced were atomically sharp should be substantiated because an experiment by Cordwell and Hull (1969) has shown that if a certain method can be used successfully to initiate sharp cracks at low temperatures, then it may not be assumed that this will also be the case at high temperatures. Their experiment on tungsten, using a spark discharge method, indicated that cracks were blunted if introduced at a temperature where the fracture surface energy was greater than the true surface energy, and it was only when the cracks were introduced at a sufficiently low temperature that the material had a fracture surface energy approximately equal to the true surface energy. It is conceivable that the hot tool (about 600^0C) used to introduce these cracks could have heated the material sufficiently to cause plastic relaxation at the crack tip. However, it is believed that the material in the vicinity of the crack tip only experienced a rise in temperature much less than 600^0C. This supposition is based on the results of an experiment in which a notched specimen was heated to about 150^0C and then quenched in water. This temperature difference was sufficient to cause propagation of a crack from the notch. (However, as the direction of propagation could not be accurately controlled, this method of introducing sharp cracks was abandoned.) Admittedly, the above experiment differs

from the present one as far as heat transfer rates are concerned, but the temperature difference required to propagate a crack from the notch should be similar in both cases.

Because the specimens were not tested in vacuo the possibility of stress corrosion should be considered. A comparison can be made with the results of experiments on soda-lime glass tested in toluene by Evans (1972). He showed that the residual water content may cause stress corrosion. However, if the strain rate was sufficiently high, the fracture surface energy was unaffected by the presence of the water. It is believed (by comparison with Evans' result) that the strain rate in the present experiment was sufficiently high and that the presence of sodium reduced the residual water content sufficiently so that the true value of γ_f was measured.

It is possible to attribute the tendency for the crack to deviate from the $(1\bar{1}00)$ plane, when introduced, to two factors, viz : anisotropy of surface energy on cleavage planes and elastic anisotropy. It has been demonstrated by Sih and Liebowitz (1968) that for a body

with sufficient elastic anisotropy, the required cleavage stress of the crack tip may be larger at an angle to the crack than directly ahead of it. This stress is given by

$$\sigma_{\theta\theta} = \frac{K_1}{2(2r)^{\frac{1}{2}}} \mathrm{Re}\left\langle \frac{s_1 s_2}{s_1 - s_2} \left\{ \left[\frac{(s_2^{-1} + s_2) + (s_2^{-1} - s_2)\cos 2\theta + 2\sin 2\theta}{(\cos\theta + s_2 \sin\theta)^{\frac{1}{2}}} \right] \right.\right.$$

$$\left.\left. - \left[\frac{(s_1^{-1} + s_1) + (s_1^{-1} - s_1)\cos 2\theta + 2\sin 2\theta}{(\cos\theta + s_1 \sin\theta)^{\frac{1}{2}}} \right] \right\} \right\rangle$$

where r is the radial distance from the crack tip and angle θ is measured from the line of the crack and is zero directly ahead of the crack. This stress is shown in fig.9 for the present case and also for the isotropic case. It is seen that the stress distribution is nearly isotropic and consequently elastic anisotropy plays little or no role in the determination of the crack propagation direction in this case. It was also established that for a crack parallel to the (0001) plane and a tensile stress applied parallel to the Z axis, the cleavage stress is again nearly isotropic. The closeness of the anisotropic stress field to the isotropic stress field has also been experimentally noted (Heavens and Ashbee, 1975).

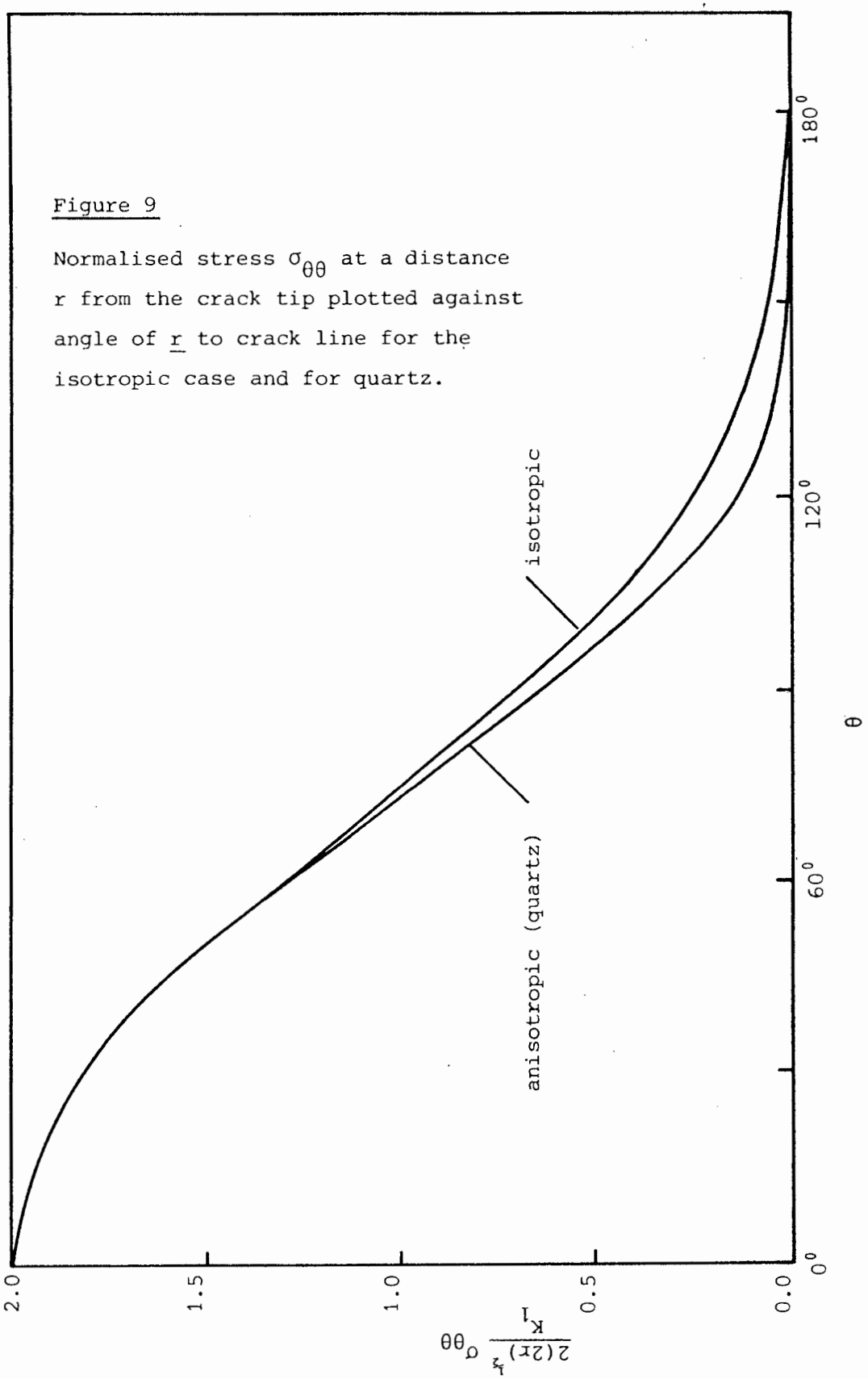

Figure 9

Normalised stress $\sigma_{\theta\theta}$ at a distance r from the crack tip plotted against angle of r to crack line for the isotropic case and for quartz.

3.5 Conclusion

A fracture surface energy of $3.0 Jm^{-2}$ was obtained for fracture along the $(1\bar{1}00)$ plane in α-quartz. A calculation of the true surface energy for this plane, based on bond energy data, gave a value of $2.9 Jm^{-2}$ which is considered to be an upper limit for the value of the true surface energy. It is thus concluded that when quartz is tested in tension at room temperature it is almost perfectly brittle. Calculations of the stress field at crack tips in quartz using anisotropic elastic theory for two crack orientations has shown that the stress field is, to a good approximation, the same as that in an isotropic body. It is therefore concluded that the role of elastic anisotropy in the determination of the direction of cleavage in quartz is insignificant and it is only the anisotropy of the surface energy that determines the deviations from isotropic behaviour.

4. CRACK PROPAGATION IN α-QUARTZ

4.1 Introduction

A knowledge of the velocity behaviour of cracks in brittle materials under given loading conditions will assist engineers in designing safer structures and will give them values of the rate of energy released during catastrophic failure. The determination of an upper limit to the crack velocity and information concerning velocity-distance/time relationships is also useful in the consideration of methods of mining and comminuting rock and in the control of rock bursts.

Until recently the only available equation of motion of a crack in a brittle solid has been the quasi-static one of Berry (1960). The motion of cracks in highly brittle and semi-brittle materials has been described in terms of this equation by adjusting various parameters in the equation. Freund (1972) has derived an exact result for the motion of a mode 1 crack in a brittle solid and the various predictions of this theory should, in addition to those of the previous theory, be compared to experimental findings.

The theory given by Berry (1960) for crack propagation under mode 1 conditions is modelled by a central crack of length 2c in an infinite body of unit thickness which is assumed to grow from rest under the action of a remotely applied tensile stress σ. This is a quasi-static model and the motion of the crack is established by the use of an energy balance equation. Thermodynamic equilibrium of the body requires that

$\dot{U} = \dot{V} + \dot{T} + \dot{D}$ where the dot refers to

differentiation with respect to time, U is the work done by external loads, V is the elastic strain energy, T is the kinetic energy and D is the dissipative energy. In its integrated form this equation becomes :-

$$V - U + T + D = \text{constant} \qquad (8)$$

the constant being determined by the initial conditions. The kinetic energy is given by

$$T = \tfrac{1}{2}\rho\dot{c}^2 \iint_R \{(\partial u_1/\partial c)^2 + (\partial u_2/\partial c)^2\}\, dxdy \qquad (9)$$

where u_1, u_2 are the displacements in the x and y

directions, c is the crack length, ρ is the mass density of the material and the region R is assumed to cover the whole body. Mott (1948) found that on dimensional grounds T is given by

$$T = \tfrac{1}{2}k'\rho c^2\dot{c}^2 \ (\sigma^2/E^2)$$

where k' is a constant which depends on Poisson's ratio. The static value of the net available energy U - V, for a constant stress at infinity is given by $U - V = \pi\sigma^2c^2/E$, see section 1.2 , and D is given by $D = 4\gamma_f c$. From the Irwin-Orowan equation we have

$\gamma_f = \sigma^2\pi c_o/2E$, where c_o is the initial crack length. Equation (8) can therefore be written in the form :-

$$\frac{k'\rho c^2\dot{c}^2\sigma^2}{2E^2} - \frac{\pi\sigma^2c^2}{E} + \frac{2\pi c_o c\sigma^2}{E} = E_o \qquad (10)$$

where E_o is a constant. For $\dot{c} = 0$ and $c = c_o$ at $t = 0$

E_o is given by $E_o = \dfrac{-\pi c_o^{\,2}\sigma^2}{E} + \dfrac{2\pi c_o^{\,2}\sigma^2}{E}$

and the following equation is obtained from equation (10) for the crack velocity

$$v = \left(\frac{2\pi E}{k'\rho}\right)^{\frac{1}{2}} (1 - c_o/c)$$

where $v = \dot{c}$. We can write this equation as

$$v = v_m (1 - c_o/c) \qquad (11)$$

where $v_m = (2\pi E/k'\rho)^{\frac{1}{2}}$ is the maximum velocity of the crack. The value of k' has been evaluated by Roberts and Wells (1954) by using the static elastic displacements and restricting the range of integration in equation (9) so that v_m has the value $0,38v_\ell$ where v_ℓ is the longitudinal wave velocity. However, Küppers (1967) has used numerical techniques and has calculated a value of $0,6v_\ell$ for v_m. Berry realised that equation (11) implied that for a crack initially at rest, the acceleration was also zero so that crack growth was impossible. He accordingly modified the equation by letting the initial stress σ_f required to propagate the crack be higher than the Griffith stress σ_g. If we make this distinction in equation (10) and insert the parameter $n = 2\sigma_g^2/\sigma_f^2$ we obtain a modified equation given by :-

$$v^2 = v_m^2 (1 - c_o/c) (1 - (n-1) c_o/c) \qquad (12)$$

This equation implies that the crack will have a finite initial acceleration provided $n < 2$. It must be realised that this result is only approximately correct as it suffers from the severe drawback that the static, instead of the dynamic value of U - V is used and also

that the kinetic energy is evaluated throughout the whole body. This is the only equation of motion that has been available for many years, and provided that v_m is interpreted as the maximum observed crack velocity, it is found, rather surprisingly in view of the assumptions made, that cracks in many brittle materials obey this equation.

A recent theory which provides an exact equation of motion for an edge crack in a semi-infinite body for mode 1 conditions has been obtained by Freund (1972). Freund first obtained an expression for the dynamic stress intensity factor of such a crack before obtaining an equation of motion. This dynamic stress intensity factor K_v is defined analogously to the static stress intensity factor except that the tensile stress perpendicular to the crack surface at the crack tip is evaluated at a velocity v. Freund found that K_v factored into a velocity component and a distance component as :

$$K_v = k(v)K_s(c) \qquad (13)$$

where $K_s(c)$ is the static stress intensity factor for a crack of length c and k is given by the equation :-

$$k(v) = \{v\, S_+(v)(1/v + 1/(v_s-v)(1-v/v_\ell)^{\frac{1}{2}}\}^{-1} \qquad (14)$$

where v_s is the Rayleigh wave velocity, v_ℓ is the velocity of longitudinal waves and $S_+(v)$ is a complicated integral

whose value is only slightly different from unity for all values of v. A graph of k(v) against v is given in fig. 10.

The method used to obtain the equation of motion in this case differs from Berry's treatment in that the energy balance is not determined for the whole body, but only for a small loop surrounding the moving crack tip.

The 'dynamic strain energy release rate', which is the dynamic analogue of Irwin's strain energy release rate for static problems, is defined as the energy released to the crack tip for unit advance of the crack. The equation of motion of the crack is then obtained by setting this quantity equal to the energy necessary to create two new surfaces. We shall assume that the body is thin so that the elastic theory of plane stress may be applied to reduce the problem to two dimensions. As the crack tip, which is surrounded by a small curve L, moves under the action of the applied loading, mechanical energy flows through L at a rate denoted by $\dot{H}$. We let $\dot{P}$, T and V denote the rate of work of the tractions on a boundary S enclosing the entire crack, the total kinetic energy of the material in the region R enclosed by S and the total strain energy of the material in R respectively. The energy flux through L is then equal to the difference between the rate of work of the applied loads on S and the rate of increase of internal energy in R i.e. $\dot{H} = \dot{P} - (\dot{T} + \dot{V})$, from which the following

Figure 10

Graph of k(v) the ratio of the dynamic stress intensity factor to the static stress intensity factor, plotted against normalised crack velocity v/Rayleigh velocity (v_s)

result is obtained :

$$\dot{H} = \int_L \{\sigma_{ij} n_i \dot{u}_i + \tfrac{1}{2}(\sigma_{ij} u_{i,j} + \rho \dot{u}_i \dot{u}_i)\ v n_x\ \}\ dL$$

given that the crack lies along the X axis, σ_{ij} and u_i are the components of stress and displacement and n_i is the normal to L. The first term in this integral represents the rate of work of the material outside of L on the material inside and the second term represents the flux of energy arising from material particles crossing L as it moves through the material. The dynamic energy release rate is then given as $G = v\dot{H}$.

This can be expressed in terms of the dynamic stress intensity factor as :-

$$G = K_v^2\ B(v)\ /\ E \qquad (15)$$

for plane stress conditions where

$$B(v) = \frac{(1 - v^2/v_\ell^2)^{\frac{1}{2}}\ v_s/v}{(1-\nu)\{\ \frac{4v_s^2}{v^2}(\frac{v_s^2}{v^2} - \frac{v_s^2}{v_\ell^2})^{\frac{1}{2}}(\frac{v_s^2}{v^2} - 1)^{\frac{1}{2}} - (\frac{2v_s^2}{v^2} - 1)^2\}}$$

From equation (13) this may also be written as

$$G = K_s^2(c)F(v)/E \qquad (16)$$

where $F(v) \equiv k(v)B(v)$. The function F(v) is shown in

fig. 11 for a material with a Poisson's ratio of $\nu = \frac{1}{4}$. (The graphs of F(v) previously published by Freund are incorrect (Freund 1976, private communication).) This graph is nearly linear and for practical purposes the relationship will be assumed to be $F(v) = 1 - v/v_s$.

If we equate the work done to create two new surfaces as equal to twice the fracture surface energy, then the equation of motion (15) becomes :

$$2E\gamma_f = K_s^2(c)(1-v/v_s) \qquad (17)$$

The result obtained by Eshelby (1969) for a mode 3 crack is equivalent in form to equation (15) and hence some of his comments apply in this case as well and the following points should be noted in connection with equation (15) :

(i) The upper limit on the velocity of a crack is the Rayleigh velocity - a result which is in agreement with other predictions (Yoffe 1951, Broberg 1960).

(ii) If the crack tip is viewed as a particle, then it behaves as though it has no inertia. This is in agreement with the observations of Küppers (1967).

(iii) If the tip of the crack is initially held closed so that the initial strain energy release rate required to propagate the crack is greater than $2\gamma_f$, then the crack will propagate with an initial finite velocity.

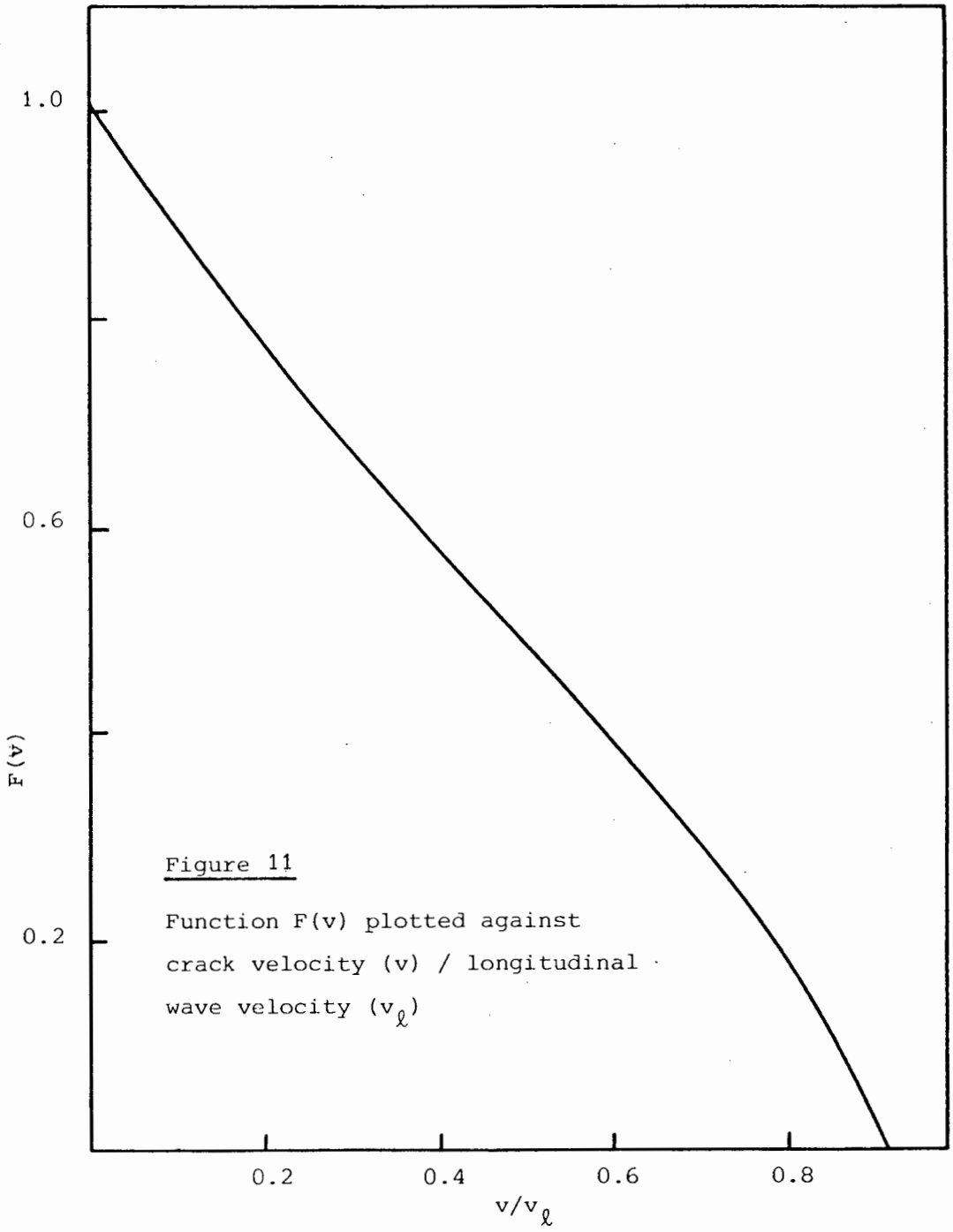

Figure 11

Function F(v) plotted against crack velocity (v) / longitudinal wave velocity (v_ℓ)

(iv) The equation does not take into account reflected waves from the edge of the specimen, but an examination of this effect indicates that it is small (Freund, 1976).

The result obtained by Freund has also been obtained by independent methods by Kostrov (1975) and by Burridge (1976). However, in the case of a finite specimen care must be used in applying Freund's result, not only because of reflected waves, but also because the equivalent static stress intensity factor in Freund's result is only strictly applicable to infinite bodies, and the static stress intensity factor for a crack where the crack tip is near a free surface, will differ greatly from that of a crack of equivalent length in an infinite medium.

4.2 Experimental methods

Crystals of dimensions 60mm x 12mm x 0.5mm cut parallel to the X,Y and Z axes respectively had notches cut into the long edges with an annular diamond saw 0.15mm wide or with a diamond impregnated copper wire 0.15mm in diameter in order to vary the sharpness of the initial notch. These specimens were tested by the application of a tensile stress along the X axis as described in section 2.2.2. This particular crystal orientation was chosen because it fulfilled the requirements of both the electrical and Wallner line methods of measuring velocity.

4.2.1 Electrical resistance grid methods

It was found that if a resistance grid was placed on a crystal surface which became polarised during fracture as a result of the piezoelectric effect, then the piezoelectric signal was so large that the resistance grid signal could not be detected. The symmetry of quartz is such that no matter how the crystal is stressed, no component of polarisation will occur perpendicular to the (0001) plane. Hence this face of the crystal was chosen for the positioning of the resistance grid.

4.2.1.1 Preparation of specimens and grids

One of the large (0001) faces of the specimen was polished to a mirror finish with 1μm diamond paste and then carefully cleaned before being coated with about 10nm of nichrome evaporated from a tungsten boat at a pressure of about 5×10^{-5} Torr. A mask of the resistance grid - which consisted of 35 equally spaced bars connected in parallel and a trigger bar - was produced on a high contrast film. The pattern of the mask was then transferred to the specimen by a standard photoresist process and the unwanted nichrome was removed by immersing the specimen in aqua regia. Good electrical contact was made with the grid by clipping gold plated transistor socket receiving pins over the edges of the specimen. A fractured specimen with the nichrome grid is shown in plate 3.

4.2.1.2 Measuring circuits

The first circuit to be described merely measured the change in resistance of the whole grid as each grid bar was broken. This circuit is shown in fig.12. There are two important points which should be noted in the design of the circuit. The first is that the change in voltage across the measuring resistor should be approximately equal each time a grid bar is broken and the second is that the time constant must be sufficiently small to allow for the detection of the

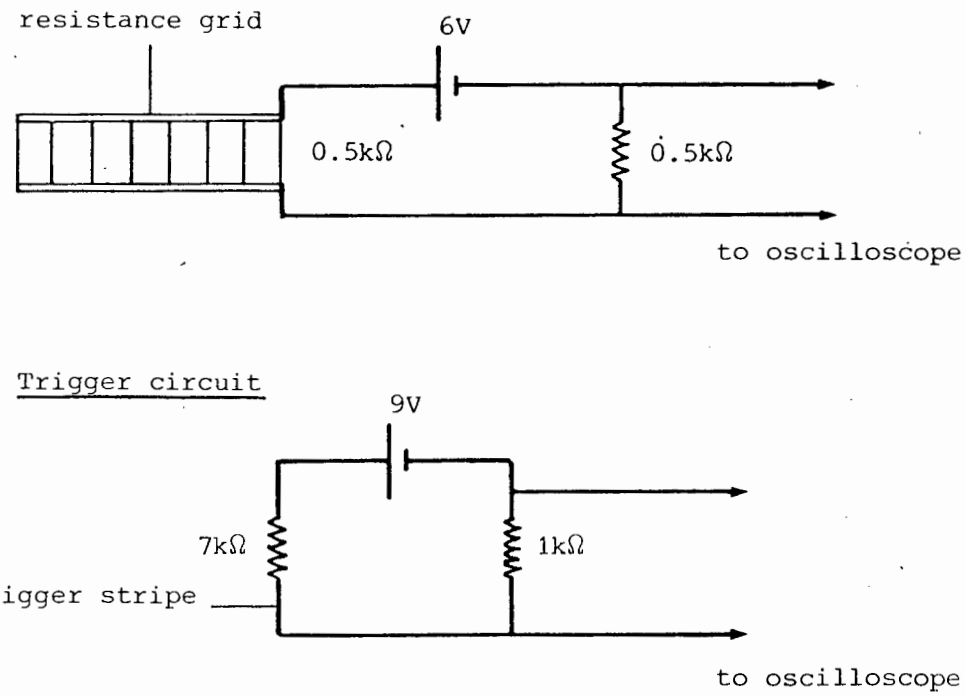

Figure 12

First measuring circuit for resistance grid method of obtaining crack velocities.

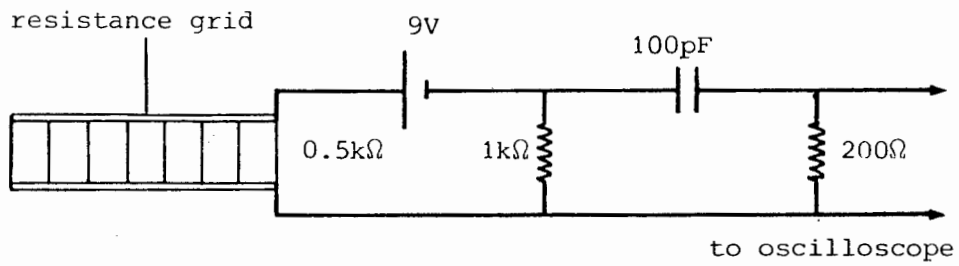

Figure 13

Second circuit containing differentiating stage.

sudden change in voltage as each grid bar breaks. The signal was recorded by photographing the screen of a fast (Hewlett Packard 180D) oscilloscope using 10 000 ASA Polaroid film. Because there were only small changes in the initial resistance of the grid, it was very difficult to separate the signals resulting from the breaking of each grid bar during the initial stage. This difficulty was overcome by designing a second circuit (shown in fig.13) which consisted of an extra stage which differentiated the signal from the first circuit and hence emphasised the points where the grid bars broke.

4.2.2 Wallner line method

It was found advantageous to have at least one of the large faces of the specimen ground with 600 grit silicon carbide, as this would provide a large number of sources of shear waves which would in turn promote the generation of Wallner lines during fracture. The directions of the crystal axes were determined by the Laué back-reflection X-ray technique, and in order to apply the theory developed in Appendix E, the positive sense of these axes was determined by the method of etch figures (Cady, 1946). Good etch figures were produced on a polished (0001) face after etching for 40 mins in 40 per cent hydrofluoric acid.

Wallner lines on the fracture surface were

photographed by oblique illumination in an optical microscope at a magnification of 100X and a composite picture of the surface was built up, from which the angles required for the theory were obtained. In order to determine the angle between the wavefront and the crack propagation direction, use was made of finely spaced surface markings which were observed in addition to the Wallner lines. These are thought to be caused by a perturbation of the crack front by waves continuously emmitted by the growing crack and subsequently reflected from the boundary at the initiation site. These markings should therefore give an approximation to the actual position of the crack front at an instant in time.

4.3 Experimental results

The signal obtained by the first electrical measuring circuit is shown in plate 4 and the result of the improved circuit in plate 5. A time-distance relationship was established by correlating the sudden change in electrical signal with the breaking of the end of a grid bar and the average velocity between the breaking of the bars was thus obtained as a function of crack length. A graph of crack velocity against normalised crack length is shown in fig.14 as obtained by both the electrical grid and Wallner line methods for a single specimen.

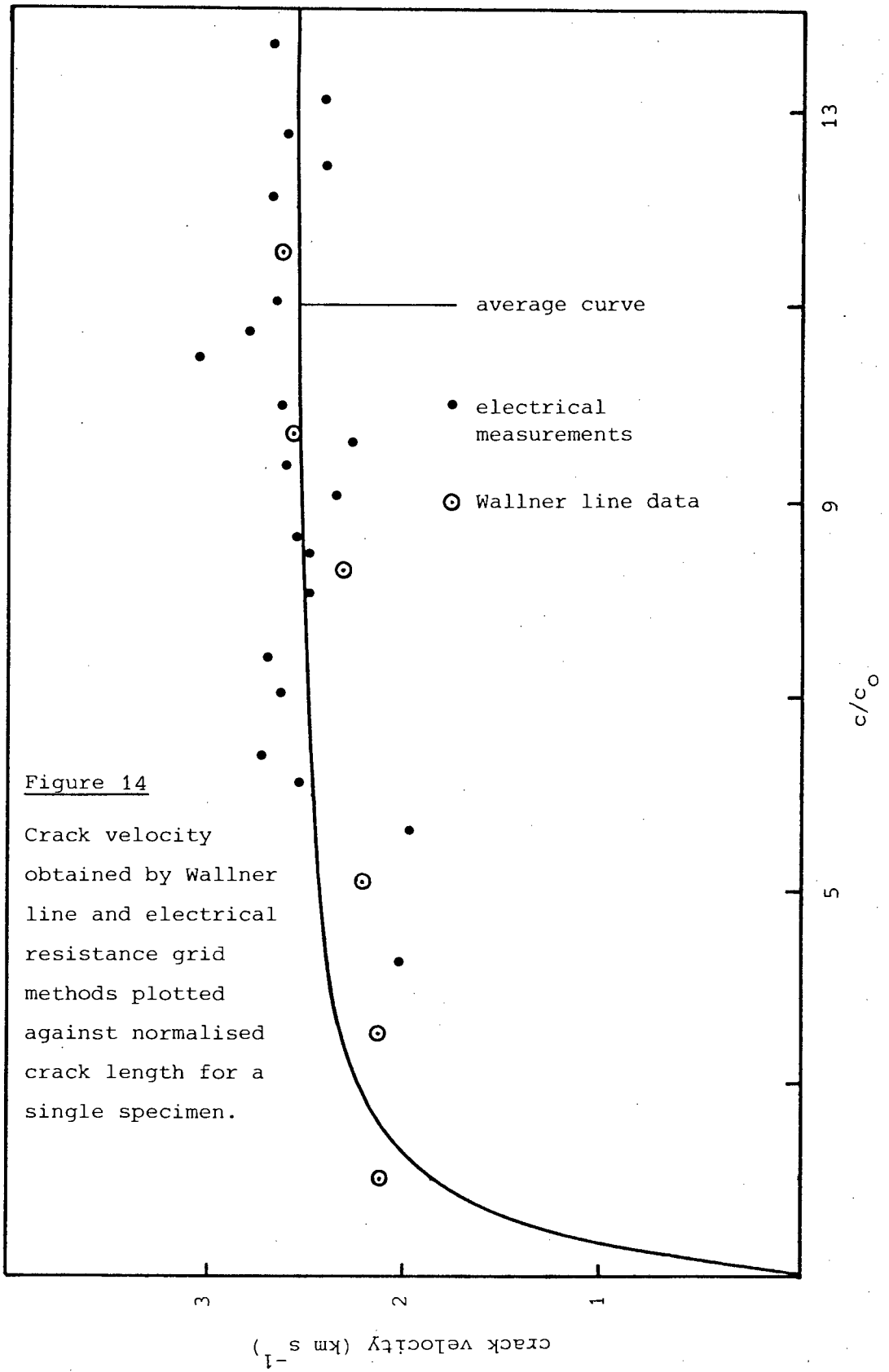

Figure 14

Crack velocity obtained by Wallner line and electrical resistance grid methods plotted against normalised crack length for a single specimen.

The fracture surfaces were usually very flat and normal to the tensile stress axis and only when a very blunt notch was introduced in the specimen did the fracture surface become rough, but no macroscopic bifurcation ever occured. This surface roughening was localised to crystallographic planes, some of which were identified as the rhombohedral planes $\{10\bar{1}1\}$. It was found that surface roughening only occured at very high crack velocities at about $0.92v_s$. A typical mirror like fracture surface showing Wallner lines is shown in plate 6 for a specimen with a sharp notch and the onset of surface roughening in a specimen with a blunt notch is shown in plate 7.

4.4 Discussion

4.4.1 Accuracy of results

The scatter in the velocities obtained by the resistance grid method arises mainly from the difficulty in taking measurements from the photographs of the oscilloscope screen. However, all the velocity measurements are subject to a systematic error of about five per cent as the time base of the oscilloscope was only calibrated to this accuracy. It is assumed that the grid bars broke at almost the same time as the specimen and so would only contribute a small error which may be neglected.

The main sources of error introduced into the

analysis of Wallner lines are the measurements of angles from the photograph and the measurement of the orientation of the crystal. These lead to a maximum error of about ten per cent on the crack velocity.

If the isotropic Wallner line theory had been used for the present case a situation where the crack front was perpendicular to the crack propagation direction would have to be found and an average shear wave velocity would have to be chosen. If the average shear wave velocity is chosen as equal to the shear wave velocity in silica, then for a typical result the isotropic value would be fifty per cent lower than the anisotropically calculated value.

4.4.2 Comparison with theories

In this section we will attempt to modify the theory of Freund, using the suggestion of Berry, to take into account the possible geometries of crack tips.

4.4.2.1 Blunt cracks

A crack in the edge of a semi-infinite solid has a stress intensity factor given by

$$K_s(c) = 1.99\sigma\sqrt{c}$$

(see equation (3) when the specimen width tends to infinity), and if we substitute this into equation (17) and impose the initial condition v=0 when $c=c_o$, then we obtain the equation

$$v = v_s(1-c_o/c) \qquad (18)$$

At high velocities this relation is only approximately correct, but at low velocities it is seen from fig.11 that F(v) accurately follows a straight line and hence equation (18) should be regarded as exact near v=0. This result is the same as Berry's for a Griffith crack if we accept $v_m=v_s$, and hence for the reasons mentioned previously the crack will not grow. Using Berry's method as an example we may suppose that if the crack was blunt an overstress would be required to propagate the crack. Hence if we take the initial condition that

$$\sigma^2_f = \alpha\sigma^2_g = \alpha\frac{2E\gamma}{(1.99)^2 c_o} \qquad (19)$$

then we obtain the result

$$v = v_s\left(1 - \frac{1}{\alpha}\frac{c_o}{c}\right) \qquad (20)$$

from equation (17). This equation implies that the crack moves with an initial velocity given by

$$v_o = v_s\left(1 - \frac{1}{\alpha}\right)$$

Fig.15 shows the velocity plotted against normalised crack length for Berry's equation (12) and the modified Freund equation (20) for different values of n and α.

In order to compare the experimental results with these two equations, c_o/c is plotted against v and the result is shown in fig.16 for three different specimens. It can be seen that the data can be fitted to the straight line,

$$v = v_{max}\left(1 - \frac{1c_o}{\beta c}\right) \qquad (21)$$

β a constant. The values of β found from the graph are compared to the values of α calculated from equation (19) in the following table.

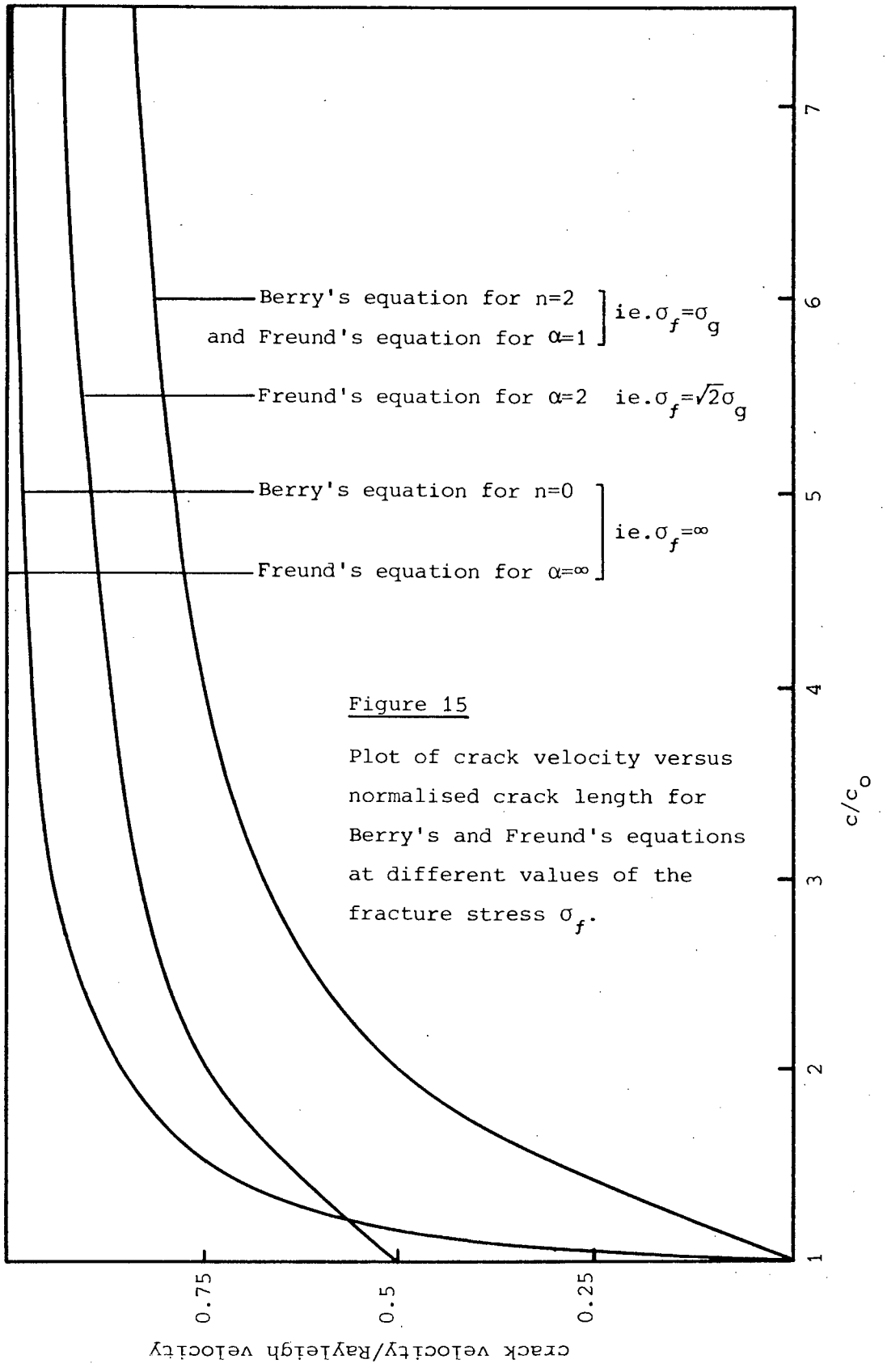

Figure 15

Plot of crack velocity versus normalised crack length for Berry's and Freund's equations at different values of the fracture stress σ_f.

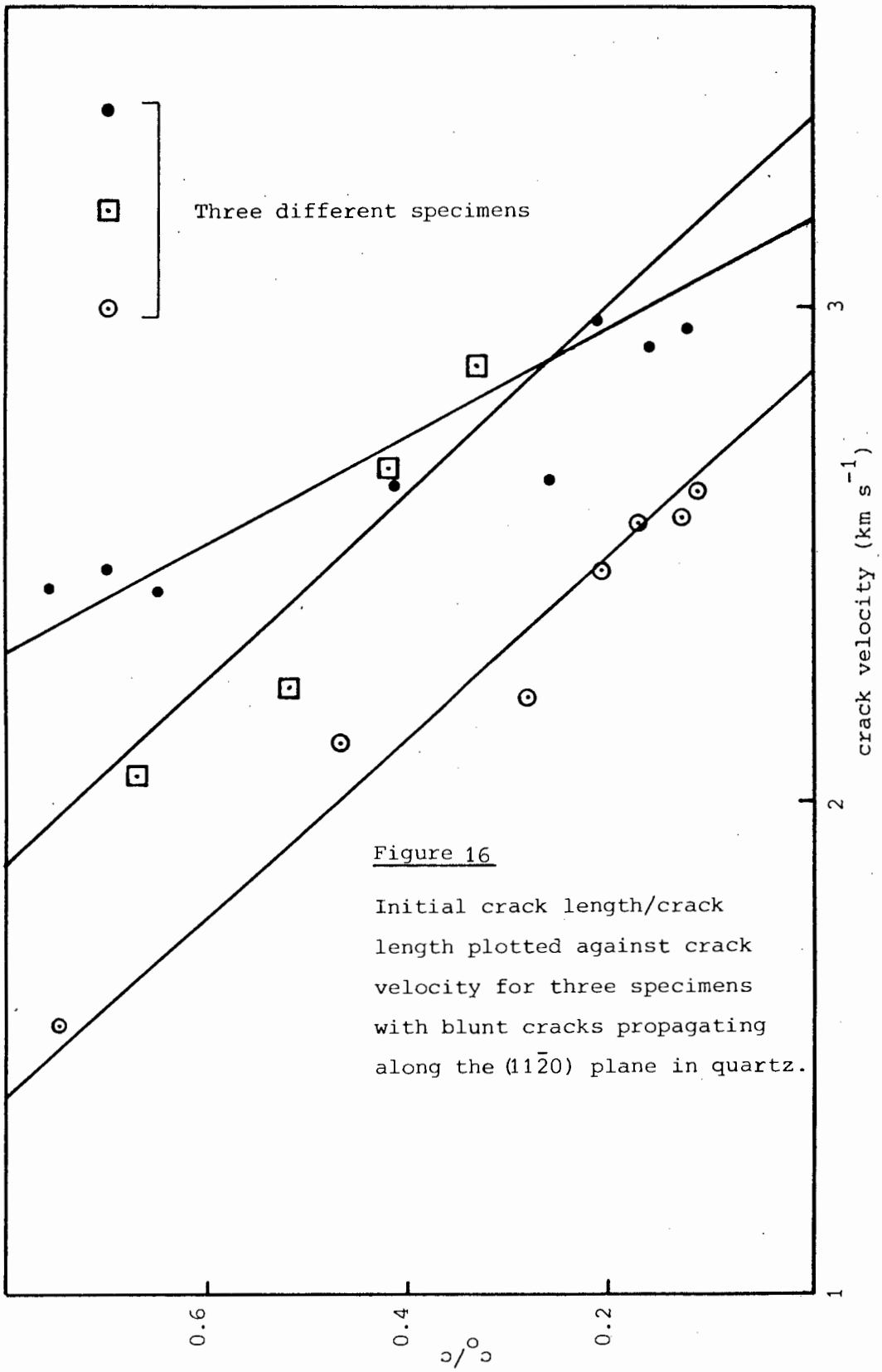

Figure 16

Initial crack length/crack length plotted against crack velocity for three specimens with blunt cracks propagating along the $(11\bar{2}0)$ plane in quartz.

β	α
1.6	2.3
1.8	2.9
3.0	4.2

Within experimental error the maximum velocity v_{max} for these specimens is the same and has the value 3.15 ± 0.25 kms^{-1}. The measured velocity of Rayleigh waves on the fracture plane in the crack propagation direction has the value 3.25 kms^{-1} (Voltmer et al, 1968).

4.4.2.2 Sharp cracks

Values of the Griffith stress for sharp cracks were obtained from the formula

$$\sigma_g^2 = \frac{2E\gamma}{Y^2 c_o} \qquad (22)$$

where E is the value of Young's modulus in the direction of the tensile stress and Y is the geometric parameter given by equation (3). The true surface energy γ for the $(11\bar{2}0)$ plane was evaluated in the same manner as

described in Appendix D for the $(1\bar{1}00)$ plane. From the results of section 3.3 it is believed that equation (22) will give a good estimate of the Griffith stress.

It was found that for sharp cracks, the fracture stress was often lower than the Griffith stress calculated for the initial crack length, since the specimens were tested in air and consequently environmentally activated crack growth probably occured. The velocity behaviour of the crack under these conditions may be expected to qualitatively be described by an equation similar to equation (11) for a Griffith crack except that the crack velocity will reach the same percentage of the maximum velocity at a greater value of c/c_o because the strain energy in the body is lower since $\sigma_f < \sigma_g$. However, once the crack enters the rapid stage of propagation, the crack tip will be moving faster than the gaseous diffusion rate and consequently we may apply equation (20) in this region but now require $\alpha < 1$. A plot of c_o/c against v for a specimen with $\alpha < 1$ is shown in fig.17 indicating a linear relationship in agreement with equation (21). The values for β and the maximum velocity obtained form the graph of three specimens is given in the table below and these values are compared to the Rayleigh velocity and the calculated values of α.

β (from graph)	v_{max} (from graph)	v_s	α (from calculation)
0.63	3.0 kms^{-1}	3.25 kms^{-1}	0.75
0.24	2.75 kms^{-1}	" "	0.20
0.06	3.32 kms^{-1}	" "	0.08

Figure 17

Plot of initial crack length/crack length against velocity for a sharp crack along the $(11\bar{2}0)$ plane in quartz.

This excellent agreement indicates that at high velocities these cracks obey the modified Freund equation.

For large values of c/c_o Berry's equation may be approximated as follows. From equation (12) we have

$$v^2 = v_m^2 (1 - n\frac{c_o}{c} + (n-1)(\frac{c_o}{c})^2)$$

and as $c_o/c << 1$ we may ignore terms higher than $O(\frac{c_o}{c})$.

Hence $v = v_m(1 - \frac{nc_o}{2c})$.

Since $\frac{n}{2} \equiv \frac{1}{\alpha}$, this equation is the same as Freund's equation if we can accept that $v_m = v_s$.

4.5 Conclusion

It has been demonstrated experimentally that cracks in quartz attain a high maximum velocity ($3kms^{-1}$) which is close to the Rayleigh wave velocity ($3.25kms^{-1}$). Freund's theory has been modified to take into account the geometry of the crack tip and experimental results indicate an excellent agreement with this modified theory for the case of a blunt notch and also for the fast fracture stage of a crack which initially propagated under stress corrosion conditions. At the start of

fracture and at low crack velocities there is a fundamental difference between Berry's and Freund's equations, but at high velocities it has been found that they are very similar if it is assumed that $v_m = v_s$ for Berry's equation. The agreement between the observed crack velocity behaviour and theory has been made on the assumption of constant fracture surface energy. Hence any increase in fracture surface energy during propagation (eg. from a temperature rise during fracture) can be discounted in the case of quartz.

5. FRACTOGRAPHY OF QUARTZ AND COMPARISONS WITH OTHER MATERIALS

5.1 Introduction

Glass rods broken in tension usually display three regions of fracture surface morphology. The first is called the 'mirror' region where the surface is optically smooth and corresponds to the first phase of crack growth. The second is called the 'mist' region and has a rough appearance. After the 'mist' region branching occurs and the surface is said to have a 'hackle' appearance. This division of fracture surface morphology into three distinct zones is usually displayed by most brittle materials. In addition, there exists a quantitative result for both brittle and semi-brittle materials regarding the starting point of the 'mist' or 'hackle' region. This result is usually stated in the form that

$$\sigma_f c_m^{\frac{1}{2}} = \text{constant or } \sigma_f c_b^{\frac{1}{2}} = \text{constant}$$

for a particular material and for a particular set of loading conditions (eg. Kirchner et al, 1976), where c_m is the crack length at the start of the 'mist' and c_b is the crack length at the onset of branching.

The phenomenon of crack branching has been recognised for some time, but practical control of

materials to either inhibit or enhance crack branching has only recently been attempted. The control of particle size and shape of shattered safety glass is of great practical importance and represents an instance where the direction and magnitude of crack branching is controlled by altering the stress distribution in the surface layers of the glass. In mining, crack branching in the extraction of rock by means of rock cutters or blasting is very important as this will determine the size of the particles removed (which may be later comminuted) and also the extent to which the remaining unmined surfaces are fissured. For instance, in tunnelling smooth walls should be produced, whereas in some mining operations the presence of cracks will act as sites for further propagation and will assist in the removal of rock.

A number of theories have been proposed to explain the onset of crack branching. The first of these was proposed by Yoffe (1951), where she found that at a critical crack velocity (for a propagating tensile crack in an infinite medium), the cleavage stress $\sigma_{\theta\theta}$ was greater on an inclined plane away from the existing crack plane at $\theta=0$. This stress could then cause the crack to deviate from its original path, and since the maximum in $\sigma_{\theta\theta}$ is equally inclined on both sides of the crack, the crack could bifurcate. While it was discovered that cracks do indeed attain a high velocity in brittle materials it was found experimentally, for instance, in normal commercial glasses that crack branching occured at about $0,5v_s$ whereas Yoffe's theory predicted a value of

about $0,7v_s$. This led other investigators to search for a new criterion for crack branching which did not depend on crack velocity. Clark and Irwin (1966) have proposed that a critical stress intensity factor could be used as a criterion, but in their analysis velocity effects could not properly be taken into account. Congleton and Petch (1967) have also attempted to formulate a criterion for crack branching in terms of stress intensity factors. They have calculated a static stress intensity factor for branching under the condition that an 'advance' crack nucleates ahead of the main crack and is propagated before the main crack reaches it. This method does not take velocity into consideration and moreover it can only predict a lower limit for the value of $\sigma_f c_b^{\frac{1}{2}}$. Johnson and Holloway (1966) have attempted to determine the onset of crack bifurcation by suggesting that a crack will bifurcate when the strain energy released by the crack is sufficient to create four new surfaces. By considering the motion of the crack to be given by the quasi-static model (Mott, 1948), they found a value of $\sigma_f c_b^{\frac{1}{2}}$ in terms of the maximum observed fracture velocity. The results of this approach are inconclusive (Kirchner et al (1976)). We will now examine Yoffe's theory in greater detail than has been done previously and also take into account the elastic properties of the material in which the crack propagates.

It can be shown (Rice, 1968) that the angular variation of the cleavage stress $\sigma_{\theta\theta}$ for a propagating

mode 1 crack under arbitrary loading is the same as the angular variation of $\sigma_{\theta\theta}$ for a crack of constant length in Yoffe's problem. The stresses, a small distance r from the crack tip for an arbitrary propagating mode 1 crack are given in terms of Poisson's ratio ν and crack velocity v as :-

$$\sigma_{\theta\theta} = \sigma_{xx}\sin^2\theta+\sigma_{yy}\cos^2\theta-2\sigma_{xy}\sin\theta\cos\theta$$

$$\sigma_{xx} = \frac{3}{4}\mu A\{(1+2\alpha^2{}_d-\alpha^2{}_s)\frac{\cos(\theta_d/2)}{r^{\frac{1}{2}}_d} - \frac{4\alpha_s\alpha_d}{1+\alpha^2{}_s}\frac{\cos(\theta_s/2)}{r^{\frac{1}{2}}_s}\}$$

$$\sigma_{xy} = \frac{6}{4}\mu A\alpha_d\{\frac{\sin(\theta_d/2)}{r^{\frac{1}{2}}_d} - \frac{\sin(\theta_s/2)}{r^{\frac{1}{2}}_s}\}$$

$$\sigma_{yy} = \frac{3}{4}\mu A\ \{-(1+\alpha^2{}_s)\frac{\cos(\theta_d/2)}{r^{\frac{1}{2}}_d} + \frac{4\alpha_s\alpha_d}{1+\alpha^2{}_s}\frac{\cos(\theta_s/2)}{r^{\frac{1}{2}}_s}\}$$

where $\alpha^2{}_d = 1 - v^2/v^2{}_\ell$, $\alpha^2{}_s = 1 - v^2/v^2{}_s$, μ is the shear modulus, v_ℓ and v_s are the velocity of longitudinal and shear waves respectively, $v^2{}_\ell/v^2{}_s = 2-2\nu/1-2\nu$,

$r_d = r(\cos^2\theta+\alpha^2{}_d\sin^2\theta)^{\frac{1}{2}}$, $r_s = r(\cos^2\theta+\alpha^2{}_s\sin^2\theta)^{\frac{1}{2}}$,

and θ is the angle of inclination to the fracture plane.

'A' is a spatial constant and may be related to the dynamic stress intensity factor K_v by :

$$K_v = \frac{3}{4}\mu \{ \frac{4\alpha_s\alpha_d - (1+\alpha^2{}_s)^2}{1 + \alpha^2} \} A$$

As already noted, the maximum value of $\sigma_{\theta\theta}$ changes its position from $\theta=0$ to larger angles with increasing velocity. The critical value of the velocity at which this will take place is given by the fact that

$\left.\frac{\partial^2\sigma_{\theta\theta}}{\partial\theta^2}\right]_{\theta=0}$ becomes zero at this velocity. This critical velocity is shown as a function of ν in fig.18.
It should be noted that as a body tends to a liquid i.e. as $\nu\to\frac{1}{2}$ the critical velocity increases.

For a fixed ν, once the critical velocity is exceeded, the maximum of $\sigma_{\theta\theta}$ moves continuously away from $\theta=0$ to a value of θ_{max} at the Rayleigh velocity (at this stage $\sigma_{\theta\theta}\Big]_{\theta=0} = 0$). The value θ_{max} is rather insensitive to ν as it only varies from 75^0 to 76^0 for $\nu=0$ to $\nu=\frac{1}{2}$.

Because the result $\sigma_f c_b^{\frac{1}{2}}$ = constant is also true for semi-brittle materials, we should examine the case of a small plastic zone around the tip of a propagating

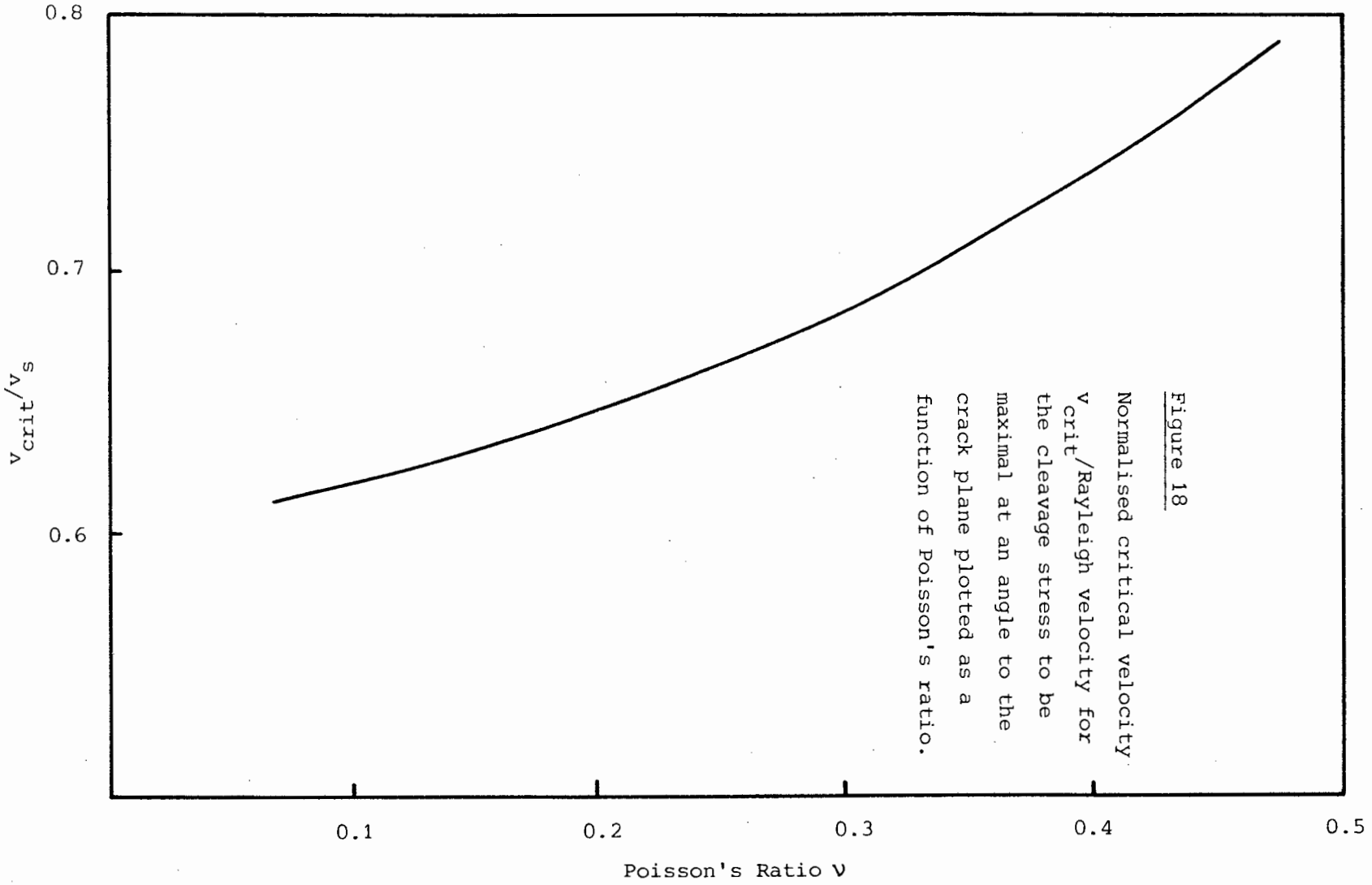

Figure 18

Normalised critical velocity v_{crit}/Rayleigh velocity for the cleavage stress to be maximal at an angle to the crack plane plotted as a function of Poisson's ratio.

crack, as this might explain the non-ideal behaviour of cracks in materials which are regarded as being brittle. It should be noted that the rise in temperature observed during fast fracture would promote plastic behaviour. Broberg (1972) obtained a solution for a crack propagating in an elastic-plastic material by considering the crack as propagating in a layer of elastic material with properties differing from that of the bulk elastic material. The elastic properties of the layer are such that the velocity of longitudinal waves in the layer is smaller than the velocity of transverse waves in the bulk material. Also, the crack is supposed to travel at a velocity greater than the velocity of longitudinal waves in the layer but below the velocity of transverse waves in the bulk material. This model may be severely criticised because of its oversimplification of plastic effects, but it does provide some interesting results. The first of these is that in the case where the layer is very 'thin', the stresses reduce to the elastic case. The second is that when the layer is 'thick', there is no singularity in either the stress or strain fields at the crack tip and therefore cracks may be propagated ahead of the crack tip. The third effect occurs at high velocities when the stress distribution will change in such a way that the maximum in $\sigma_{\theta\theta}$ will not occur at $\theta=0$ as in the Yoffe case. The fourth is that the equation of motion, while being different to Freund's (see section 4.1), still predicts a maximum crack velocity of v_s.

The extreme brittleness of quartz suggests that

it could be used as a basis for the understanding of crack branching in comparison to other materials. Furthermore, because of the practical significance of quartz as mentioned previously an investigation into the crack branching behaviour of this material should be undertaken in its own right.

5.2 Experimental methods

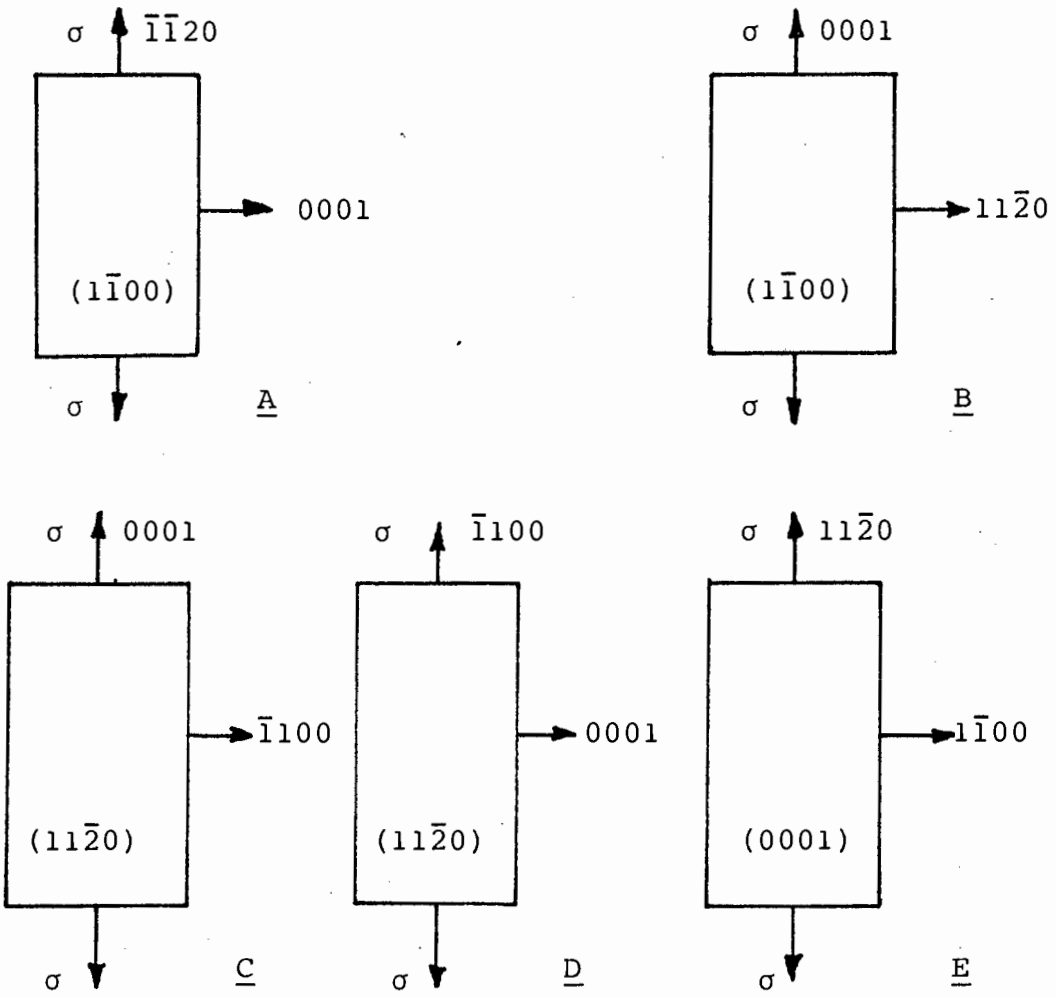

Crystals of orientation A, B, C and D were notched and tested in air as described for specimens of orientation E in section 4.2 . Measurements from the edge of the crystals to the crack branching distance were made by either measuring a 100X micrograph or by using the vernier on an optical microscope stage. After fracture, one of the matching pieces of each crystal was etched for 2 minutes in 40 per cent hydrofluoric acid in order to enlarge and therefore to detect if any stopped cracks occured before the main branching event; both matching pieces were then examined in the scanning electron microscope.

5.3 Experimental results

Fig.19 shows a graph of the fracture stress σ_f plotted against $c_b^{\frac{1}{2}}$ where c_b is the distance from the edge of the crystal to the branching point for the given conditions. The values are for the four different orientations and it can be seen that the product $\sigma_f c_b^{\frac{1}{2}}$ is constant and within experimental error has the same value for the four orientations.

Unlike glass, the fracture surface morphology does not simply become rough in the 'mist' region, but reflects the crystalline nature of quartz. The initial region of crack propagation is optically smooth as in glass but subsequently small zig-zag steps appear and

Figure 19
Values of fracture stress σ_f plotted against crack branching distance c_b for 4 different quartz specimen orientations.
Slope = $\sigma_f c_b^{\frac{1}{2}}$ = 1.64MPam$^{\frac{1}{2}}$
Orientation
A - A
B - B
C - C
D - D
σ_f MPa
40
30
20
10
$c_b^{-\frac{1}{2}}$ m$^{-\frac{1}{2}}$
5
10
15
20
25

grow in length before branching occurs as shown in plates 5 and 8 (These steps have been identified as the rhombohedral planes (Ball and Payne, 1976)). In the case of glass, etching with hydrofluoric acid has revealed the presence of microcracks beneath the surface in the 'mist' region (Johnson and Holloway, 1968). However, etching of quartz and examination in the scanning electron microscope did not reveal any such microcracks in the zig-zag region and hence if these were present, they were presumably of shorter extent than those found in glass.

Velocity guages were placed on specimens of orientations A, B, C and D, and even though the piezoelectric effect distorted the signals from the guages, the total time for a crack to traverse a guage could be measured. From these results estimates were made for the crack velocity at branching and these varied from 0,7 to 0,9v_s. The fractography of crystals of orientation E has been described in section 4.3.

5.4 Discussion

Table 1 contains crack branching data relating to crystalline and amorphous materials which vary from highly brittle to semi-brittle. In section 5.4.1 an explanation of the onset of crack branching and the subsequent behaviour of the cracks will be attempted in terms of the theories presented in the introduction

and previous sections and the crack branching behaviour of quartz is compared to that of the other materials. In section 5.4.2 criteria for crack branching in brittle and semi-brittle materials are presented.

5.4.1 We shall initially consider isotropic materials for which some theoretical results on propagating cracks are known and then, after modification, apply them to crystalline materials.

We may predict from Yoffe's result that in an ideally brittle material which is both elastically isotropic and isotropic with respect to the surface energy on various planes, crack branching can occur once the crack velocity exceeds the critical velocity for the material, but the branching angles should not be greater than 75^0 with respect to the line of the crack. Because the maximum in $\sigma_{\theta\theta}$ is rather flat near the critical velocity, it is expected that in real materials crack branching will only occur at velocities rather greater than those shown in fig.18 when the maximum is better defined. A material taken from table 1 which best approximates the conditions of isotropy and is highly brittle is silica glass. It can be seen from columns 5 and 6 of this table that cracks in silica do indeed only branch when the crack velocity is greater than the critical velocity. It should be noted at this point that when bifurcation occurs the fracture velocity has been observed to decrease only a few per cent and

Material	$\sigma_f c_b^{\frac{1}{2}}$ MPa $m^{\frac{1}{2}}$	Average E GPa	γ_{f_0} Jm^{-2}	Average ν	Experimental v_{max}/v_s	Yoffe v_{crit}/v_s	Freund v_{crit}/v_s	K_{vc}/K_c
Quartz	1.64	100	3	0.25	0.7→0.95	0.68	0.99	1.5
Sapphire	7.3	400	2	0.24	0.71→0.8	0.68	0.99	3.5
MgO	4.3	300	1.5	0.23	-	0.67	0.99	-
Si	5.8	182	2.5	0.32	0.81	0.72	0.96	3.6
Soda lime glass	2.04	70	4	0.28	0.51	0.70	0.97	3.3
PMMA	8.5	4	400	0.40	0.68	0.75	0.99	3.5
Flint glass	2.0	78	3.9	0.22	0.5	0.66	0.96	3.2
Silica	2.3	73	2	0.17	0.68	0.65	0.98	3.4
Cr	4.5	270	2.9	0.2	-	0.65	0.98	-
W	-	362	6.3(20^0K)	0.28	> 0.9	0.70	(≃0.96)	-

Table 1. (values measured at 20^0C)

thereafter to remain almost constant (Field, 1971), so that the measured values of maximum velocities in table 1 should be interpreted as being approximately equal to the crack branching velocities.

We may extend this model to include cases where a material in elastically isotropic, but not isotropic with respect to its surface energies. We may expect that if the crack was initially propagating along a plane of low surface energy as is the usual situation, it would only move to one of higher surface energy if the cleavage stress were much greater on that plane. Hence we would expect branching to occur at a velocity much closer to v_s than for isotropic materials. From table 1 tungsten (when fractured along the (100) plane) best suits the description and one finds that the maximum velocity is very close to v_s.

If the material is anisotropic in its surface energies and elastically anisotropic then two interactive effects are expected. The first is that the crack would not want to deviate from a low surface energy fracture plane as discussed above, and the second is that the dynamic stress field may be more or less favourable in promoting a deviaition of the crack from its plane than in the isotropic case. Three materials having these properties are given in table 1 viz. quartz, sapphire and silicon. In each case the maximum velocity exceeds that predicted by Yoffe's analysis. In the case of quartz it has been shown in section 3.4 that the elastic stress field around the crack tip is

very similar to the isotropic field. Hence there should not be too great a deviation from the isotropic stress field for a crack travelling in a specimen of this orientation and the only anisotropic effect to be considered is that of the anisotropy of surface energy. The ease of cleavage in quartz has been experimentally established to follow the following order (Bloss and Gibbs, 1963) :-

Order of Cleavage	Cleavage plane	
1	$(10\bar{1}1)$	Positive rhombohedron
2	$(01\bar{1}1)$	Negative rhombohedron
3	$(11\bar{2}2)$	Second order trigonal pyramid
4	(0001)	Basal pinacoid
4	$(11\bar{2}1)$	Second order trigonal dipyramid
4	$(10\bar{1}0)$	Unit prism
5	$(11\bar{2}0)$	Second order prism

For the case of a specimen of Orientation E, none of the easy cleavage planes (i.e. order 1 to 4) is perpendicular to the (0001) plane of the crystal face and at a suitable angle to the $(11\bar{2}0)$ fracture plane along which the crack could branch. We should therefore expect a crack in this specimen to behave in a similar manner to a crack in tungsten. This is in fact the case and as mentioned in section 5.3 , the crack reached a velocity of $0,92v_s$ before any attempt at branching occured and when this did begin, cleavage steps parallel to the rather inaccessible, but low surface energy rhombohedral planes occurred. In the

other orientations of quartz and for sapphire and silicon the above two anisotropic effects cannot be separated, but it is clear that these anisotropies contribute to a high crack branching velocity.

In semi-brittle materials such as PMMA, the crack branching velocity is lower than that predicted by Yoffe's equation and consequently it would appear that the above analysis is not directly applicable to them. If we assume that in these materials a small plastic zone accompanies the crack tip, then we may apply the results of Broberg's (1972) analysis to them. In terms of this model the subsurface cracking observed in these materials may be explained by the fact that there is no singularity in the stress or strain fields at the crack tip, and therefore cracks may be initiated in a plane adjacent to the crack plane. The direction of the cleavage stress during propagation will be inclined to the plane of the crack as in Yoffe's case, but the critical velocity at which this occurs will be different (and presumably lower if this is to be consistent with observation).

5.4.2 The fracture surface greatly increases in roughness in the region between the onset of surface roughening and crack branching. This may be explained by recognising that an instability has set in and that as the crack grows it becomes more unstable until branching occurs. Of course, once the crack has deviated from a plane, Yoffe's solution no longer

applies in the immediate vicinity of the crack tip, but if the roughening is not severe, we may estimate an average stress field. In fact, if the average stress field is assumed to be the same as the original solution, then we may propose an equation which will predict that $\sigma_f c_b^{\frac{1}{2}}$ is a constant for the material under given conditions. If we develop the picture of the 'mist' region as consisting of a growing instability, then we ought to expect that branching will occur at a critical velocity. Using Freund's equation (15) and letting $G = 2\gamma_f$ we obtain the equation :

$$\frac{k^2{}_s(c_b)F(v_c)}{E} = 2\gamma_f \qquad (23)$$

where v_c is the critical velocity. Writing $K^2{}_s(c_b)$ in terms of the fracture stress and geometric parameter Y, we obtain :-

$$\sigma^2{}_f c_b = 2E\gamma_f / F(v_c) Y^2 \qquad (24)$$

Hence if fracture is to occur at this critical velocity then $\sigma_f c_b^{\frac{1}{2}}$ will be a constant for the material if γ_f is constant or a function of velocity only. If we insert the experimental values of $\sigma_f c_b^{\frac{1}{2}}$ into equation (24) and use the static value of γ_f we arrive at a set of critical velocities for crack branching as shown in table 1, column 7 (assuming that $F(v) = 1-v/v_s$ and $Y = 2$, see section 4.4). It can be seen that for the materials

already discussed, the only occasion when the experimental velocities approximate the ones derived from equation (24) occur when oscillations off the fracture plane are prevented because of surface energy anisotropy viz. quartz orientation E and tungsten. We may suppose that, because of the increased area in the 'mist' region and because energy may be dissipated in the form of plastic work as the crack velocity increases, the effective surface energy is greater than the static surface energy. An examination of equation (24) will show that the critical velocity will be decreasedin this case.

Another approach to the problem is to follow the method of Clark and Irwin, and specify that the dynamic stress intensity factor attains a critical value for branching to occur. The work of Freund has given the velocity dependance of the dynamic stress intensity factor explicitly for mode 1 cracks and from equation (15) and setting $G = 2\gamma_f$, we obtain the result

$$K_v = \sqrt{\frac{2E\gamma_f}{B(v)}} \qquad (25)$$

A graph of K_v/K_c for constant γ_f against velocity is shown in fig.20, where $K_c = \sqrt{2E\gamma_{f0}}$ and γ_{f0} is the fracture surface energy at zero velocity. It can be observed from this graph that K_v is still within 90 per cent of its static value up to half v_s. If γ_f were to increase with velocity, then for an increase of 24 per cent of γ_f above its static value, K_v will exceed its static value at a velocity of half v_s.

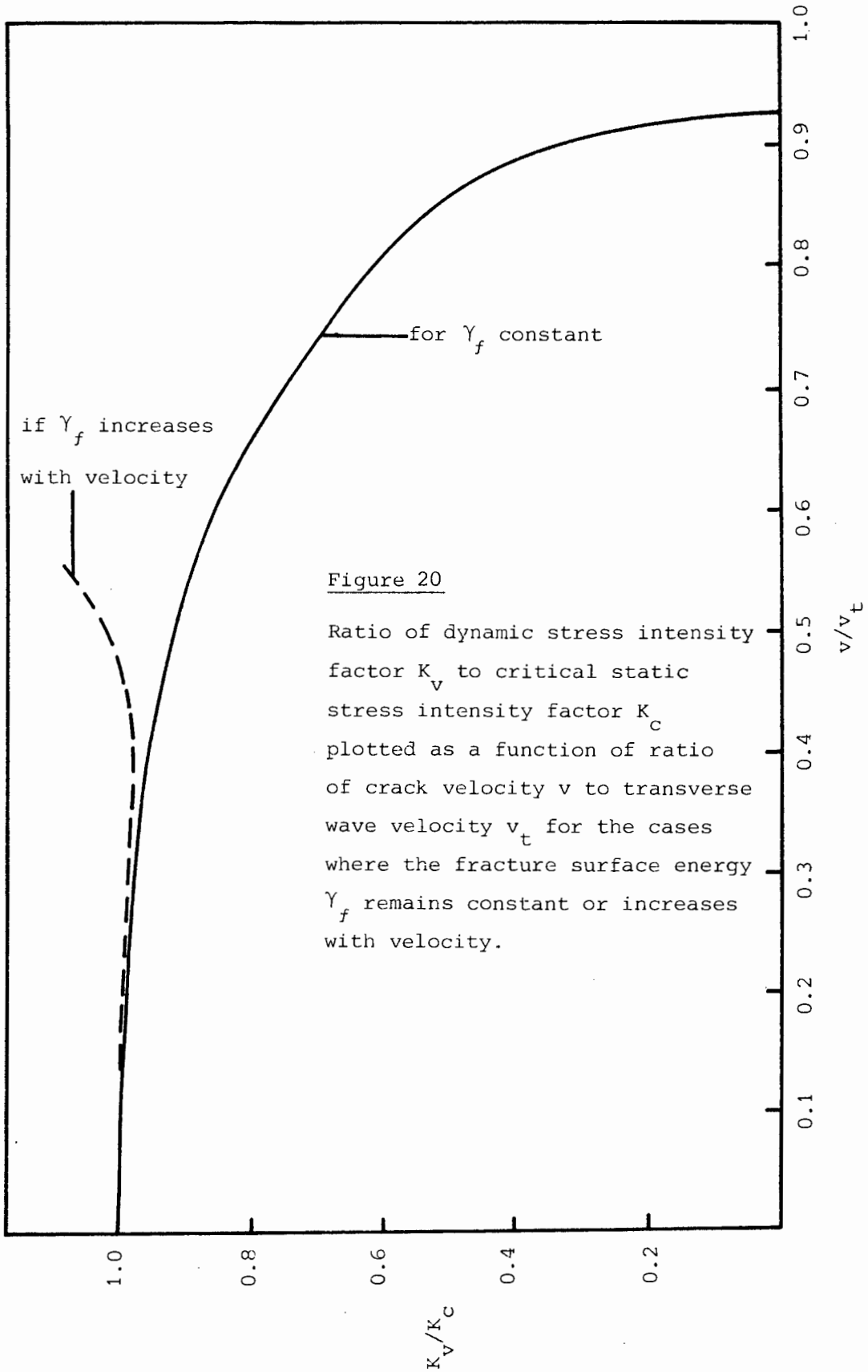

Figure 20

Ratio of dynamic stress intensity factor K_v to critical static stress intensity factor K_c plotted as a function of ratio of crack velocity v to transverse wave velocity v_t for the cases where the fracture surface energy γ_f remains constant or increases with velocity.

If we postulate that branching will occur when the dynamic stress intensity factor reaches a critical value K_{vc} above K_c then from equation (24) and (25) :

$$\frac{K_{vc}}{K_c} = \frac{k(v_c) Y \sigma_f c_b^{\frac{1}{2}}}{\sqrt{2E\gamma_{f0}}} \qquad (26)$$

Some values of K_{vc}/K_c derived from equation (26) are shown in table 1. From equation (15) we have :-

$$\frac{K_{vc}}{K_c} = \sqrt{\frac{\gamma_f}{\gamma_{f0} B(v)}}$$

so that K_{vc}/K_c takes into account both velocity and surface energy. With the exception of quartz, the values of K_{vc}/K_c for the brittle and semi-brittle materials listed in table 1 is approximately the same (3,2 to 3,6). This remarkable fact indicates that if the increase in fracture surface energy and velocity are both taken into account a single criterion might be used to predict the onset of crack branching. The fact that quartz does not fit into the pattern may be related to the unusual fractography observed in this material.

5.5. Conclusion

It has been shown that for highly brittle materials including quartz, Yoffe's result is appropriate

for establishing the onset of fracture surface roughening. Once this roughening has established itself, it increases in magnitude and the dynamic value of γ_f increases until a critical velocity or stress intensity is attained and branching ensues. This increase in γ_f may be attributed to surface roughening and a plastic dissipative process caused by the heat generated by the running crack. The behaviour of quartz is similar to that of other highly brittle materials and its fractography can be explained in terms of differences in the surface energies of its various planes.

In the case of non-ideally brittle materials such as glass and PMMA, Broberg's model can be used to establish a reason for surface roughening at velocities below that predicted by Yoffe's equation and also to explain the existence of subsurface cracking in these materials.

6. TRANSMISSION ELECTRON MICROSCOPY OF THE DAMAGE PRODUCED BY INDENTATION AND POLISHING ON QUARTZ

6.1 Introduction

There is a great interest in replacing the traditional drill-and-blast techniques of mining and excavation through hard rocks by rock tunnelling and cutting machines. As these new techniques are more efficient in selective mining operations, do not cause large quantities of dust and increase the safety of mining in deep gold mines, they are highly desirable. These techniques are at present the subject of extensive engineering research, but there is a sparsity of knowledge about the physical behaviour of brittle rock when cut by hard tools such as tungsten carbide or diamond and the optimisation of cutting conditions could result from such knowledge. Quartz is a very attractive and almost ideal material to study for this purpose not only from the scientific viewpoint, but also from commercial considerations as many hard rocks contain quartz, and gold is extracted from quartzites.

Laboratory experiments were therefore designed to study in microscale the action of a cutting tool (in this case a diamond stylus) on the surface of a single crystal of quartz. Two electron microscopy experiments were performed in which the nature of the

damage zone under such a stylus was simulated in the static case by a Vickers hardness indenter and in the dynamic case by small diamond polishing particles. Similar transmission electron microscopy studies in other brittle materials such as alumina, silicon and silicon carbide at 25^{0}C (Hockey 1971, Eremenko and Niketenko 1972, Hill and Rowcliffe 1974, Hockey and Lawn, 1975) have revealed that plastic deformation has taken place by the generation of twins and many dislocations. The generation of twins and dislocations has two important effects. Firstly, they absorb energy during the sliding of the stylus which would increase the coefficient of friction and would also inhibit the propagation of cracks. Secondly, it has been shown that indentation of certain brittle materials in various active environments can cause the promotion or retardation of dislocation motion (Westwood, 1974) which will effect the rate of cutting in these materials.

At atmospheric pressure, synthetic quartz will only deform plastically in uniaxial compression at temperatures above 550^{0}C (Baëta and Ashbee, 1970), but if the crystal is tested at a confining pressure of 10 - 15 kbars, fracture is prevented and plastic deformation will occur at a temperature as low as 300^{0}C (McLaren and Retchford, 1969). As the large shear stresses and confining pressures underneath a hardness indenter are of the order of tens of kbars (Brace, 1963) it is likely that plastic flow will occur in preference to fracture and dislocations and twins may develop in

quartz as in other brittle materials. Brace has observed that the surface beneath a Knoop indenter on quartz contains facets of rhombohedral planes and he has suggested that microcracking has accompanied deformation.

6.2 Experimental methods

6.2.1 Specimen preparation for indentation and electron microscopy

Slices of synthetic quartz 0.5mm thick with faces parallel to $(10\bar{1}0)$ were glued to a brass disc with 'lakeside' resin and were ground successively with 320,400 and 600 silicon carbide grit on a cast iron disc, ensuring that the damage introduced by each preceeding treatment was fully removed. These slices were then ground on a glass plate with 0.3μm alumina powder in distilled water and when examined in an optical microscope the surface was found to be covered with a random array of pits about 10μm in diameter. Polishing of these slices was performed on a vibratory polisher (Buehler 'Vibromet') on a paper cloth with a slurry of 0.3μm alumina in distilled water. The subsequent surface had a 'mirror' finish and no surface defects could be resolved even when examined at the highest magnification in an optical microscope. The crystals were cut into 4mm squares and etched for one hour in a five per cent hydrofluoric acid solution in order to remove any

surface damage. A square array of sixteen indentations 200μm apart were made on these 4mm squares with a Vickers microhardness indenter of a Reichert microscope at a load of 100g which took about 20 seconds to apply. The samples were glued to a glass slide with 'lakeside' and were prepared for subsequent ion beam thinning (for examination in the electron microscope) by grinding the side opposite the indentations with two grades of silicon carbide grit (400 & 600). The 400 grit was used to reduce the specimen thickness to 150μm and the 600 grit reduced the thickness to 60μm. The samples were finally ground with 0.3μm alumina in distilled water on a glass plate to a thickness of 30μm. The final thickness being determined by the interference colour of the quartz as observed through crossed polaroids. The sample was then mounted on a copper grid with 'Seccotine' adhesive and the parts of the sample projecting over the edge of the grid were cut away with a scalpel. Thinning was performed on the side opposite the indentation using an 'Ion Tech' ion beam thinner operating at 6kV and at a sputtering rate of about $5\mu m\,h^{-1}$. Some specimens were annealed at 800^0C for 12 hours prior to thinning and the rate of heating and cooling through the $\alpha \rightleftharpoons \beta$ transition was set at 1^0C per min. The specimens were coated with carbon and sometimes with carbon and a gold-palladium alloy by vacuum evaporation in order to prevent charging during examination in a Phillips EM300 transmission electron microscope operating at 100kV.

Electron beam induced damage in quartz is very rapid and at normal intensities a specimen may only be observed in the T.E.M. for a few minutes before it vitrifies. Consequently the specimens were observed at low beam intensities and examined as quickly as possible.

6.2.2 Specimen preparation for the examination of the effects of a diamond polish

Synthetic quartz crystals with faces parallel to $(11\bar{2}0)$ were ground to a 600 grit silicon carbide finish and then polished with 6μm diamond paste. A number of visible scratches remained on the surface after polishing, but no attempt was made to remove them. Some specimens were also etched as described in section 6.2.1 and all the specimens were also thinned and examined as described in section 6.2.1.

6.3 Experimental results

In order to explain some of the features observed in the transmission electron microscope, calculations of the extinction distances for a number of low order reciprocal lattice vectors was made. The extinction distance is defined relativistically as :-

$$\xi_g = \frac{\pi V_c \cos\theta}{\lambda |F_g|} \qquad \text{(Hirsch et al, 1965)}$$

where V_c is the volume of the unit cell, λ is the relativistic wavelength of the electrons, $\sin\theta = \lambda/2d_{hk\ell}$ where $d_{hk\ell}$ is the interplanar spacing, F_g is the structure factor for the reciprocal lattice vector $\underline{g}$ and is given by :-

$$F_{hk\ell} = \sum_i f_i(\theta)\exp\{-2\pi i(hu_i+kv_i+\ell w_i)\}$$

where u_i, v_i and w_i are the fractional coordinates of atom i in the unit cell and $f_i(\theta)$ is the atomic scatteirng factor for atom i. Smith and Burge (1962) have given an analytical representation of the atomic scattering factors for silicon and oxygen as a function of θ by fitting a polynomial to values of these factors calculated by other authors at particular values of θ. The fractional coordinates of the atoms in the unit cell were obtained from Frondel (1962). The following values were obtained for ξ_g for 100kV electrons.

Reflection	Extinction distance (nm)
$\{10\bar{1}0\}$	153
$\{10\bar{1}1\}$	68 or 105
$\{10\bar{1}2\}$	176 or 375
$\{11\bar{2}0\}$	172
$\{11\bar{2}2\}$	152
{0003}	953

The relatively large extinction distances occuring in

quartz arise because of the low atomic scattering factor of oxygen.

Because of the short lifetime for observations in these specimens there was insufficient time to obtain two beam conditions and the photographs presented were generally obtained under multiple beam conditions. If the deviation parameter s of the operating reciprocal lattice vector from the Ewald sphere is approximately zero then a dislocation will have a width of about $\xi_g/3$. For low order reflections and $s \simeq 0$ dislocation images in quartz should have widths from about 20nm to 100nm. If s is large then the images will be smaller but will lack contrast and if multiple beam conditions are operating, single dislocation images will no longer appear. In order to establish the type of the defect which gave rise to diffraction contrast, the specimens were tilted and the resulting change in contrast noted and those features which were identified as dislocations had image widths which varied from 15nm to 150nm according to the particular imaging conditions.

6.3.1 Indented samples

It can be seen in the typical indentation shown in plate 9 that the indenter profile is preserved and that cracking has occured at the sharp corners of the indentation. It was found that carefully taken diffraction patterns of undeformed areas of the crystal away

from the indentation yielded patterns which showed that radiation damage had not yet occured. Hence the carefully taken diffraction pattern shown in plate 10 of the central area of an indentation similar to the one shown in plate 9 is considered to reflect the true state of the material at the base of the indentation. The tendency for the diffraction spots to be broadened suggests that there is a large amount of strain present in the material and that misorientation of the material probably arises from microcracking. In regions where the material was sufficiently thin around the hardness indentation, there was only a small density of defects as shown in a typical area in plate 11. Besides the linear polishing scratches observed in the plate there are features at A and B which show diffraction contrast and are shown at a higher magnification in plates 12 and 13. The white areas at the ends of the lines C in plate 12 were seen to be completely transparent in the original micrograph (i.e. the electrons penetrated the foil at the point without scattering or absorption). Consequently, these must be cracks which are opened at one end and the contrast which arises along the rest of their length is presumably caused by a mismatch between the crack faces after relaxation and closure. (The black dots are caused by radiation damage (Baëta and Ashbee, 1973)). In plate 13 and around another indentation (plate 14) lines XY run to the centre of the indentation. It was not possible to establish the origin of these features, but most of the defects transverse to the lines XY showed systematic contrast changes and the oscillatory features which are

indicative of dislocations. At D in plate 14 a defect showing fringes can be observed. Unfortunately, the way in which the fringes changed in contrast during tilting of the specimen was not observed. However, it would appear that the fringes are associated with a crack in the material as the fringes and boundaries are curved and therefore the feature would not be a twin or a stacking fault. If two crack interfaces do not mate perfectly after fracture, then a displacement of the two faces with respect to each other will give rise to fringes. There are two independent ways in which this can occur. Firstly, the two faces can be separated by a rigid body displacement $\underline{c}$ measured from one interface to the other. This will give rise to a set of fringes with loci given by $\underline{g}\cdot\underline{c} = N$ where N is an integer (Bonse et al, 1969). For example, if the two interfaces are displaced so that $\underline{g}$ is parallel to $\underline{c}$, then for the present case in which there are 7 fringes and for $|\underline{g}| \simeq 1/0.2\text{nm}$, the interfaces would be $\simeq$1.4nm apart. Secondly, a rotated moiré pattern could be generated at an interface by the rotation of one side of the interface with respect to the other. This will produce a small change in the diffraction vector, i.e. $\delta\underline{g} = \underline{g}_1 - \underline{g}_2$ where $|\underline{g}_1| = |\underline{g}_2|$ but $\underline{g}_1$ is not parallel to $\underline{g}_2$, and fringes with a spacing of $1/|\delta\underline{g}|$ will appear (Gevers, 1962). This can be related to the amount of angular rotation θ by the equation $|\underline{g}|/|\delta\underline{g}| \simeq 1/\theta$ for θ small. In the given case the seperation of the lattice planes will be typically $1/|\underline{g}| \simeq 1/0.2\text{nm}$ and

$1/|\delta \underline{g}| \simeq 10nm$ from the photograph, so that $\theta \simeq 2x10^{-2}$rad.

After annealing, a deformation zone such as that shown in plate 15 was observed around the indented area which, from the contrast behaviour and geometries, appeared to consist of dislocations and twins.

6.3.2 Diamond polished specimens

The tracks left by diamond polishing particles on the surface of quartz are accompanied by the generation of dislocations as seen in plate 16. These dislocations, although showing similar contrast to that discussed by Baëta and Ashbee (1973), do not show much oscillatory contrast and consequently it would appear that they lie nearly parallel to the surface of the foil. There is little evidence of dislocation movement away from the main width of the scratch and those that do extend from the line of the scratch usually appear to follow crystallographic directions (see also plate 17). Since hydrofluoric acid attacks the strained material around the dislocations preferentially, further etching of the foil surface removed most dislocations and dislocation sites within the scratches could then be observed by absorption contrast as in plate 18. About ten dislocations per μm were observed for a scratch width of about ½μm (i.e. extent of main

dislocation generation), giving a total dislocation length of about 5μm per μm of scratch length.

When large particles are pulled across the quartz surface dynamic Hertzian cracking occurs and chatter marks remain in the wake of the track produced. Some of these chatter markings are shown in plate 19 and regions in the immediate vicinity of these cracks showed diffraction contrast except where the cracks had fully opened (as arrowed in the plate). The contrast is thought to originate from elastic strain fields which are caused by a mismatch at the crack interfaces when closure and relaxation occur.

6.4 Discussion

The marked difference in the number of dislocations generated when the crystal was indented quasi-statically compared to being scratched dynamically at a speed of about $1ms^{-1}$, can possibly be explained in terms of a high local rise in temperature occuring during scratching as observed in other materials (McPherson, 1973). A locally high temperature and the presence of a large hydrostatic pressure would both favour production of dislocations rather than cracks.

6.5 Conclusion

During the quasi-static indentation of quartz

it has been found that permanent deformation produced by the indenter occurs mainly through cracking, and a high degree of elastic strain is still present underneath the indenter even on its removal. This stress is relieved on annealing by the generation of dislocations and possibly twins. The low density of dislocations or twins generated by the indenter as compared to the other materials mentioned in the introduction is indicative of the highly brittle nature of quartz.

During rapid loading with diamond polishing particles dislocations are generated and this may be explained in terms of a high local rise in temperature.

7. THE DAMAGE PRODUCED BY A SLIDING DIAMOND STYLUS ON THE SURFACE OF QUARTZ

7.1 Introduction

The mechanisms and influences of external variables on the deformation produced during hard rock cutting was investigated by performing a small scale laboratory experiment. Similar laboratory experiments have been carried out by many workers by drilling with rotary drilling bits into granite. However, there are a number of disadvantages in using such an experimental system viz.

(i) the cutting tool only cuts into virgin rock on the first rotation and thereafter debris interferes with the process.

(ii) there are a number of cutting edges of different orientations embedded in a matrix which is subject to continuous wear and only the average properties of the cutting tool can be characterised.

(iii) granite is an inhomogeneous material and hence the form of the damage will vary from grain to grain and will therefore be difficult to assess.

In order to eliminate these adverse effects the present

experiment was performed by linearly translating a diamond stylus of known dimensions over prepared surfaces of single crystals of quartz.

The deformation character is intimately related to the coefficient of friction and measurements of the coefficient of friction and the observation of surface damage in brittle materials have been carried out by a number of investigators (eg. Bowden and Brookes 1966, Bowden and Hanwell 1966). Most measurements have been performed on diamond but the form of the fracture patterns has also been studied for diamond sliding on glass and quartz by Preston (1922) and Graham (1972). Seal (1958) observed that when large loads were applied to a diamond stylus sliding on diamond, Hertzian cracks appeared and the coefficient of friction increased. A similar effect was noted by Bowden and Brookes (1966) for diamond sliding on magnesium oxide. Bowden and Tabor (1964a) could not explain this increase in the coefficient of friction and they discounted the theory that the increase could have been caused by the propagation of Hertzian cracks, since the amount of energy expended in creating the amount of new area per unit length of scratch observed in their experiment, was very small.

If a hard spherical indenter is forced against the flat surface of an elastically isotropic brittle material, a ring crack is formed around the indenter which extends into the material in the form of a cone which follows a principal stress trajectory (i.e. normal to the greatest principal tensile stress) (Frank and Lawn, 1967). However, in the case of materials with

elastic and surface energy anisotropy, the situation is more complicated and the crack pattern may no longer be simple (Lawn, 1968). From observations of Hertzian cracks on quartz, Heavens and Ashbee (1975) found that while the surface crack is almost circular, the cone crack follows easy cleavage planes beneath the surface. The geometry of these cracks will also be changed by differences in elastic modulii of the indenter and surface as frictional forces will come into play (Johnson et al, 1973).

The stress field generated by a sliding spherical indenter with friction was obtained by Hamilton and Goodman (1966) and the critical condition for fracture was deduced by Lawn (1967). The maximum tensile stress now occurs at the trailing edge of the indenter for all values of the coefficient of friction and the crack will again follow principal stress trajectories. Hertzian crack patterns on diamond under sliding loads has been observed by Seal (1958) and these cracks showed a marked tendency to follow easy cleavage planes. Graham (1972) has observed the form of cracking on quartz and glass surfaces using diamonds of radii 0.5mm and 1.0mm. He found that the cracking pattern deviated from the ideal Hertzian pattern especially beneath the surface where cracking extended in an irregular way at a considerable depth below the surface. He also observed that the spacing between the cracks could either increase or decrease with increased sliding speed, depending on the load. Material was supposed to be

removed by a process of intersecting cracks in the track and sometimes large pieces would chip out.

The fracture behaviour of brittle materials in chemically active environments has been the subject of much recent study (Westwood, 1974) and in particular, the fracture of glass and quartz has also received much attention (Macmillan et al 1974, Swain et al, 1973). The controlling factor appears to be that of the zeta potential (ζ) of the material in the liquid environment. A brief definition of the zeta potential is given in Westwood (1974). The above studies have shown that the hardness of brittle materials, including quartz, is maximised when $\zeta \simeq 0$ and that the drilling rate is also maximised when $\zeta \simeq 0$. The drilling rate of a diamond bit in quartz is shown to increase dramatically in environments of heptyl alcohol and undecyl alcohol, and an increase of fourteen-fold can be achieved. A number of mechanisms have been proposed to explain this effect but the most attractive is that of the effects these environments have on dislocation motion. Westwood (1974) has shown that the increased hardness of materials when $\zeta \simeq 0$ is accompanied by a decrease in dislocation motion away from the indented region and has concluded that the polarity of the solid-liquid interface influences the mobility of dislocations. Mills et al (1976) have shown that the energy expended for a given depth of indentation in granite is the same for different liquids, but the amount of cracking is most severe in liquids where the hardness of the granite is a maximum. They have explained

this result by proposing that,in the absence of plastic flow which dissipates elastic strain energy (for liquids where $\zeta \simeq 0$), removal of the load will release the accumulated strain energy in the form of severe cracking.

However, as already mentioned, there are a number of complicating effects in a drilling experiment and in addition to the influence of dislocation motion, there are a number of other possibilities which depend on the polarity of the solid-liquid interface and could give rise to the observed environmental increase in cutting efficiency viz.

(i) The viscosity of the fluid plus debris may inhibit or enhance the rate of debris removal which in turn may interfere with the cutting process, (eg. in milling experiments this is known to have a marked influence on milling efficiency, (Clark and Kitchener, 1968)).

(ii) A static-fatigue mechanism may be operative by reducing the surface energy and as in the case of quartz hydrolytic weakening of the Si-O bond in the presence of water, may occur. However, such static-fatigue cracking is a relatively slow process and may not play a significant role in rapid cutting.

(iii) Surface charging effects on small debris material in certain environments may cause agglomeration

of these particles and interfere with the mechanics of the cutting process as well as changing the cooling properties of the liquid plus debris.

A fourth effect which is unrelated to charging effects, but is very important is the thermal capacity of the fluid which will control the local temperature rise during cutting and hence influence the amount of plastic deformation produced. The plastic blunting of cracks will, in turn, effect the advance of the drill by the inhibition of fracture.

7.2 Experimental methods

Previous experiments on the friction of diamond (Seal, 1958) and of glass (Macmillan et al, 1974) suggested that the experiment should be carried out as a function of the following five variables :

(i) normal load applied to stylus
(ii) speed of sliding
(iii) orientation of the quartz crystal
(iv) surface finish of the quartz crystal
(v) chemical environment

Only those combinations of the above variables which were thought might yield the most information on the nature of the cutting process were investigated.

7.2.1 The testing machine

The testing apparatus is illustrated in plate 45. The sample, mounted on a table which could be rotated through 15^0 intervals, was moved at constant velocity on a carriage which was attached to the base by two linear bearings. A high quality commercial diamond glass-cutter was mounted on a pivoted arm above

the specimen which allowed the cutter to be adjusted to give a maximum score depth with as little side chipping as possible. Forces were applied to the stylus by placing various dead loads centrally on the platform above the diamond cutter. The whole device was mounted on the crosshead of an Instron testing machine and the carriage was pulled along by a stiff cord (a waxed forward and reverse wound cord) which was attached via two pulleys to the load cell of the testing machine. In order to ensure that the geometry of the diamond stylus changed as little as possible during the course of experimentation, a well used (but still sharp) diamond glass-cutter was used in preference to a new one. The geometry of the tip of the diamond was determined by scanning electron microscopy.

7.2.2 Sample preparation and examination techniques

The samples were single crystals of quartz with dimensions 60mm x 12mm x 0.5mm and the scratching was done on the large faces of the crystals. The samples were divided into three groups, each with a different surface finish. The first finish was a 0.3μm alumina polish, the second was obtained by grinding the sample on a glass plate with 0.3μm alumina and the third consisted of polishing with 0.3μm alumina and then etching in 40 per cent hydrofluoric acid for 40 minutes. Great care was taken with samples with the last finish in order to ensure that the surfaces were not damaged before testing.

After a specimen had been scratched it was cut into two sections. Both sections were ultrasonicated in ethanol in order to remove the debris formed during scratching. One of these sections was then etched in 40 per cent hydrofluoric acid for 30 minutes. These specimens were given a coating of approximately 10nm of carbon and approximately 5nm of gold-palladium alloy in a vacuum coating unit which had facilities for revolving and rotating the specimens to ensure even coating. This treatment eliminated any charging phenomena during subsequent examination in the S.E.M.

It was found that a cross-section of these scratches could be obtained, without altering the existing crack pattern, by tapping an unmounted crystal with a sharp diamond stylus (away from the scratch) which caused the crystal to break along major cleavage planes across the line of the scratch.

7.2.3 Testing methods

The samples were glued to the rotatable table with 'lakeside' resin and set parallel to lines scribed on the table surface. Scratches were made on four crystal faces and in the directions as indicated below.

(i) $(10\bar{1}0)$ face in the direction of the X and Z axes
(ii) $(1\bar{2}10)$ face in the direction of the Y and Z axes

(iii) (0001) face in the direction of the X and Y axes

(iv) $(1\bar{2}10)$ in directions which were at angles of 15^0, 30^0, 45^0 ..., 165^0 to the Y axis.

The speed of scratching was varied from 8.5×10^{-4}mm s^{-1} to 8.5mm s^{-1} and the load applied to the stylus was varied between 4.9×10^{-2}N and 9.8N. In some experiments the environment was altered by flooding the specimen surface and stylus with either distilled water or n-heptyl alcohol.

7.3 Experimental results

7.3.1 Accuracy of results

A force of approximately 0.2N was required to overcome the inherent friction of the carriage. This force was independent of applied load and presumably arose from the side forces holding the linear bearings in position. As this friction force also varied with the position of the carriage, no measurements of friction were taken when the force required to move the carriage was less than 0.4N. The friction in the two pulleys was negligible and the frictional moment in the pivot of the counterbalanced arm was 3×10^{-3}Nm, which corresponded to a load of 0.02N on the loading platform. The level of the pivot was slightly above the plane of the specimen surface and an allowance for this should be

made in the calculation of the coefficient of friction. However, the error this gives the coefficient of friction is never greater than 2 per cent and this allowance has consequently been ignored as the accuracy of the measured friction force varied from about 5 per cent at 9.8N applied load to about 10 per cent at 2.9N applied load because of statistical scatter and the limited accuracy of the load cell. Measurements of scratch and crack dimensions taken by scanning electron microscopy have an accuracy of about 5 per cent.

7.3.2 Friction measurements

A record of the measured friction force at three different speeds on one specimen at the same load is given in fig. 21. The curves show a stick-slip type pattern and over the range of speeds from 8.5×10^{-4}mm s^{-1} to 8.5×10^{-1}mm s^{-1}, the same average peak value of the friction force was obtained. However, at 8.5mm s^{-1}, the friction force had a large oscillation of about 2N and a mean value of 5N. Parts of the friction force curve at the slowest testing speed could be correlated with a true stick-slip process - where the carriage does not move in the stick region and the cord only stretches until a critical load when the carriage slips forward and the load suddenly drops. However, there were other parts of the curve where the carriage was pulled along with the string. The frequency of these stick-slip points depends on the

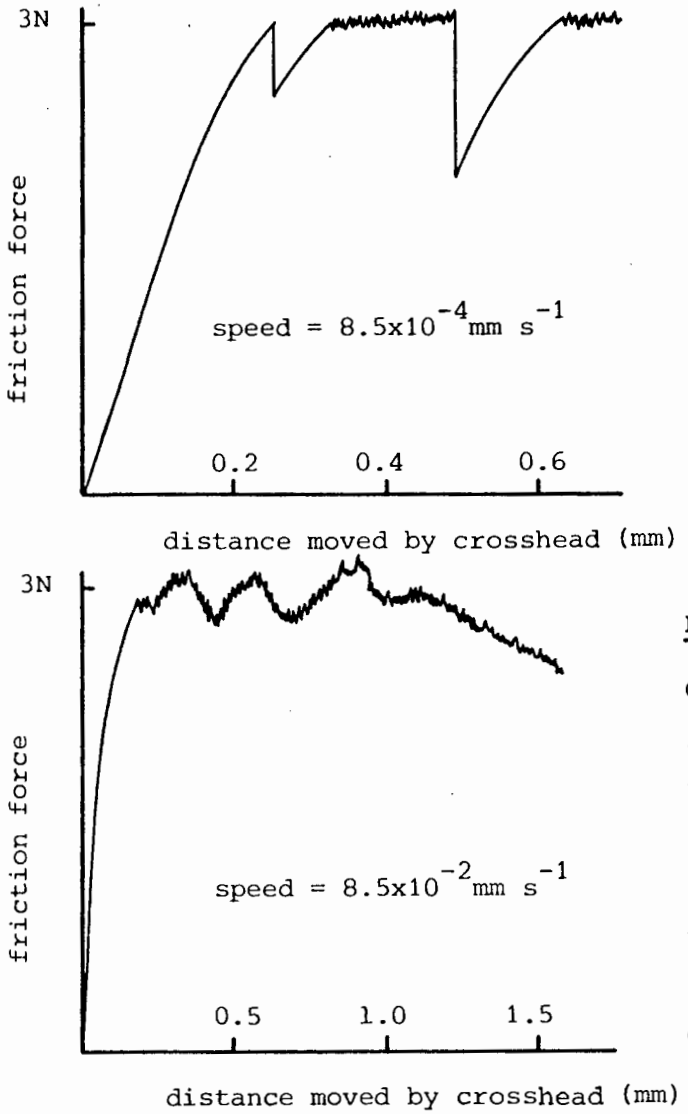

Figure 21

Change in form of friction force for three different speeds at a load of 9.8N on the $(11\bar{2}0)$ face of quartz scratched in the direction of the Y axis.

mass and stiffness of the system. At high speeds, where the carriage is pulled along with a velocity comparable to the velocity during the slip stage, inertia effects occur and this is thought to be the explanation for the large oscillations and high value of the friction force at velocities of 8.5mm s^{-1}.

All the experiments described in the rest of this section were performed at a speed of 8.5×10^{-2} mm s^{-1}.

The results of measurements of the maximum friction force for varying loads on one specimen are presented in fig. 22. The resulting coefficient of friction is shown as a function of applied load in fig. 23. The coefficients of friction at applied loads of 9.8N and 2.9N were measured as a function of all the crystal orientations previously tabulated for polished specimens tested in air and the same mean value of the coefficient of friction was obtained for all these orientations. For a fixed orientation, the surface finish was varied and the mean value of the coefficient of friction at the two loads mentioned above was found to be identical for all three surface finishes when the samples were tested in air. The same mean value of the coefficient of friction was also found for the three different environments when tested at the two above mentioned loads for a polished surface in a fixed orientation.

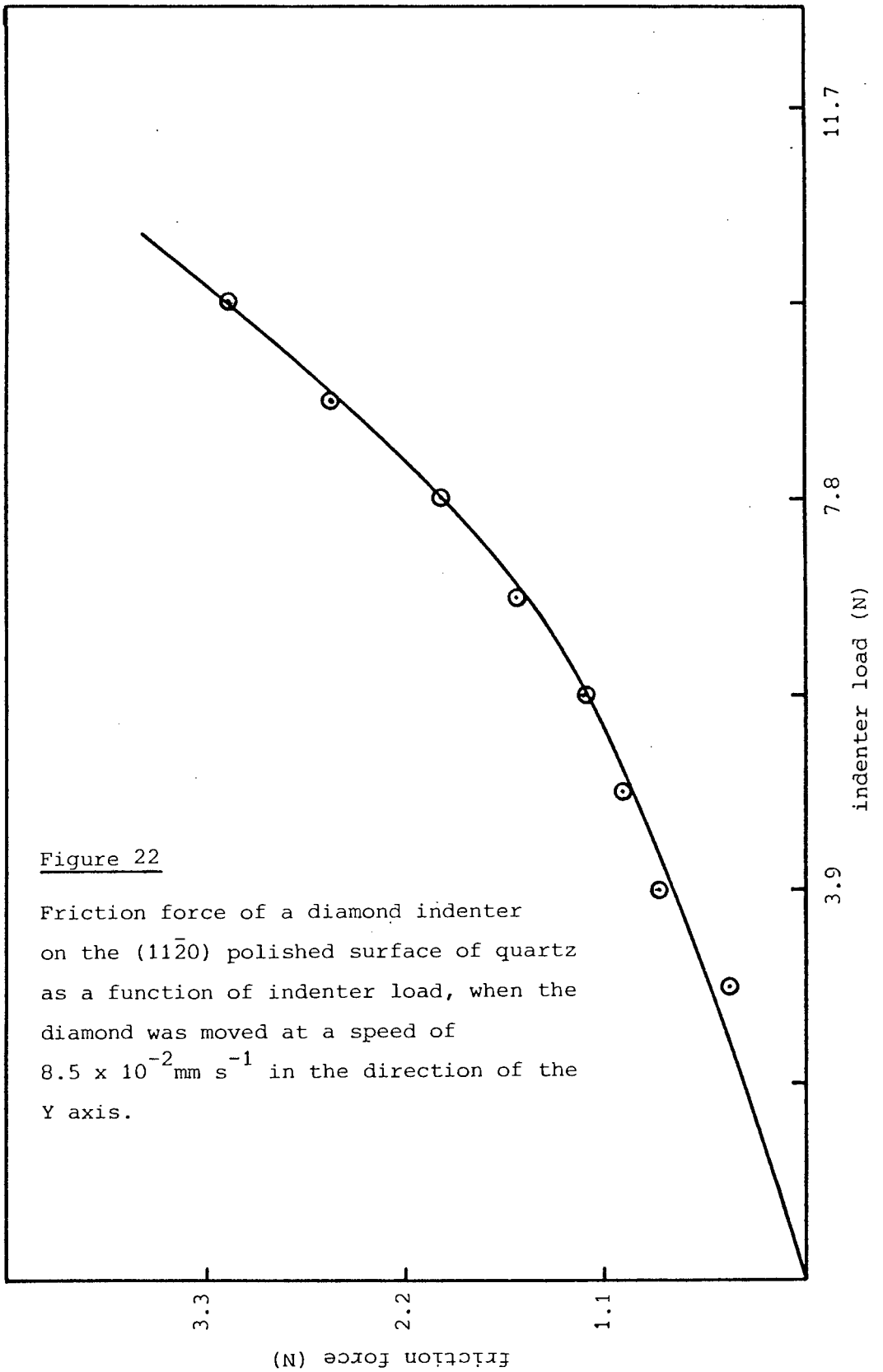

Figure 22

Friction force of a diamond indenter on the $(11\bar{2}0)$ polished surface of quartz as a function of indenter load, when the diamond was moved at a speed of 8.5×10^{-2} mm s^{-1} in the direction of the Y axis.

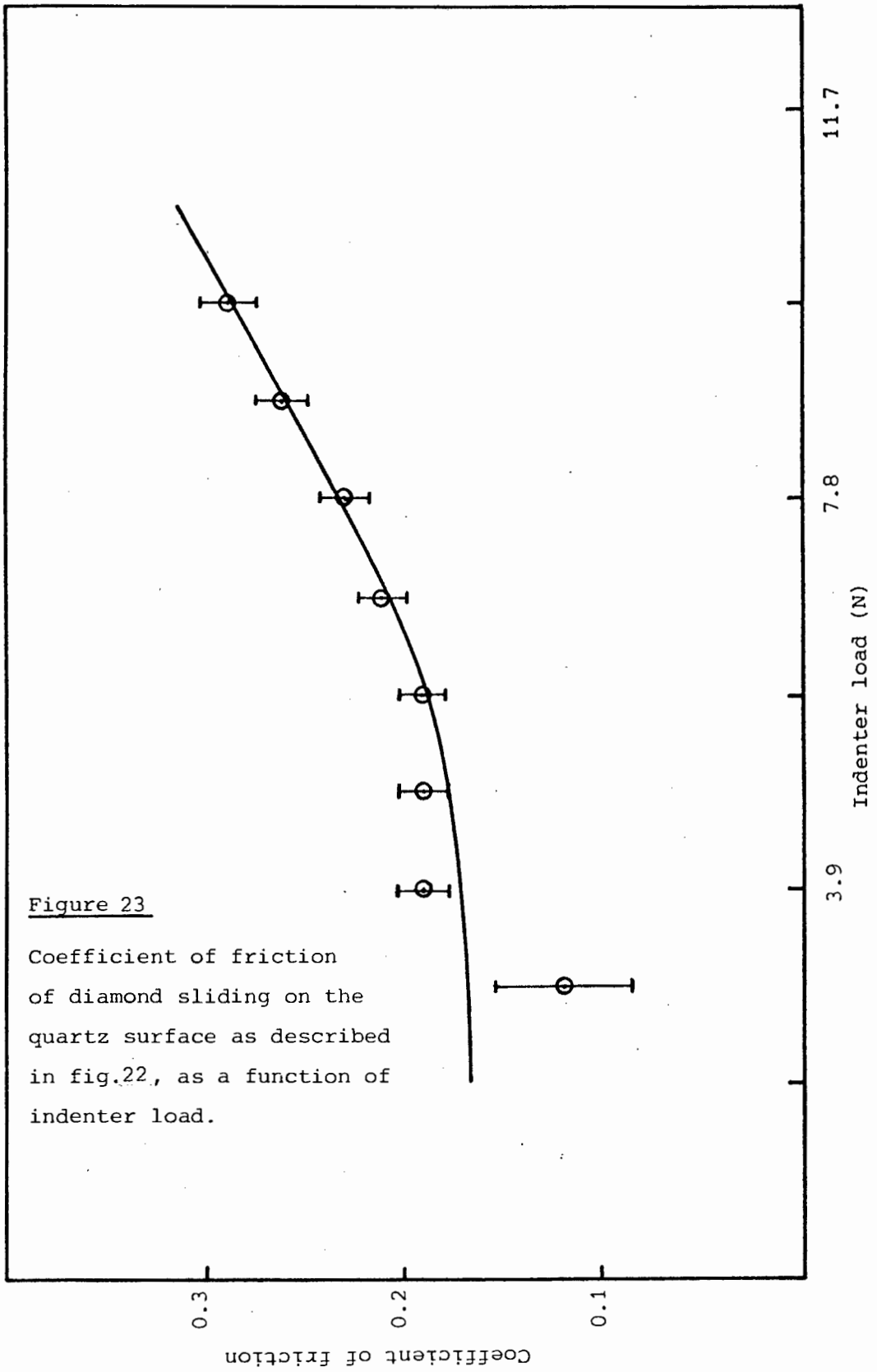

Figure 23

Coefficient of friction of diamond sliding on the quartz surface as described in fig.22, as a function of indenter load.

7.3.3 Deformation character

Typical scratches under 9.8N, 2.9N and 0.78N loads for the same surface finish, cutting speed, orientation and environment, are shown in plates 20, 21 and 22 respectively, and a scratch under a 9.8N load taken at a higher magnification is shown in plate 24 Loads less than 0.78N produced no observable deformation, but after etching, deformed areas could be seen. The appearance of the scratches after etching is shown in plates 25, 26, 23, 27 and 28 for loads of 9.8N, 2.9N, 0.78N, 0.2N and 4.9×10^{-2}N respectively.

7.3.3.1 Crack widths (constant: orientation, environment, speed, surface finish)

It is believed that the widths of the central damage zone represent the contact area between the diamond stylus and the specimen. This is indicated in a few cases where not all of the material was removed from the damage zone and score lines in the direction of scratching across the full width of this zone are evident (see plate 29). The widths of the central damage zone in unetched samples caused by 9.8N and 2.9N loads were found to be equal to the widths measured in the etched samples. Hence in the case of light loads where the damage region could not be observed without etching, it is assumed that the widths measured in the etched specimens are equal to the widths of the actual

damage zone. These widths are plotted against the applied load in fig.24 and a logarithmic plot of these quantities is shown in fig.25. If a straight line is fitted to the points in fig.25 the relationship between half the width of the damage zone w and applied load L

is $w = 1.3 \times 10^{-5} L^{\frac{1}{3}}$

where w is measured in metres and L in Newtons.

It was established that the tip of the diamond stylus could be approximated by two radii of curvature at right angles to each other with values of 310μm and 75μm, with the direction of scratching parallel to the plane containing the 310μm principal radius of curvature. These values were substituted into an analysis for a Hertzian indenter of this geometry loaded onto a quartz surface and the result (given in Appendix F) shows that there is an elliptical area of contact between the surfaces given by semi-axes a and b, where

$b = 0.63 \times 10^{-5} L^{\frac{1}{3}}$ and $a = 2.6b$, where b is measured in metres and L in Newtons. Hence for purely elastic contact, the width of the central damage zone of the scratch should be 2b. As 2w is about twice the value of 2b it must be assumed that some inelastic deformation has taken place beneath the stylus.

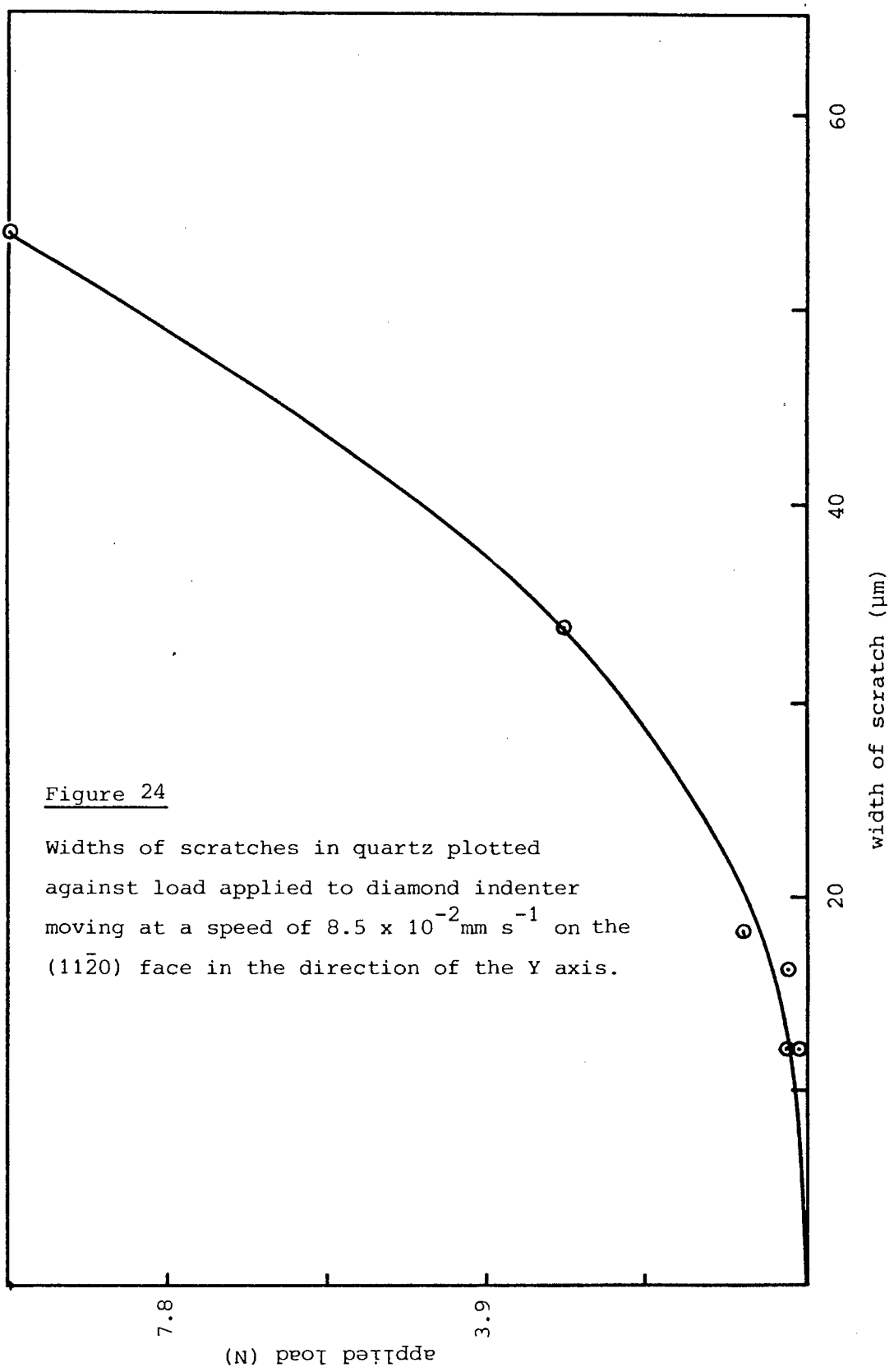

Figure 24

Widths of scratches in quartz plotted against load applied to diamond indenter moving at a speed of 8.5×10^{-2} mm s^{-1} on the $(11\bar{2}0)$ face in the direction of the Y axis.

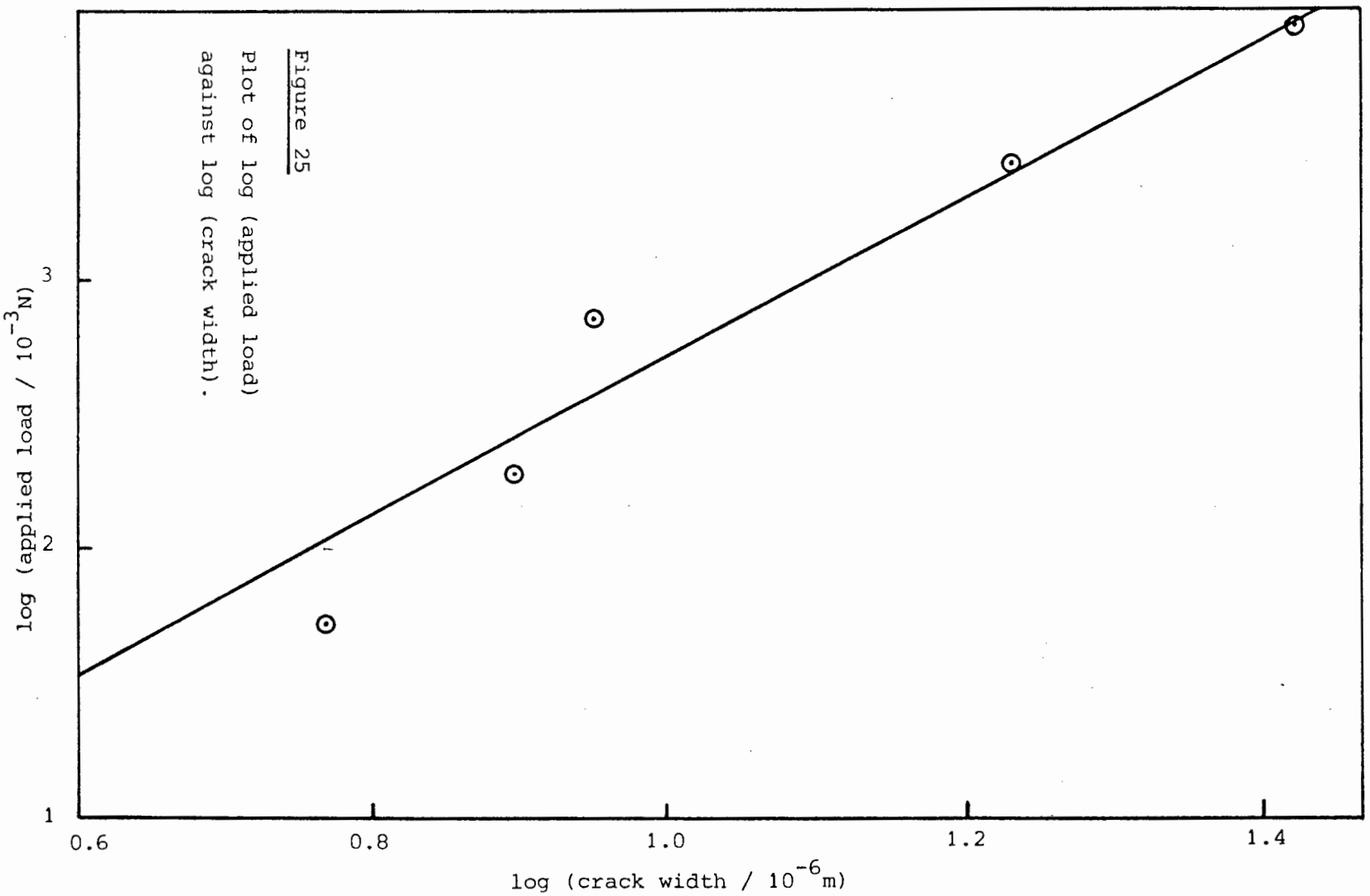

Figure 25

Plot of log (applied load) against log (crack width).

7.3.3.2 Median vent cracks (constant: orientation, environment, speed, surface finish)

Sections through scratches revealed that cracks formed at right angles to the surface and penetrated into the material at all applied loads as shown in plates 30, 31 and 32 for loads of 9.8N, 0.78N and 4.9×10^{-3}N respectively. These are identified as being the same as the median vent cracks described by Lawn and Swain (1975). A plot of applied load against vertical crack length is presented in fig.26.

7.3.3.3 Hertzian cracking

Typical Hertzian cracking occured away from the main width of the scratch and an example is shown in plate 33 and etched in plate 34. The average separation of these cracks was found to be independent of speed of sliding, environment and orientation at a load of 9.8N. There was no difference in crack patterns observed between the polished or ground surfaces, but in the case of the etched surfaces, fewer Hertzian cracks were observed in the surface as shown in plate 35, but further etching showed that Hertzian cracks did extend below the surface as seen in plate 36. However, the geometry of these Hertzian cracks showed a marked effect with change in crystal orientation. Examples of etched surfaces are shown in plates 37, 38 and 39. Included in these figures are arrows which show the intersection of

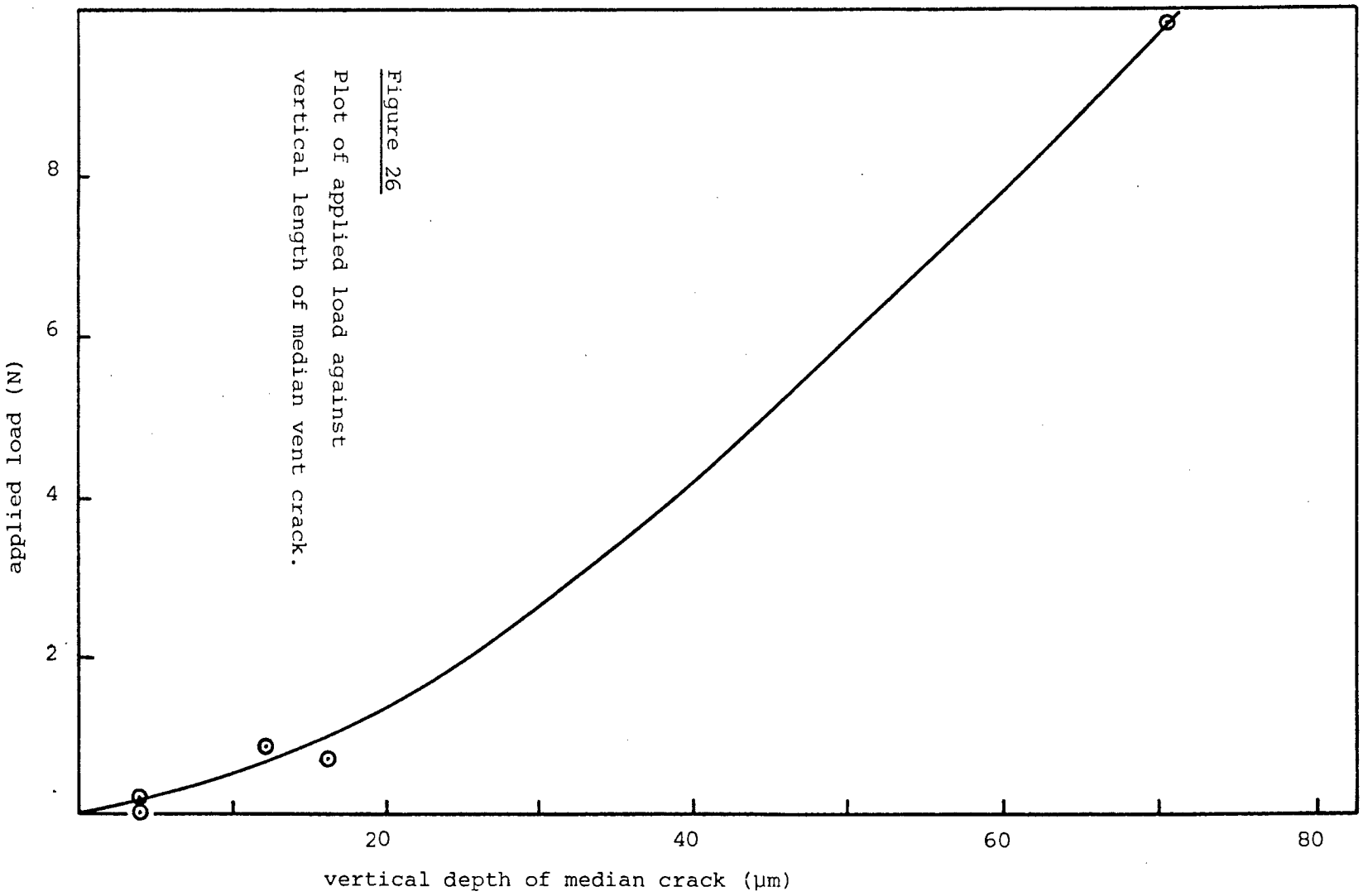

Figure 26

Plot of applied load against vertical length of median vent crack.

the major cleavage planes in quartz (the positive and negative rhombohedron planes) with the surface. The manner in which these cracks extend beneath the surface is shown in plate 30 and after etching in plate 40. At high magnification steps are often seen on the etched Hertzian crack surfaces as shown in plate 41 which is an area of plate 24 taken at a higher magnification.

7.3.3.4 Effect of environment (on central damage zone)

Tests were carried out at loads of 9.8N and 2.9N and at speeds of 8.5×10^{-2} mm s^{-1} and 8.5mm s^{-1} on one polished specimen with three different environments. The width of the central damage zone for etched and unetched specimens was the same on average in all three environments. However, after identical subsequent etching conditions more material was removed from the central damaged zone when the specimen was tested in water rather than in air, and more material was removed when the environment was heptyl alcohol instead of water as can be seen from plates 37, 42 and 43 for environments of air, water and heptyl alcohol respectively.

7.4 Discussion

7.4.1 Dynamic Hertzian cracking

The results of Hamilton and Goodman (1966) for

the static stress field of a spherical indenter loaded onto an elastic surface with friction are shown in fig.27 where the principal stress trajectories are indicated. The Hertzian crack patterns in quartz are seen to correspond to the theoretical results in principle, as cracks formed on the surface in an arc behind the indenter where the tensile stresses are a maximum and as cracks also extended in an arc below the surface of the material as shown in plates 33 and 44. However, the crystallography of quartz clearly has an influence in determining on which surfaces fracture would occur,and the cracks tended to form on low surface energy rhombohedral planes where possible. A second effect noted was that the Hertzian cracks tended to follow one of the rhombohedral planes in preference to the other. This can be explained by the fact that the positive rhombohedron is a preferred cleavage plane compared to the negative rhombohedron (Heavens and Ashbee, 1975).

In the present study, it was noted that Hertzian cracks could be seen on the surface in the S.E.M. as in plate 23 and consequently the crack faces must have moved with respect to each other in order to be visible. There are two possible explanations for this. One is that there is some plastic deformation beneath the scratch which creates an elastic displacement field of sufficient strength to open the cracks (Lawn and Swain, 1975) and a second is that cleavage steps (which were made visible after etching) prevented the cracks from closing properly. This latter explanation has been successfully used to explain the

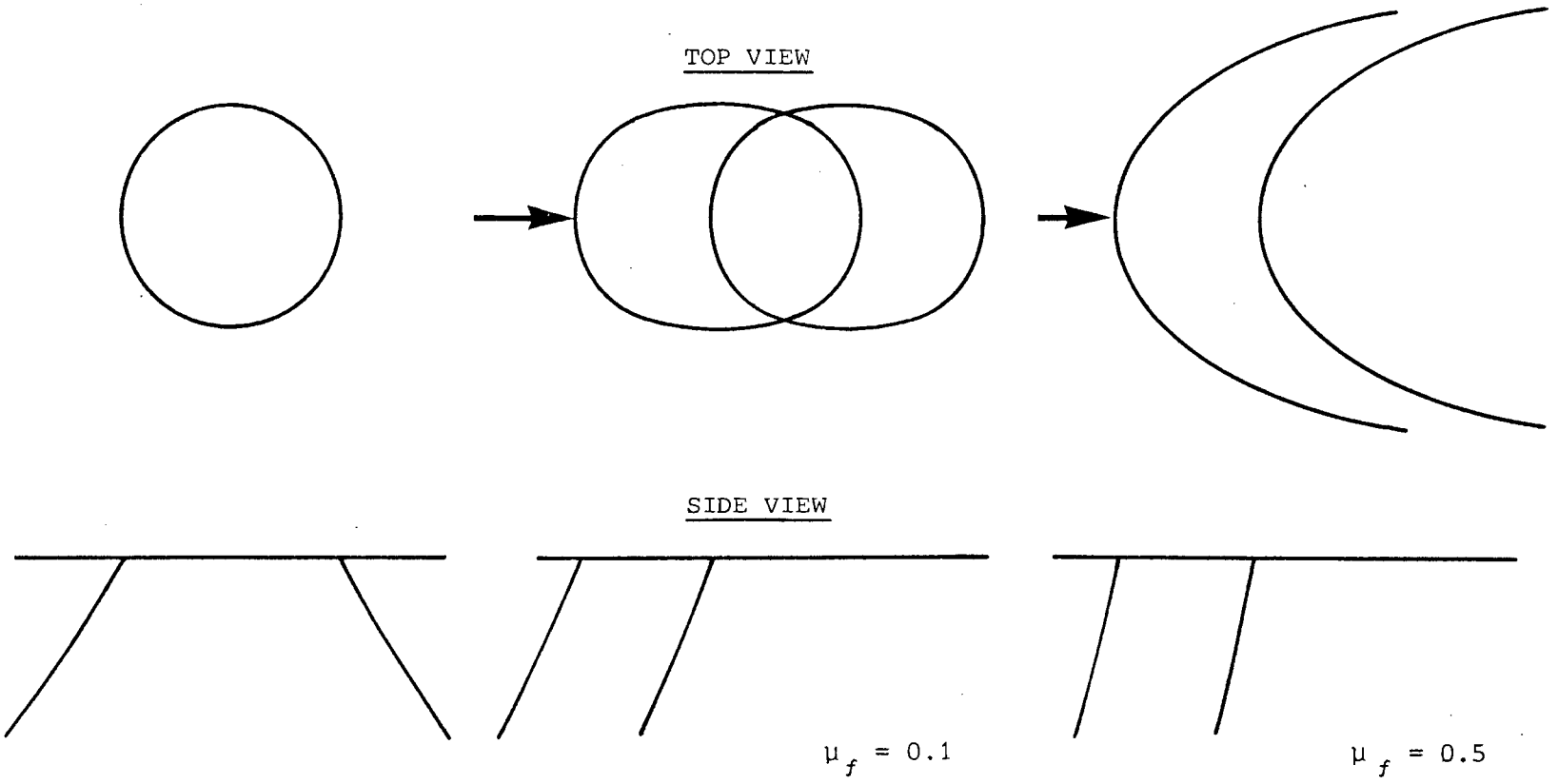

Figure 27

Theoretical Hertzian crack shapes caused by a static and a sliding spherical indenter at two coefficients of friction. The arrows indicate the direction of sliding.

residual deformation resulting from Hertzian indentations in diamond (Lawn and Komatsu, 1966). It is quite probable that both of these mechanisms are operative here.

Regions of elastic strain in a crystal are attacked by acid more rapidly than unstrained material. The preferential attack at the cracks by hydrofluoric acid can then be explained if we assume that there is a mismatch at the crack interfaces and elastic strain fields occur adjacent to them as observed in transmission electron microscopy (see section 6.4).

Sometimes cracks were produced on the specimen surface in a direction opposite to that expected for a Hertzian stress field, but subsequent etching revealed that they lay close to the surface (see plates 33 and 34 before and after etching). If we apply the results of Lawn and Swain discussed in the previous section, then these cracks could be propagated from a damage region beneath the surface to intersect the surface in the observed manner once the indenter passed and the elastic strain energy was released.

7.4.2 Subsurface damage

Lawn and Swain (1975) have shown that the length of the median vent crack developed beneath a geometrically similar sharp indenter, will grow in direct proportion to the indenter load. In the present case, the cracks do

indeed deepen with increasing load, but not linearly. The presence of an inelastic region beneath the scratch has already been noted, but because the indenter was not geometrically similar, it is not expected that a linear relationship should hold between indenter load and crack length. It was also shown in the above mentioned paper that when the load on the indenter was released, the stress field changed from compressive to tensile. This tensile stress field would then propagate cracks initiated in the damage region and the direction of crack propagation would be lateral and towards the specimen surface which would result in the creation of chips. This result would account for the observed high degree of chipping in the present case at high loads and presumably the presence of a tangential force on the indenter would only modify the detailed nature of the crack pattern.

7.4.3 Coefficient of friction

In order to calculate the coefficient of friction of diamond sliding on quartz, the first approach will be to use the classical theory of friction for metals as described by Bowden and Tabor (1964b). This theory assumes that the friction arises from the sum of two terms. The first originates from the shearing of a welded region between the asperities of the two surfaces and the second originates from the ploughing of one surface into the other. Bowden and Hanwell (1966) have shown that there is a tenacious contaminant layer on the surfaces of both

diamond and quartz in air and that only repeated sliding (of the order of a few hundred times) in ultra-high vacuum conditions removes this layer. It is therefore thought that the adhesion between diamond and quartz in air is small and that the shearing term is therefore very small. Striations such as those in plate 29, about 0.5μm wide or less were observed on debris material and at low loads (plate 22), when no cracking occured, they were found to have similar widths. These tracks must arise from asperities on the diamond stylus and if they occur through dislocation motion as seen in section 6.3.2 for diamond polishing particles, then this plastic flow would make a contribution to the coefficient of friction. The amount of energy dissipated by this plastic flow per unit scratch length for a given load is difficult to estimate from the observed dislocation density, since the energies required for dislocation motion, for dislocation self energy and for the creation of dislocations in a dislocation free crystal, cannot easily be calculated in the present circumstances.

There are another three mechanisms which should be considered in the evaluation of the coefficient of friction. The first is that of Hertzian fracture and even though Bowden and Tabor (1964a) showed that Hertzian cracks dissipate little energy during sliding, the present results show a great amount of cracking occuring in the central damage zone and this should be taken into account. However, it is shown in Appendix G that even if it is assumed that when the stylus moves, all the elastic energy

in the material beneath the stylus is transformed into surface energy by cracking, this contribution to the coefficient of friction is an order of magnitude lower than the observed coefficient of friction. The second is a ratchet mechanism whereby the asperities on the stylus are assumed to rise over those on the surface and therefore do work against the applied load. It is conceivable that a modification of this idea could be a mechanism in the present case. The stylus might plough into the surface and then rise out again for a short distance as the specimen moves along and then as new cracks are formed, dig in again. The coefficient of friction calculated this way will be equal to the tangent of the angle with which the stylus rises to the surface. At greater loads the depth of ploughing will be greater and consequently the stylus might rise at a greater angle to the surface and an increase in the coefficient of friction will result. In order to verify this theory the displacement of the stylus normal to the surface has to be measured, but because of the small distances involved this is experimentally very difficult. The third mechanism is that friction has taken place by the fracturing of asperities (Byerlee, 1967). This mechanism also predicts that the coefficient of friction should increase with increasing load because of the interlocking of asperities, but there is no way of checking the validity of this mechanism in the present experiment.

High rises in temperature at asperity tips can occur and it is shown in Bowden and Tabor (1964b) that the

temperature rise is proportional to the sliding velocity. If we accept that a dislocation mechanism contributes to the coefficient of friction, then an increase in sliding velocity has two effects. Firstly, higher velocities imply higher temperatures which in turn promote dislocation activity so that plastic work is done and the coefficient of friction will rise. The second effect is that higher velocities mean higher rates of strain and a subsequent lowering of dislocation activity and thus a consequent decrease in the coefficient of friction. In the present case the coefficient of friction remained constant over a velocity range of 10^3 and therefore if the contribution from plastic flow is significant, it is suggested that over this range the above two effects remained in the same proportion to each other so that the net dislocation activity remained roughly constant.

7.4.4 Effect of surface finish

Frank and Lawn (1967) and Wilshaw (1971) have developed fracture mechanics equations for the prediction of the growth of Hertzian cone cracks in isotropic materials. Their analyses depend on the fact that there is a distribution of flaws on the surface of the material and that the material fails because the longest of these flaws propagate. Hence, if these flaws are shortened by polishing or shortened and rounded by etching, higher loads are required to propagate Hertzian cracks. The present study has revealed that the frequency of Hertzian cracking

beneath the surface is independent of surface preparation and a possible explanation for this is that, unlike the case of static Hertzian indentation, the stylus creates its own flaws as it moves and the tensile stress behind the slider then propagates them, and therefore the prior presence of surface flaws will not have a marked influence on the coefficient of friction.

7.4.5 Effect of environment

Macmillan et al (1974) have shown that for a sapphire ball sliding on soda-lime glass, the width of the track produced and the coefficient of friction decreased dramatically when the environment was changed from water to heptyl alcohol. The present study indicates that neither of the above two effects occured when large loads were used and severe cracking took place. The only difference noticed with the use of these two environments was that the damage produced below the surface of the scratch was more severe (i.e. a greater amount of material was released on etching), in water than in air and even more severe in heptyl alcohol than in water. A similar effect has been found to occur in alumina (Gruver and Kirchner, 1974) when the material is scratched in environments such that $\zeta \simeq 0$. In section 7.4.3 it was suggested that plastic flow in quartz could make a significant contribution to the coefficient of friction. If we assume that the environments used decreased dislocation activity for the reasons given by Macmillan et al (1974), then the behaviour of quartz

during scratching should reflect this assumption. The observation that the width of the scratch was independent of environment may be explained by the fact that the area of contact between the stylus and the quartz surface, and the amount of Hertzian cracking, is controlled mainly by elastic deformation, and hence the width of the scratch will only be influenced to a small degree by a change in the amount of plastic deformation produced. The observed increase in the damage beneath the stylus in the environments used is consistent with the idea that a decrease in plastic flow in the environments would favour the production of cracking as discussed in previous sections. However, the fact that the coefficient of friction remains approximately the same for the liquid environments as for air may be explained by assuming that the decrease in plastic flow, although significant in terms of the extent of cracking, is not significant in terms of total energy expended and therefore has a negligible effect on the coefficient of friction.

Of the other possible environmental sensitive mechanisms mentioned in the introduction, the effect of the cooling properties of the liquid environments as well as that of static fatigue, need only be considered, since the ramainder involve debris which in the present case does not interfere with the cutting process. The presence of a heat absorbing liquid environment will reduce the amount of plastic flow and hence will have the same effect as zeta potential effects of the liquid on dislocation activity. If static fatigue had played a major role in

the change in scoring properties with environment, then one would expect the extent of Hertzian cracking to increase in a similar manner to the increase in damage produced beneath the stylus. As the extent of Hertzian cracking did not change with environment, it must be concluded that static fatigue can only make a small contribution to environmental effects during cutting actions.

7.5 Conclusion

It has been established that the geometry of dynamic Hertzian cracking produced by a moving stylus on quartz obeys, in principle, the theoretical calculations of the stress field, but the variations in surface energies play an important role in determining the direction of crack propagation. The presence of a high degree of chip production at large indenter loads and uncharacteristic Hertzian cracking have been explained in terms of the theory of Lawn and Swain, whereby the stored elastic energy beneath the indenter is converted into surface energy on unloading.

The coefficient of friction was observed to vary from about 0.15 at an indenter load of 3N to about 0.3 at an indenter load of about 10N. Five mechanisms have been examined which could explain the value of the coefficient of friction and its rise with increasing load. The first of these mechanisms is based on the fracture of welded regions between the two materials and has been regarded as

making a negligible contribution to the coefficient of friction. It has been shown that the contribution to the coefficient of friction arising from the energy released in creating new surface area is also negligible. By identifying dislocation activity under diamond polishing particles (as observed in the transmission electron microscope) with striations on the scratch surface, it is believed that plastic flow plays a role in the determination of the coefficient of friction, but the size of this contribution could not be calculated. The two other mechanisms, viz. ratchet and fracturing of asperities, could not in principle be determined in the present type of experiment and if present, their effect on the coefficient of friction could not be guaged. It is thus concluded that the origin of the coefficient of friction and its increase with load is not clearly determined.

The absence of any effects of surface finish on the coefficient of friction or on the form and extent of cracking has been explained by proposing that the stylus generates its own initiating flaws as it moves.

The only effect caused by a change of environment was that of an increase in the severity of subsurface damage beneath the stylus. An explanation in terms of decreased dislocation activity and hence more fracturing has been proposed.

8. GENERAL CONCLUSION

The deductions and conclusions derived from experimentation and calculations are divided into two sections : (i) those which can be generalised to embrace the class of brittle materials and (ii) those which are restricted to quartz.

(i) It has been established that crack geometries to within 0.1μm of the crack tip in brittle materials, are the same as that predicted by linear elastic methods. Theories have been developed for determining the onset of fracture if the loading conditions and crack geometry are known, and also for the determination of fracture velocities in anisotropic materials by the use of Wallner lines. Freund's exact equation of motion for a propagating crack has been shown to allow for modification, so that the initial geometry of cracks may be taken into account. Crack branching has been found to be governed by the simultaneous influences of fracture velocity and dynamic fracture surface energy, and the prediction that the ratio of the dynamic stress intensity factor to its static value should be a constant has been shown to be accurate for a number of different materials.

(ii) The stress field near the crack tip in quartz has been shown to be very similar to the isotropic case and it is concluded that only the anisotropy of surface energies will determine the deviation of the direction of crack propagation from isotropic behaviour. Calculations of surface energy and accurate measurements of fracture surface energy have shown that the fracture surface energy is almost the same as the true surface energy and therefore quartz is almost perfectly brittle when tested in tension. The maximum crack velocity in quartz was observed to be very close to the Rayleigh wave velocity and also to obey Freund's modified equation. From this result it has been concluded that the dynamic fracture surface energy is equal to the static fracture surface energy. The anisotropy of surface energies in quartz can be used to explain crack branching behaviour and the observation of high crack velocities. The fact that relatively few dislocations or twins were generated beneath a Vickers hardness indenter as compared to other brittle materials suggests that even under high hydrostatic pressures quartz is very brittle at room temperature. However, dislocation activity observed beneath diamond polishing particles has been attributed to a local increase in temperature. The value of the coefficient of friction between diamond and quartz and its increase with

increasing load has been shown to be related to plastic flow but no definite mechanism has been found to predict the observations. The form of the damage arising from cracking produced by a diamond stylus on the surface of quartz may be concluded to arise from the release of strain energy from an inelastic zone beneath the indenter. No firm conclusion can be given for the fact that the subsurface damage is more severe in heptyl alcohol than in water and more severe in water than in air, but the known increase in hardness in these environments suggests that the amount of plastic flow is decreased and brittle failure therefore favoured.

The wide variety of experiments which have been carried out during this study has enabled an appreciation of the relationship between the behaviour of quartz under pure tension and under more complex loading conditions to be gained. The results of these basic studies can now be used to advantage in order to devise laboratory scale experiments which could model the more complex, but real conditions which exist in a mill or beneath a drill or cutting tool. Such studies may ultimately lead to more efficient excavation and comminution of mineral bearing rock.

A P P E N D I X A

Introduction of sharp cracks into glass and quartz by thermal shock treatments

Samples of glass and quartz were notched in the centre of their long lengths by an annular diamond saw 0.15mm wide to a depth of 0.5mm to 1mm. The samples were purposely hand held during this notching operation in order to try to introduce distortional stresses so that short sharp cracks might be produced at the ends of the notches.

A chisel shaped steel tool was heated to red heat in the flame of a bunsen burner and the tip of the tool was applied at an angle to the specimen surface as shown in fig. 28. By bringing the tool closer to the specimen surface, a crack could be produced on the underside of the specimen to the desired length.

Figure 28

Method of introducing sharp cracks into glass or quartz

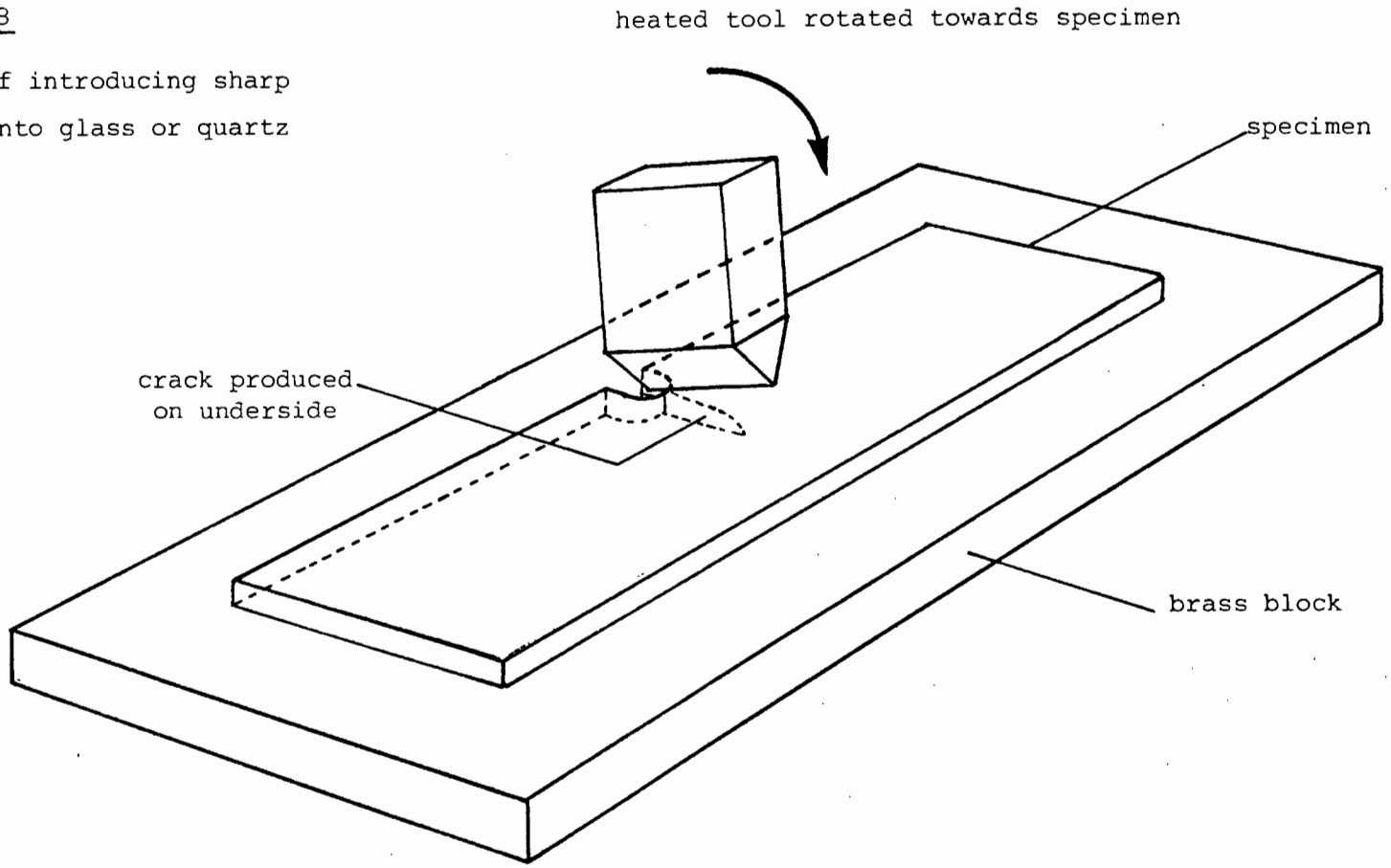

A P P E N D I X B

The shape of an edge crack in a semi-infinite medium subjected to uniform tension at $\pm\infty$ is deduced from the work of Wigglesworth (1957). Using the coordinates shown in the diagram below, and setting

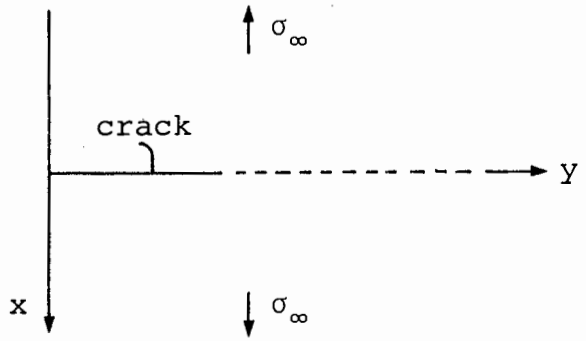

the crack length and the tensile stress σ_∞ both equal to unity, Wigglesworth obtained the displacements u and v of the material in the x and y directions respectively

as $$8\mu(u+iv) = 4(1-\nu)\Omega(z) - F(z,\bar{z})$$

for a state of plane strain or if ν (Poisson's ratio) is replaced by $\nu/1-\nu$ for a state of plane stress, μ is the modulus of rigidity, $z = x+iy$, Ω a complex function and $F(z,\bar{z}) = (z-\bar{z})\bar{\Omega}'(\bar{z}) + \Omega(z) - \Omega(\bar{z})$ where the bar refers to conjugation and the dash to differentiation. Hence for plane stress

$$u(x,y) = \frac{1}{2\mu}\mathrm{Re}\left\{\frac{\Omega(z)}{1-\nu} - \frac{F(z,\bar{z})}{4}\right\}$$

and the shape of the crack is given by $u(0,y)$.

If we let $F(z,\bar{z}) \equiv G(x,y)$ then $G(0,y) = -4iy$.
Ω may be expanded in an infinite series as follows

$$\Omega(z) = U(z) + V(z) - 2z$$

where $$U(z) = \sum_{n=0}^{\infty} A_n (1+iz)^{n+\frac{1}{2}}$$

and $$V(z) = i\sum_{n=0}^{\infty} B_n (1+iz)^{n}$$

hence $$u(0,y) = \frac{1}{2\mu(1-\nu)} \sum_{n=0}^{\infty} A_n (1-y)^{n+\frac{1}{2}}$$

Now $A_n = 3.17214\ a_n$ and the a_n are tabulated by Wigglesworth, but only the first ten terms were used to evaluate

$$\tilde{u}(0,y) = \sum_{n=0}^{10} a_n (1-y)^{n+\frac{1}{2}}$$

and the values $\tilde{u}(0,0) = 0.9185$ and $\tilde{u}(0,1) = 0$ were obtained. The values of $\tilde{u}(0,0)$ and y were scaled to fit the limits of the experimental curve and the result of the full curve is shown in fig.3.

A P P E N D I X C

Evaluation of the integral

$$\frac{d}{dc} \left\{ \int_o^c u(y,c)\,dy \right\}$$

where $u(y,c)$ is the shape of the crack

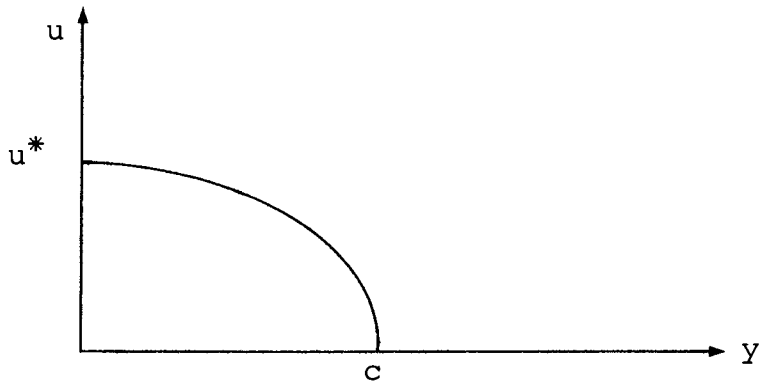

where $u^* = u(0,c)$

We assume that u depends on c such that if $c \to c'$ then the axes will change only by a scale factor.

i.e. $\frac{c}{c'} u(y,c') = u\left(\frac{c}{c'} y, c\right)$

Let $c' = c + \Delta c$

then $u(y,c+\Delta c) = \frac{c+\Delta c}{c} u\,(y-\Delta y, c)$

where $\frac{c}{c+\Delta c} \simeq \frac{c-\Delta c}{c}$ for small Δc and $\Delta y = \frac{\Delta c}{c} y$

$$\therefore \quad u(y,c+\Delta c) = u(y-\Delta y,c)+\frac{\Delta c}{c}u(y-\Delta y,c)$$

$$\text{i.e.} \quad \frac{u(y,c+\Delta c)-u(y,c)}{\Delta c}+\frac{u(y,c)-u(y-\Delta y,c)}{\frac{c}{y}\Delta y}=\frac{u(y-\Delta y,c)}{c}$$

$$\therefore \lim_{\Delta c\to 0} \Rightarrow \frac{\partial u}{\partial c} + \frac{y\partial u}{c\partial y} = \frac{u}{c} \qquad (C1)$$

$$\text{now} \quad \frac{d}{dc}\{\int_o^c u(y,c)dy\} = u(c,c) + \int_o^c \frac{\partial u(y,c)}{\partial c}dy$$

$$= \int_o^c \frac{u}{c}dy - \int_o^c \frac{\partial u}{\partial y}\frac{y}{c}\,dy$$

as $u(c,c) = 0$ and by (C1)

$$\text{and} \quad \int_o^c y\frac{\partial u}{\partial y}dy = \int_{u^*}^{o} ydu \qquad \begin{matrix}\text{as } y=o,\ u=u^* \\ y=c,\ u=o\end{matrix}$$

$$= yu\Big]_{u=u^*}^{u=o} - \int_o^c udy = -\int_o^c udy$$

Therefore the final result is

$$\frac{d}{dc}\{\int_o^c udy\} = \frac{2}{c}\int_o^c udy$$

A P P E N D I X D

Derivation of the surface energy for the $(1\bar{1}00)$ plane in α-quartz

A brief description of the theory, outlined by Blakely (1973), on which the calculation of true surface energy is based is provided as a guide to the level of approximation used in the evaluation of the surface energy in quartz.

The thermodynamic surface energy γ is defined as the reversible work involved in creating unit area of new surface at constant temperature, volume and total number of moles.

i.e. $$\gamma = \lim_{dA \to 0} \frac{đw}{dA}$$

where $đw$ is the amount of work associated with the increment da in Area. For a one component system, the following relation holds between the surface energy at an absolute temperature T, the internal energy per unit area e and the entropy per unit area s :-

$$\gamma(T) = e(T) - Ts(T)$$

Now e(T) will consist of changes in potential energy of interaction and vibrational energy and the contributions to s(T) will arise mainly from lattice vibrations. If it is assumed that the freshly created area is planar

and that there are no surface defects, e(T) may be expressed in terms of the potential energy at 0^0 K, $e_{pot}(0)$ and a vibrational term $e_{vib}(T)$ as follows :-

$$e(T) = e_{pot}(0) + \int_0^T \left(\frac{\partial e_{pot}}{\partial T}\right) dT + e_{vib}(T)$$

which therefore becomes :-

$$e(T) = e_{pot}(0) + \left(\frac{\partial e_{pot}(0)}{\partial a}\right) \Delta a + e_{vib}(T)$$

where Δa is the change in lattice parameter between 0^0 K and T. The potential energy at 0^0 K can also be sub-divided into two parts. If the crystal is divided into two parts such that the atoms or ions maintain their relative spacings, this will contribute an amount $e^0_{pot}(0)$ to $e_{pot}(0)$. If these atoms or ions are then allowed to relax to their new equilibrium positions, this will contribute an amount $\Delta e_{pot}(0)$ to $e_{pot}(0)$.

Hence :

$$\gamma(T) = e^0_{pot}(0) + \Delta e_{pot}(0) + \left(\frac{\partial e_{pot}(0)}{\partial a}\right) \Delta a + e_{vib}(T) - Ts_{vib}(T)$$

An indication of the relative importance of these various terms may be obtained by examining KCl as an

example.

Energies in mJm^{-2}

Temp. (^0K)	$e^0_{pot}(0)$	$\Delta e_{pot}(0)$	$(\frac{\partial e_{pot}(0)}{\partial a})\Delta a$	$e_{vib}(T)$	$-Ts_{vib}(T)$	$\gamma(T)$
298	175,3	-34,0	4	-1,3	-25,6	118

In the case of quartz an estimate is made of the bond energy between two atoms and this together with a knowledge of the co-ordination number and bond density on the surface plane is used to calculate the surface energy. However, this semi-empirical method suffers from two drawbacks in the case of quartz. Firstly, by evaluating the bond energy from the free energies of formation of the various components as shown below we neglect all entropy and lattice relaxation contributions to the calculation of the surface energy. Secondly, as the Si-O bond is half ionic, one should not consider the bond as being between nearest neighbours only. It can be seen from the example above of KCl that the contributions to the surface energy arising from the relaxation and entropy terms will both lower the estimate of γ given by the bond energy calculation by approximately 35 per cent. The effect of the Si-O bond being partly ionic also implies that the estimate based on bond energies will be too high. Hence it may be concluded that the value of γ derived in this section will represent an upper limit to the actual value of γ.

	Free energy of formation at standard temperature. $\Delta H_{f\,0}$	
$Si(s) + O_2(g) \rightarrow SiO_2(\alpha\text{-quartz})$	$-879\ kJmole^{-1}$	1
$Si(g) \leftarrow Si(s)$	$-454\ kJmole^{-1}$	2
$2O(g) \leftarrow O(g)$	$-497\ kJmole^{-1}$	3
$Si(s) + 2O(g) \rightarrow SiO_2(s)$	$-1830\ kJmole^{-1}$	

The average energy of a Si-O bond in α-quartz is determined from the free energies of formation of the various compounds. Hence for four fold co-ordination, a single Si-O bond has a value of 458 $kJmole^{-1}$ or $7{,}63 \times 10^{-19}$J. The number of bonds per unit area in the $(1\bar{1}00)$ plane is given by Bloss and Gibbs (1963) as 7,56 bonds $(nm)^{-2}$. Since two new surface sites are formed when one bond breaks, the surface energy is thus equal to 2,88 Jm^{-2}.

---

1. Handbook of Chemistry and Physics (1970) p. D-49, (ed. R.C. Weast), The Chemical Rubber Co., Cleveland.
2. ibid p. F-162
3. ibid p. F-158

A P P E N D I X E

The measurement of crack velocities using Wallner lines is well known (Field, 1971), but workers who have used Wallner lines to determine crack velocities in crystalline materials have used planes of high symmetry in which the velocity of shear waves is isotropic (Hull and Beardmore 1966, Greenwood 1971). In order to include cases where the velocity of shear waves is anisotropic in the fracture plane, the analysis of Shand (1954) will be generalised.

Fig.29 shows a crack initiated at O and propagating from left to right in the plane of the paper. The state of stress responsible for the fracture is assumed to be uniform tension perpendicular to the fracture plane. This will allow the fracture front to diverge uniformly. When the crack front reaches a defect at S, the rapid change in stress at the point will result in the generation of an elastic disturbance. In general, three sheets of elastic waves will propogate from S. Consider one of them, travelling with velocity V_R, which has associated with it a component of particle displacement perpendicular to the fracture surface. This wave will modulate the crack front and a Wallner line will result. In general, the tangent to the wave front and the wave propagation direction will not be perpendicular, nor will the crack propagation direction be generally perpendicular to the crack front : let

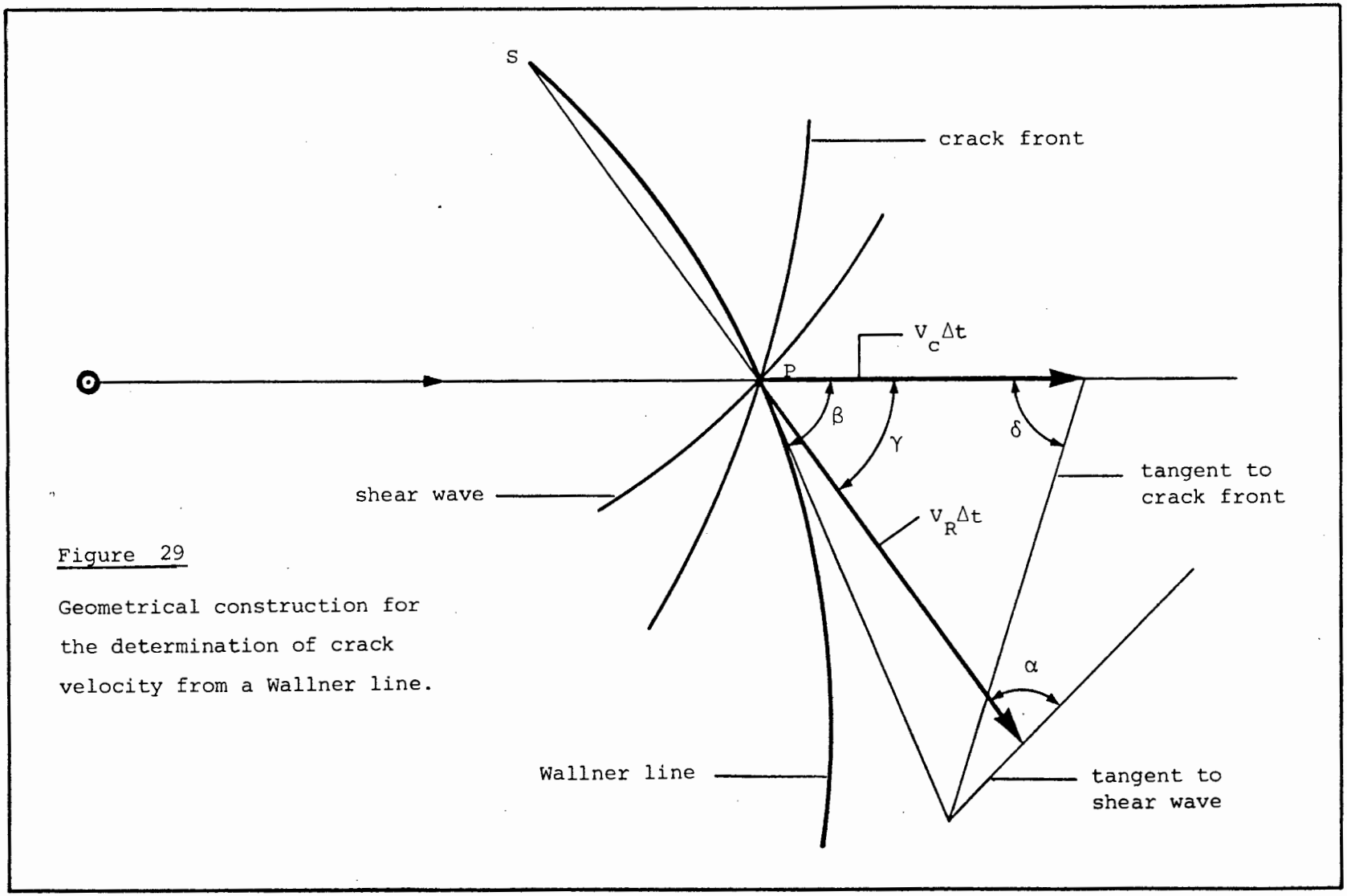

Figure 29

Geometrical construction for the determination of crack velocity from a Wallner line.

the angle between the tangent to the wave front and the wave propagation direction be α and the angle between the crack propagation direction and the crack front be δ as shown in fig.29. The velocity of the crack deduced from the geometrical construction shown in fig.29 is given by

$$V_C = V_R \frac{\sin(\beta + \delta)\sin\alpha}{\sin(\alpha + \gamma - \beta)\sin\delta} \qquad (E1)$$

Fracture along the YZ plane in α-quartz

The velocity of a sheet of elastic waves propagating from a point source (called the ray velocity $\underline{V_R}$) is given by Love (1892), Musgrave (1970) as

$$\underline{V_R} = (\partial v/\partial \nu_1 \ , \ \partial v/\partial \nu_2, \ \partial v/\partial \nu_3) \qquad (E2)$$

where v is the magnitude of the velocity of a plane wave propagating in a direction defined by the direction cosines ν_1, ν_2, ν_3. Geometrically (Musgrave, 1970), the ray velocity surface (called the wave surface) is the envelope of plane wave fronts with respect to the plane wave velocity surface (called the velocity surface).

The only tractable case occurs when

(i) one of the plane waves on the fracture surface is pure shear and has a particle displacement normal to the fracture surface and

(ii) the ray velocity corresponding to this pure shear wave also lies in the fracture plane. These two conditions will both occur if the plane is one of elastic symmetry (i.e. normal to a two-fold rotation axis). The YZ plane in α-quartz is one of elastic symmetry, although the crystal structure is not mirrored across this plane. (The contribution of the piezoelectric effect to the determination of ray velocities in α-quartz is small and will therefore be ignored.)

The direction cosines p_i for plane wave particle displacements are given by Love (1934) as

$$p_1 (\Gamma_{11} - \rho v^2) + p_2\Gamma_{12} + p_3\Gamma_{13} = 0$$
$$p_1\Gamma_{12} + p_2 (\Gamma_{22} - \rho v^2) + p_3\Gamma_{23} = 0$$
$$p_1\Gamma_{13} + p_2\Gamma_{23} + p_3(\Gamma_{33} - \rho v^2) = 0$$

where ρ is the density of the material and the Γ_{ij} are quadratic functions of the direction cosines ν_i and depend on the elastic stiffness constants c_{ij}. In the case of the YZ plane in α-quartz the above equations become

$$p_1\Gamma_{11} = p_1\rho v^2 \qquad \text{(E3)}$$
$$p_2\Gamma_{22} + p_3\Gamma_{23} = p_2\rho v^2$$
$$p_2\Gamma_{23} + p_3\Gamma_{33} = p_3\rho v^2$$

where $\Gamma_{11} = c_{66}\nu_2^2 + c_{44}\nu_3^2 + 2c_{14}\nu_2\nu_3$

If $v^2 = \Gamma_{11}/\rho$ (E4)

is taken as a solution to equation (E3), then the plane wave is polarised in the X direction and is therefore the one of interest. (Since the particle displacement vectors are orthogonal, the other two waves are polarised in the fracture plane and hence do not interfere with the fracture front.) The ray velocities also lie in the plane and therefore the one corresponding to the pure shear wave can be obtained from equation (E4) as

$$\partial v/\partial \nu_2 = (c_{66}\nu_2 + c_{14}\nu_3)/\rho v$$

$$\partial v/\partial \nu_3 = (c_{44}\nu_3 + c_{14}\nu_2)/\rho v$$

Let θ be the anticlockwise angle from the Y axis to the X asis, then $\nu_1 = 0$, $\nu_2 = \cos\theta$ and $\nu_3 = \sin\theta$. If we write $\underline{V_R}$ in polar form $\underline{V_R} = (V_R, \eta)$ and set the sense of η the same as that of θ, then

$$\tan\eta = \frac{\partial v/\partial \nu_3}{\partial v/\partial \nu_2} = \frac{c_{44}\tan\theta + c_{14}}{c_{66} + c_{14}\tan\theta}$$

$$\text{hence} \quad \tan\theta = \frac{c_{14} - c_{66}\tan\eta}{c_{14}\tan\eta - c_{44}} \qquad \text{(E5)}$$

V_R can then be found as a function of η from equation (E5) and

$$V_R^2 = \frac{1}{\rho^2 v^2}\{\cos^2\theta(c_{66}^2+c_{14}^2) + \sin^2\theta(c_{14}^2+c_{44}^2) \qquad \text{(E6)}$$

$$+ 2\sin\theta\cos\theta(c_{66}c_{14}+c_{44}c_{14})\}$$

Fig.30 shows the velocity and wave surfaces of the shear wave polarised in the X direction and the relation between the tangent to the wave surface and the direction of the ray and plane wave velocities. Hence α is given by

$$\alpha = \eta + \pi/2 - \theta$$

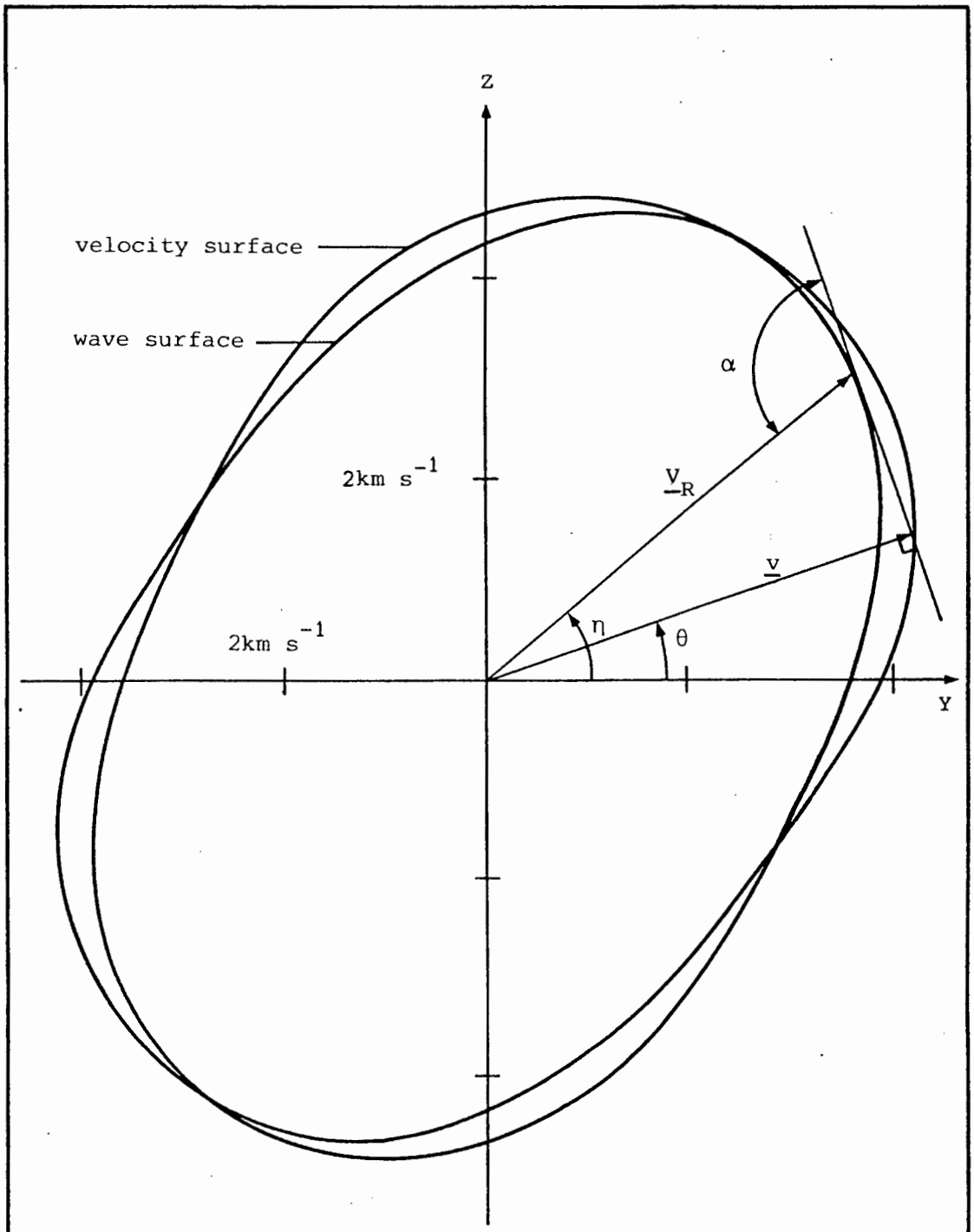

Figure 30

Velocity and wave surface for the X polarised shear wave in the YZ plane of α-quartz, showing the relationship between a tangent to the ray surface and a point on the wave surface.

A P P E N D I X F

A solution, giving the size of the contact area as a function of load for the general case of two elastic bodies in contact as developed by Hertz is given in Timoshenko and Goodier (1970).

If the two bodies have principal radii of curvature R_1, R_1' and R_2, R_2' at the tangent plane of the point of contact, then the contact area will be an ellipse with semi-axes a and b given by

$$a = m \left(\frac{3\pi}{4} \frac{L(k_1+k_2)}{A+B}\right)^{\frac{1}{3}}$$

and $$b = \frac{n}{m}a$$

where L is the applied load and $k_1 = \frac{1-\nu_1^2}{\pi E_1}$ and $k_2 = \frac{1-\nu_2^2}{\pi E_2}$

$$A + B = \tfrac{1}{2}\left(\frac{1}{R_1} + \frac{1}{R_1'} + \frac{1}{R_2} + \frac{1}{R_2'}\right)$$

and $$A - B = \tfrac{1}{2}\left[\left(\frac{1}{R_1} - \frac{1}{R_1'}\right)^2 + \left(\frac{1}{R_2} - \frac{1}{R_2'}\right)^2 + 2\left(\frac{1}{R_1} - \frac{1}{R_1'}\right)\left(\frac{1}{R_2} - \frac{1}{R_2'}\right)\cos 2\psi\right]^{\frac{1}{2}}$$

where Ψ is the angle between the normal planes containing the curvatures $1/R_1$ and $1/R_2$. The coefficients m and n are determined form the ratio of B - A to B + A and the result is given in a table by Timoshenko. In the present case $R_1 = 75\mu m$, $R_1' = 310\mu m$ and

$$\frac{1}{R_2} = \frac{1}{R_2'} = 0$$

If we choose average values of elastic modulii for diamond and quartz as below, then we obtain the values

$$b = 0.63 \times 10^{-5} L^{\frac{1}{3}} \quad \text{and} \quad a = 2.6b$$

where b is measured in metres and L in Newtons

Quartz : $E_1 = 10^{11} Nm^{-2}$, $\nu_1 = 0.25$

Diamond : $E_2 = 8 \times 10^{11} Nm^{-2}$, $\nu_2 = 0.3$

A P P E N D I X G

Evaluation of the friction force arising from fracturing in the damage zone

The elastic energy released when the indenter moves forward on the surface may be calculated as follows. The elliptical area of contact on the surface is approximated by a rectangle of dimensions 2a by 2b where a and b are the semi-axes of the ellipse. The elastic energy transfered through this area is given by $\frac{1}{2}L\delta$ where L is the load applied to the indenter and δ is the distance the indenter moves below the surface of the material. (As diamond has a much higher Young's modulus than quartz this expression should be accurate). If the indenter were to move a distance 2a, the elastic energy would be released behind the indenter and would appear under the present position of the rectangle. If all of this elastic energy was transformed into an amount of surface energy $\gamma_f A$ where A is the total area of new surface created, then the friction force F would do an amount of work $F2a = \frac{1}{2}L\delta$ each time the indenter moved a distance 2a. Therefore the coefficient of friction is:-

$$\mu_f = \frac{F}{L} = \frac{\delta}{4a}$$

From the Hertzian analysis it was found that $a = 2.6b$ where b is now regarded as the half width of the track.

For a circular form of the cross section of the indenter

$$2r\delta \simeq b^2$$

where r is the radius of the circular cross section.

Hence $\mu_f \simeq \frac{b}{20r}$

For a Hertzian indenter $b \propto L^{\frac{1}{3}}$ and hence μ_f is expected to increase with load. However, at a load of 9.8N, $b \simeq 30\mu m$ and r is $75\mu m$, so that $\mu_f \simeq 0.02$, whereas the actual value of the coefficient of friction at this load is 0.2.

ACKNOWLEDGEMENTS

It is a great pleasure to express my appreciation to those who have been so helpful in the preparation of this thesis.

I am greatly indebted to Professor A. Ball for his invaluable assistance, his interest and encouragement, as well as the many stimulating discussions, during my research.

I wish to thank Dr. E.D.F. Williams for his generous assistance given in electron microscopy.

Many thanks are also due to Ms. S. Payne, Mr. I. Charvat and Mr. A. Kanellopoulos for their help in the final stages of this thesis.

REFERENCES

Baëta, R.D., and Ashbee, K.H.G., (1970), Phil. Mag., 22, 601

Baëta, R.D., and Ashbee, K.H.G., (1973), Phys. Stat. Sol. (a), 18, 155

Ball, A., and Payne, B.W., (1976), J. Mater. Sci., 11, 731

Berry, J.P., (1960), J. Mech. Phys. Solids, 8, 194

Blakely, J.M., (1973), Introduction to the Properties of Crystal Surfaces, Pergamon Press, Oxford

Bloss, F.D., and Gibbs, G.V., (1963), Am. Mineral.,48, 821

Bonse, U., Hart, M. and Schwuttke, G.H., (1969), Phys. Stat. Sol., 33, 361

Bowden, F.P., and Brookes, C.A., (1966), Proc. Roy. Soc., A295, 244

Bowden, F.P., and Hanwell, A.E., (1966), Proc. Roy. Soc., A295, 233

Bowden, F.P., and Tabor, D., (1964a), The Friction and Lubrication of Solids, Part II, Oxford University Press, Oxford

Bowden, F.P., and Tabor, D., (1964b) ibid Part I

Brace, W.F., (1963), J. Geology, 71, 581

Broberg, K.B., (1960), Arkiv Fysik, 18, 159

Broberg, K.B., (1972), Proceedings of an International Conference on Dynamic Crack Propagation, ed. G.C. Sih, p.461, Noordhoff, Leyden

Brown, W.F., and Srawley, J., (1966), ASTM STP No. 410

Burridge, R., (1976), Int. J. Engng. Sci., 14, 725

Byerlee, J.D., (1967), J. Appl. Phys., 38, 2928

Cady, W.G., (1946), Peizoelectricity, McGraw-Hill, New York

Charles, R.J., (1958), J. Appl. Phys., 29, 1549

Clark, A.B.J. and Irwin, G.R., (1966), Expl. Mech., 6, 321

Clarke, B. and Kitchener, J.A., (1968), Br. Chem. Eng. 13,991

Congleton, J. and Petch, N.J., (1967), Phil. Mag., 16, 749

Cordwell, J.E., and Hull, D., (1969), Phil. Mag., 19, 951

Eremenko, V.G., and Nikitenko, V.I., (1972), Phys. Stat. Sol. (a), 14, 317

Eshelby, J.D., (1969) J. Mech. Phys. Solids, 17, 177

Evans, A.G., (1972), J. Mater. Sci., 7, 1137

Field, J.E., (1971), Contemp. Phys., 12, 1

Frank, F.C. and Lawn, B.R., (1967), Proc. Roy. Soc., A299, 291

Freund, L.B., (1972), J. Mech. Phys. Solids, 20, 141

Frondel, C., (1962), Dana's System of Mineralogy, Vol.3, John Wiley and Son, New York

Galileo, (1638), Two New Sciences, translated by Crew, H. and De Salviro, A., (1933), Macmillan, New York

Gevers, R., (1962), Phil. Mag., 7, 1681

Goodier, J.N.,(1968), Fracture - an Advanced Treatise, Vol.2, ch.1, ed. H. Liebowitz, Academic Press, London

Goodier, J.N., and Kanninen, M., (1966) discussed in Fracture - an Advanced Treatise, Vol.2, (1968), ch.1, ed. H. Liebowitz, Academic Press, New York

Graham, J., (1972), Rock Mech., 4, 191

Greenwood, J.H., (1971), J. Mater. Sci., 6, 390

Griffith, A.A., (1920), Phil. Trans. Roy. Soc. A221, 163

Gruver, R.M., and Kirchner, H.P., (1974), J. Am. Ceram. Soc., 57, 220

Hamilton, G.M., and Goodman, L.E., (1966), Trans. A.S.M.E. J. Appl. Mech., 33, 371

Heavens, J.W., and Ashbee, K.H.G., (1975), J. Mater Sci., 10, 1938

Hill, M.J., and Rowcliffe, D.J., (1974), J. Mater Sci., 9, 1569

Hirsch, P.B., Howie, A., Nicholson, R.B., Pashley, D.W. and Whelan, M.J., (1965), Electron Microscopy of Thin Cyrstals, Butterworths, London

Hockey, B.J., (1971), J. Am. Ceram. Soc., 54, 223

Hockey, B.J., and Lawn, B.R., (1975), J. Mater. Sci., 10, 1275

Hull, D., and Beardmore, P., (1966), Int. J. Frac. Mech., 2, 468

Inglis, C.E., (1913), Trans. Inst. Naval Archit., 55, pt.I, 219

Irwin, G.R., (1958), Handbuch der Physik, Vol.6, P.551, ed. Flügge, S., Springer-Verlag, Berlin

Johnson, J.W. and Holloway, D.G., (1966), Phil. Mag., 14, 731

Johnson K.L., O'Conner, J.J., and Woodward, A.C., (1973) Proc. Roy. Soc., A334, 95

Keer, L.M., and Freedman, J.M., (1973), Int. J. Engng. Sci., 11, 1265

Kirchner, H.P., Gruver, R.M., and Sotter, W.A., (1976) Phil. Mag., 33, 775

Kostrov, B.V., (1975), Int. J. Frac. 11, 47

Küppers, H.,(1967), Int. J. Frac. Mech., 3, 13

Lawn, B.R., (1967), Proc. Roy. Soc., A299, 307

Lawn, B.R., (1968), J. Appl. Phys., 39, 4828

Lawn, B.R., and Komatsu, (1966), Phil. Mag., 14, 689

Lawn, B.R., and Swain, M.V., (1975), J. Mater. Sci., 10, 113

Lekhnitskii, S.G., (1963), Theory of Elasticity of an Anisotropic Elastic Body, Holden-Day, San Francisco

Linger, K.R., and Holloway, D.G., (1968), Phil. Mag., 18, 1269

Love, A.E.H., (1892), A Treatise on the Mathematical Theory of Elasticity, Cambridge University Press Cambridge

Love, A.E.H., (1934), ibid 4th ed.

Macmillan, N.H., Huntington, R.D., and Westwood, A.R.C., (1974), J. Mater. Sci., 9, 697

McLaren, A.C., and Retchford, J.A., (1969), Phys. Stat. Sol., 33, 657

McPherson, R., (1973), Wear, 23, 83

Mills, J.J., Huntington, R.D. and Westwood, A.R.C., (1976), Int. J. Rock Mech. Min. Sci. & Geomech. Abstr., 13, 289

Mott, N.F., (1948), Engineering, 165, 16

Musgrave, M.J.P., (1970), Crystal Acoustics, Holden-Day

Orowan, E., (1949), Rep. Prog. Phys., 12, 185

Orowan, E., (1955), Weld. J. Res. Supp., 34, 157-s

Preston, F.W., (1922), Trans. Op. Soc., 23, 10

Rajapakse, Y.D.S., (1975), Int. J. Frac., 11, 57

Rice, J.R., (1968), Fracture - an Advanced Treatise, Vol.2, ch.3, ed. H. Liebowitz, Academic Press, New York

Roberts, D.K., and Wells, A.A., (1954), Engineering, 178, 820

Schoening, F.R.L., (1960), J. Appl. Phys. 31, 1779

Scholz, C.H., and Martin III, R.J., (1971), J. Am. Ceram. Soc., 54, 474

Seal, M., (1958), Proc. Roy. Soc., A248, 379

Shand, E.B., (1954), J. Am. Ceram. Soc., 37, 52

Sih, G.C., Paris, P.C. and Irwin, G.R., (1965), Int. J. Frac. Mech., 6, 189

Sih, G.C., and Liebowitz, H., (1968), Fracture - an Advanced Treatise, Vol.2, ch.2, ed. H. Liebowitz, Academic Press, New York

Sinclair, J.E., and Lawn, B.R., (1972), Proc. Roy. Soc. A329, 83

Smith, G.H. and Burge, R.E., (1962), Acta. Cryst., 15, 182

Swain, M.V., Williams, J.S., Lawn, B.R., and Beek, J.J., (1973), J. Mater. Sci., 8, 1153

Timoshenko, S.P., and Goodier, J.N., (1970), Theory of Elasticity, 3rd ed., McGraw-Hill, New York

Voltmer, F.W., Ippen, E.P., White, R.M., Lim, T.C., and Farnell, G.W., (1968), Proc. IEEE, 56, 1634

Westwood, A.R.C., (1974), J. Mater. Sci., 9, 1871

Wiederhorn, S.M. and Bolz, L.H., (1970), J. Am. Ceram. Soc., 53, 543

Wigglesworth, L.A., (1957), Mathematika, 4, 76

Wilshaw, T.R., (1971), J. Phys. D, 4, 1567

Yoffe, E.H., (1951), Phil. Mag., 42, 739

JOURNAL OF MATERIALS SCIENCE 11 (1976) 731–740

The tensile fracture of quartz crystals

A. BALL, B. W. PAYNE
Department of Metallurgy and Materials Science, University of Cape Town, South Africa

Quartz crystals of five orientations have been fractured in tension at temperatures below 800 K in air and water-free environments. The radius of the initial crack nucleus determines the fracture stress which, in turn, controls the velocity–distance relationship. The unusual fractography is described in which fracture occurs predominantly along facets of the rhombohedral planes and requires a surface energy of 2 J m^{-2}.

1. Introduction

The purity, perfection and the resistance to plastic flow at low temperatures make synthetic α-quartz crystals ideal for the investigation of brittle fracture. The chemical similarities with glass allow a close comparison between fracture behaviour of crystalline and amorphous solids. An examination of the fracture behaviour of quartz is valuable from the technological point of view since quartz provides an important electrical device material and the mining of minerals often involves the blasting, cutting and comminution of quartzite. Studies of the plastic deformation by the uniaxial compression of single crystals of quartz have confirmed that dislocation generation and movement are only possible under atmospheric pressure at temperatures above 820 K [1]. However, plastic flow has been induced at lower temperatures (~600 K) if a superimposed hydrostatic pressure prevents fracture [2]. A number of workers have examined the fracture of single crystals during compression and indentation [3–5] and a statistical investigation of cleavage was made by Bloss and Gibbs [6]. These have led to the conclusion that quartz possesses no distinct cleavage plane although a preference was shown for fracture along the positive and negative rhombohedron planes, $\{1\,0\,\bar{1}\,1\}$ and $\{0\,1\,\bar{1}\,1\}$ repectively. The present paper describes the fracture behaviour of quartz crystals tested in tension and the known influence of water on the fracture of silica glass [7, 8] suggested that the investigation of quartz should be made as a function of environment.

2. Experimental

Single crystals of synthetic and natural quartz were sliced with a diamond saw into specimens with five distinct crystallographic orientations (Fig. 1) and with dimensions 60 mm × 10 mm × 1 mm. After polishing the surfaces with 1 μm alumina, approximately 1 mm deep notches were cut in the narrow faces at the mid-point of the specimens with a 0.05 mm thick annular diamond saw. The cutting pressure was very small and care was taken to avoid vibrational and distortional stresses. The diamond grit of the cutting wheel was quoted by the manufacturers to be less than 60 μm. The end of the notch was square but scanning electron microscopy revealed the presence of

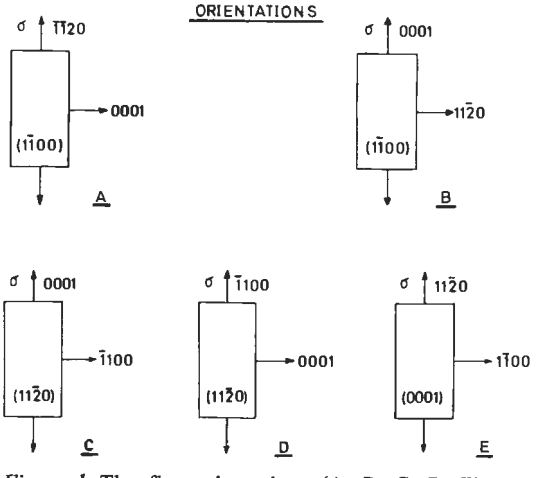

Figure 1 The five orientations (A, B, C, D, E) of the crystals which were fractured by a tensile stress applied in the direction of the long edges.

fine cutting grooves. Sharp notches of starting cracks were produced in a number of specimens by thermal shock treatments.

The specimens were mounted on freely rotating gimbal attachments of the tensile machine using "Eastman's 910" adhesive for tests at ambient temperatures and below, and "Aremco Ceramacoat 512" ceramic adhesive for the elevated temperature tests. The experiments were carried out under liquid nitrogen at 77 K, water-free toluene for temperatures up to room temperature, and in a vacuum of better than 10^{-4} mm Hg for room temperature and above. The temperature of the toluene was attained by passing liquid nitrogen around the copper container and the elevated temperatures *in vacuo* were obtained by a resistance wire furnace. A number of room temperature tests were performed in air. In order to test the influence of water at the notch tip prior to testing, several specimens were out-gassed in a vacuum of better than 10^{-5} mm Hg at 473 K for 24 h and then mounted, without exposing the notch to the atmosphere, and tested under toluene. All tests were carried out in uniaxial tension at a strain-rate of approximately 7×10^{-5} sec^{-1}. The load at fracture was recorded and the original notch lengths to the point of bifurication were measured by photographing at a magnification of x 100. The fracture surfaces were examined by both optical and scanning electron microscopy. Fine features such as Wallner lines were photographed by optical differential interference techniques.

The velocity of crack propagation was determined by the resistance grid method and by an analysis of Wallner lines which included the effects of crystal anisotropy [9] (see Field [10] for a discussion of these methods). A grid of 36 lines of "Nichrome" was vapour deposited perpendicular to the expected fracture path. The line at the tip of the notch acted as a trigger for the recording oscilloscope and the remaining lines were connected to a circuit which differentiated the sudden change in voltage as each line of the grid was broken during crack propagation. The piezoelectric quartz crystals develop electric charges on their surfaces on account of strain changes which occur during fracture. In order to avoid the interference of this effect with the resistance grid signals, crystals of orientation E (Z cut) were chosen for these velocity experiments. The crystal symmetry of this orientation is such that piezoelectric charges are not developed on the specimen faces on which the resistance grids were deposited.

3. Results and discussion

3.1. Fracture strength

The results of the tensile tests performed *in vacuo* or toluence are presented in Fig. 2; the product of the stress at fracture σ_f and the square root of the initial notch or crack length (c_0) is plotted as a function of temperature. Included in the same figure are values of the product of the fracture stress and square root of the crack length at the point of branching (c_b) for those specimens in which the crack bifurcated. The majority of the values fall between the curves which have been drawn and it can be seen that the temperature dependencies of $\sigma_f c_0^{\frac{1}{2}}$ and of $\sigma_f c_b^{\frac{1}{2}}$ show plateaux

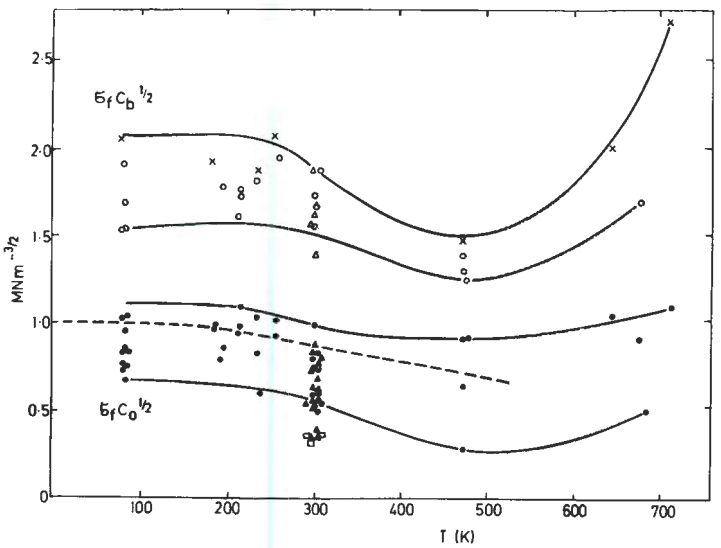

Figure 2 The temperature dependence of the fracture stess σ_f expressed as the products $\sigma_f c_0^{1/2}$ (closed circles) and $\sigma_f c_b^{1/2}$ (open circles) where c_0 is the initial notch length and c_b is the crack length at the point of crack bifurcation. The points (marked X) are values of $\sigma_f c_b^{1/2}$ for specimens of orientation C (see Fig. 1). The results for the "sharp" cracks are shown by squares (□) and the results for experiments performed in air are shown by triangles (△, ▲). The broken line represents the value of σ_f/σ_f^0 given by the theoretical model of Gilman [17] (see text).

at low temperatures and minima around 500° K. The ratio $\sigma_f c_b^{\frac{1}{2}}/\sigma_f c_0^{\frac{1}{2}}$ has a value of about 2. The average of $\sigma_f c_0^{\frac{1}{2}}$ for specimens tested in air at room temperature was found to be 0.60 MN m$^{-3/2}$ and is somewhat lower than that for specimens tested in toluene or *in vacuo*. The value of 0.35 MN m$^{-3/2}$ was found for the specimens containing sharp thermally induced cracks and tested in toluene at room temperature. There was no systematic influence of de-gassing the quartz specimens before testing and no significant difference in value obtained for synthetic and natural quartz crystals.

In view of the dependence of the fracture stress on the length and sharpness of the initial notch, the following treatment for the estimation of the surface energy for fracture is appropriate. For fracture to occur, the Griffith energy criterion $\sigma_f \geqslant (2E\gamma/\pi c_0)^{\frac{1}{2}}$ must be satisfied and, in addition, the concentrated stress at the tip of the crack $[2\sigma_f(c_0/r)^{\frac{1}{2}}$ where r is the radius of the initial crack tip] must exceed the theoretical bond strength given approximately by $(E\gamma/a)^{\frac{1}{2}}$, where E is Young's modulus, γ is the surface energy and a is the equilibrium separation of atoms. The observed fracture stress should, therefore, be given by

$$\sigma_f \simeq (E\gamma r/4ac_0)^{\frac{1}{2}}. \quad (1)$$

Thus a crack with a tip radius of about 2.5a corresponds to spontaneous crack growth according to the Griffith equation. Cracks which are initially blunt will require an overstress for the process of sharpening to a Griffith crack. This overstress will result in an excess of strain energy in the specimen and a large dissipation as kinetic energy when fracture occurs.

The sharp cracks introduced by thermal shock in the quartz crystals will have tip radii approaching atomic dimensions and the measured value of $\simeq$0.35 MN m$^{-3/2}$ for $\sigma_f c_0^{\frac{1}{2}}$ for these specimens gives a surface energy of approximately 2 J m^{-2} when the mean value of 100 GN m^{-2} for E is used in the Griffith equation. This value of surface energy agrees quite well with values calculated from bond energy data. The energy of the Si–O bond has an experimentally determined value of 36.8×10^4 J mol^{-1} [11]; thus the bond energy four-fold co-ordination is 6.2×10^{-19} J. The number of bonds per square metre lies in the range 6 to 8×10^{18} for the low index planes of quartz and hence surface energy values between 1.8 and 2.4 J m^{-2} are expected. Using a mean value of 2 J m^{-2} for γ and the experimental values of $\sigma_f c_0^{\frac{1}{2}}$ for the notched specimens, Equation 1 indicates that the crack nuclei on the notches have radii between 5a and 20a. The finer edges of the diamonds on the cutting wheel can reasonably be expected to produce grooves with radii of this size. Since the details of the crack tip geometry determine the fracture stress, the random variation of the parameter r from specimen to specimen is expected to mask any systematic variation in elastic modulus and surface energy due to crystal orientation or the difference between synthetic and natural crystals. The range of values of $\sigma_f c_0^{\frac{1}{2}}$ shown in Fig. 1 for any given temperature is, therefore, due to the range of r for the specimen.

The tendency for the notched specimens which are tested in the presence of water vapour, to fracture at lower stress values suggests that water vapour assists the sharpening of the initial cracks in the presence of an applied stress. The presence of water vapour in the notch before testing does not sharpen the cracks since a prior de-gassing treatment does not lead to a significant difference in fracture stress on subsequent testing in toluene or *in vacuo*. It is also improbable that the presence of water vapour during the test lowers the fracture stress through a lowering of the surface energy since the gaseous diffusion rate is less than the crack velocity [8].

The temperature dependence of $\sigma_f c_0^{\frac{1}{2}}$ and $\sigma_f c_b^{\frac{1}{2}}$ (Fig. 2) cannot be ascribed in full to the temperature dependence of interatomic forces which would be reflected by the values of the elastic constants and surface energy. The maximum decrease in the measured values of Young's modulus between 100 and 500 K is only 6% [12], whereas the value of $\sigma_f^2 c_0$ decreases by approximately 30%. Moreover, the modulus decrease is continuous while the fracture stress becomes independent of temperature below about 200 K. Above 500 K the elastic modulus continues to decrease in contrast to the observed increase in fracture stress. Fracture stress values have been measured as a function of temperature for other brittle materials by previous authors and minima have also been observed. (See [13] for a discussion.) The reduction of temperature sensitivity at low temperatures has also been noted [14, 15]. Since the stress for fracture is determined by the geometry or sharpness of the initial notch, the source of the observed temperature dependence must be sought in a mechanism of crack sharpening or, in the case of fracture at

temperatures above the minimum, in the mechanism of crack blunting. Congleton *et al.* [16] explained the temperature dependence of the stress required for the fracture of alumina in terms of localized plastic flow at the crack tip. They argued that at lower temperatures dislocation slip or twinning might somehow be necessary for fracture propagation and thus the thermal activation of these processes would account for the experimental fracture behaviour. Our electron microscopy and X-ray topography studies have provided no evidence for such a mechanism in quartz, although it is recognized that the localized nature of the plastic flow would make confirmation difficult. However, any conventional thermal activation theories would predict a linear increase in fracture stress with decreasing temperatures and not the observed diminshing temperature sensitivity with decreasing temperature. Gilman [17] has suggested that low temperature brittle fracture can proceed by stress activated "tunnelling of the atomic bonds" at the crack tip. The increase in temperature reduces the average height of the energy barrier and an equation

$$\sigma_f/\sigma_f^0 = [1 - B \coth (\theta/2T)] (1 - B)^{-1}$$

is derived which describes the dependence of temperature (T) of the fracture stress σ_f in relation to the fracture stress σ_f^0, at 0 K. The characteristic Debye temperature θ is related to the magnitude of the energy barrier in the presence of a stress U_m by the expression $B = k\theta/2U_m$ where k is Boltzmann's constant. This equation successfully accounts for the form of the temperature dependence at low temperature of the fracture stress of Al_2O_3 filaments. The dashed line of Fig. 2 shows that observations on quartz fit such an expression when a reasonable value of $U_m = 0.1$ eV ($\sim 1.6 \times 10^{-20}$ J) is taken and $\theta = 470$ K. A stress-activated crack sharpening mechanism based on this theory may, therefore, be applicable and the stress required to sharpen a crack of a given radius to the Griffith radius will be temperature dependent in the manner observed. The presence of water at the crack tip must reduce the magnitude of the energy barrier U_m in the presence of a stress. The stress induced hydrolysis of the Si–O bonds at the tip of the crack is probably responsible for the reduced barrier.

The increase in fracture stress above 500 K is likely to be due to an increasing amount of plastic blunting by the action of the high stress concentration at the initial notch, since general macroscopic plastic deformation has been observed in uniaxial compression [1. 2] at 600 K and evidence for dislocation generation and movement was given in both publications.

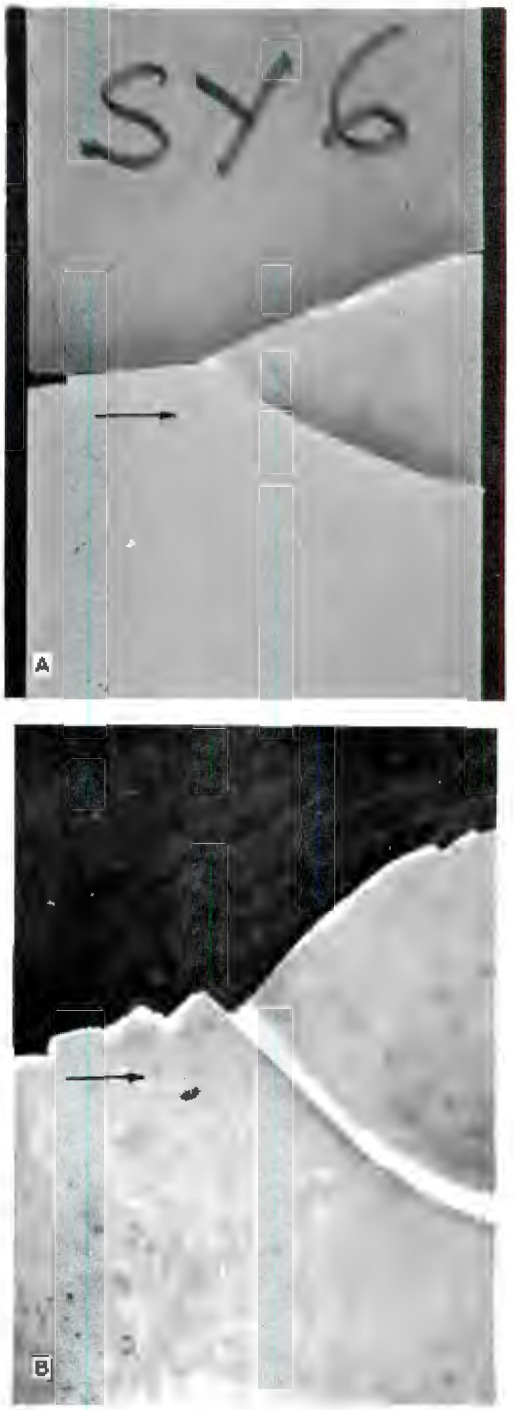

Figure 3 Typical fracture paths across the 10 mm wide faces of the specimens of the five orientations (A, B, C, D, E).

3.2. Fractography

The existence of a low energy cleavage plane in α-quartz was indicated by the behaviour of crystal wafers when subjected to thermal shock treatments. Fracture occurs by planar cleavage along a rhombohedral plane across the width of the plates. However, when tested in tension the fracture surfaces are not always planar and their exact form is determined by the direction along which the tensile force is applied, the anisotropy of surface energies for crystal planes and the magnitude and shape of the dynamic stress field at the tip of the moving crack. The detailed consideration of these influences will be subject of a future communication. Here we merely present the experimental findings.

Fracture paths, typical for each of the five crystal orientations of Fig. 1, are shown in the photographs of Fig. 3. Fracture surfaces are presented in Fig. 4. The specimens of orientations A to D are similar in that their fractures show initial flat mirror-like regions, which acquire steps or zig-zags of increasing size. If the fracture stress is sufficiently high, then the cracks subsequently bifurcate. Thus, the specimens which fractured in air or from sharp cracks at low stress values have less tendency to zig-zag or bifurcate. The cracks which propagate in a zig-zag fashion do so on two planes equally inclined to the stress axis and the size of the steps increases systematically until the fracture is completed or bifurcation occurs. If bifurcation eventuates, the branch cracks propagate on the same planes on which the zig-zag propagation occurred; this has enabled a crystallographic identification of these planes to be made.

Analysis of these planes on many specimens of

Figure 3 continued.

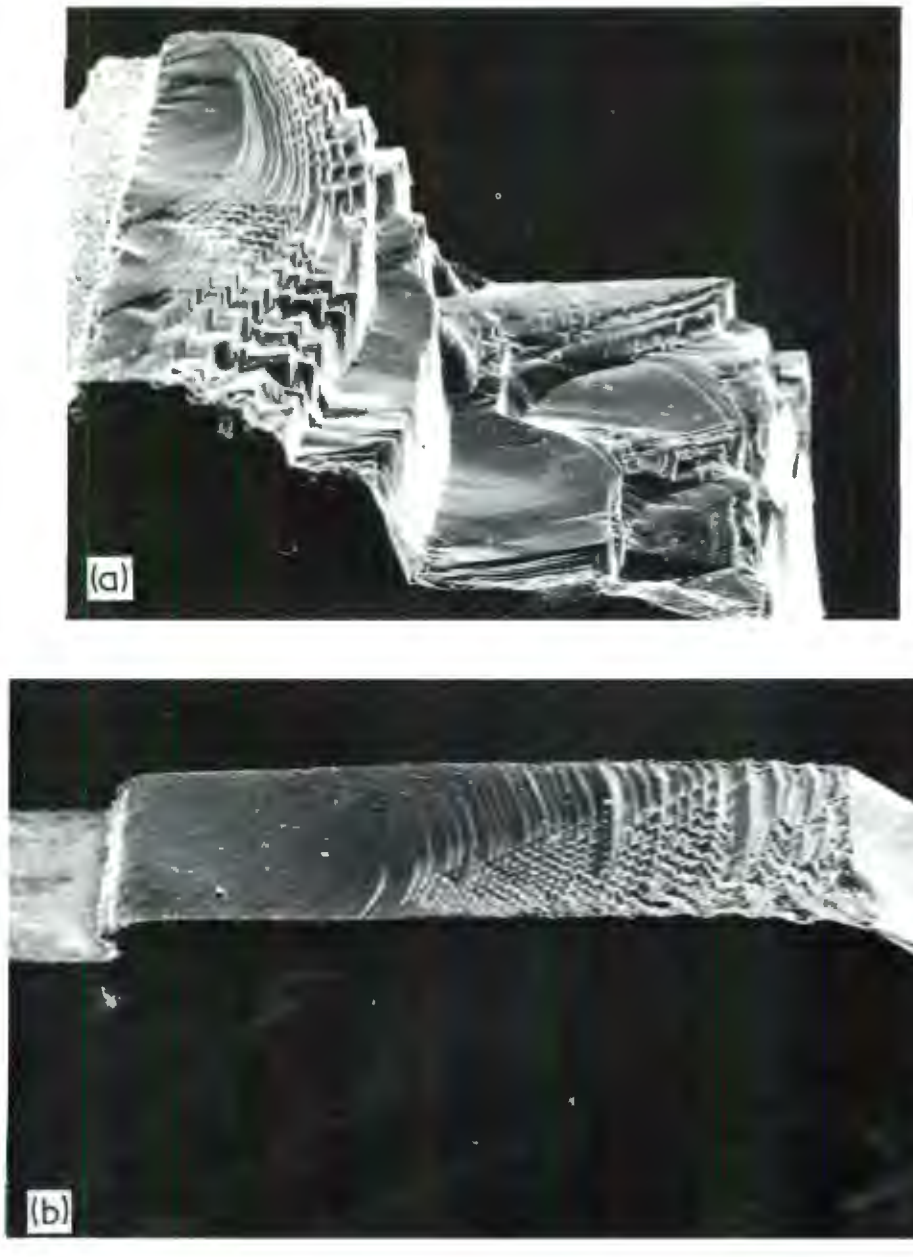

Figure 4 Fracture surfaces typical of specimens of orientations (a) B (× 100),(b) C (× 20), (c) C (× 135), (d) E (× 56). The surface of crystal E shows Wallner lines together with the values obtained for crack velocity expressed as fractions of the shear velocity (~3.8 km sec^{-1}).

each orientation A to D has been made with the aid of stereographic projections. Within the experimental error of the Laué determinations of the crystal orientations, the zig-zag and bifurcation planes can be rationalised in terms of cleavage on the rhombohedral planes. The results thus confirm previous indications [6] that quartz does possess a preferred cleavage plane, although it is very apparent from our experiments that the detailed stress field at the crack tip has an important influence.

Crystals of orientations E never fractured in a zig-zag manner and well defined bifurcation was not observed. Failure occurred in a planar fashion along the $(1\,1\,\bar{2}0)$ plane normal to the tensile axis. Even propagation from small, blunt notches at high stresses failed to promote steps or coherent crack branching of these specimens. The fracture

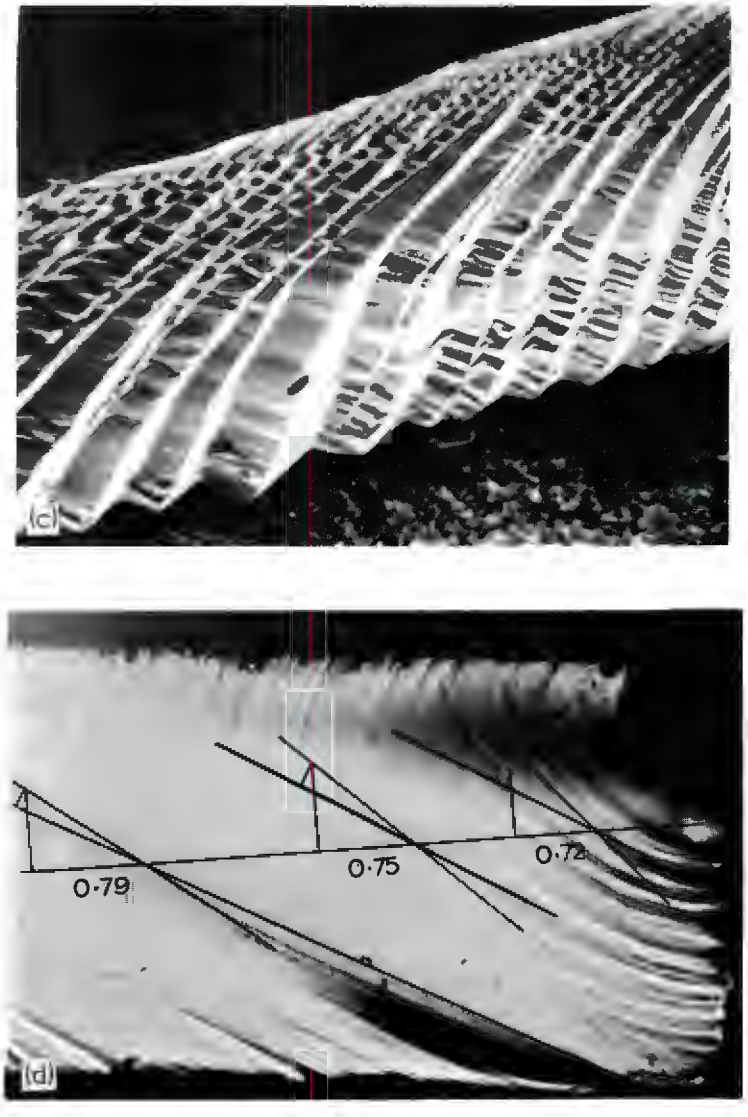

Figure 4 continued

surfaces are very like those of glass broken in tension in that they contain mirror and hackle regions. In addition, they display the Wallner lines (Fig. 4d) in the initial mirror regions which have been used to obtain fracture velocity data for this orientation. The $(1\,1\,\bar{2}0)$ fracture plane for this orientation is a flat maximum with regard to number of Si–O bonds per unit area [6] and has been reported as a very minor cleavage plane [18, 19]. The planar fracture normal to the applied stress and the glass-like behaviour of crystals of this orientation (E) must, therefore, be a consequence of the unsuitable orientation of the preferred rhombohedral cleavage planes with respect to the stress axis.

3.3 The velocity of fracture

The crack velocity, as obtained by the resistance grid method from a specimen of orientation E, is shown as a function of crack length c in Fig. 5. The solid line represents a least squares fit to the equation

$$V = V_m + d_1 (c_0/c) + d_2 (c_0/c)^2 ,$$

where the constants V_m, d_1 and d_2 determine the shape of the curve and are such that the curve passed through the point $(c_0/c = 1, V = 0)$. Fracture velocities obtained from an analysis of Wallner lines on the same specimen are also shown in this figure. The results of the two independent methods show an excellent agreement.

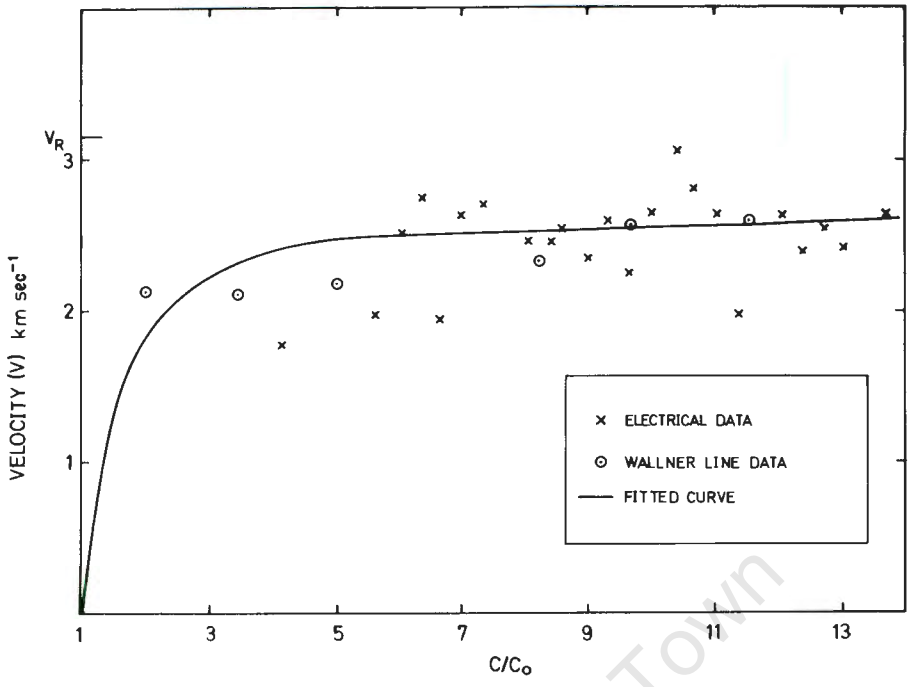

Figure 5 The velocity–distance relationship obtained by both the electrical method and an analysis of Wallner lines for a specimen of orientation E.

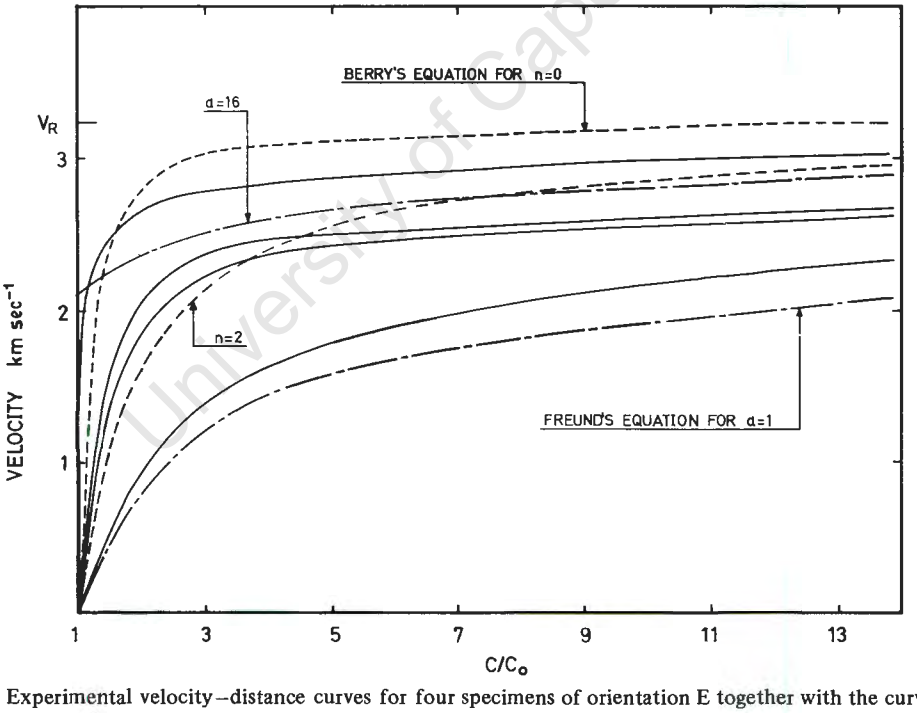

Figure 6 Experimental velocity–distance curves for four specimens of orientation E together with the curves predicted by the theories of Berry [20] and Freund [25].

Fig. 6 shows the smooth curves drawn through the data obtained by both experimental methods for four crystals of orientation E. The curves have the same form, but have different initial slopes corresponding to different accelerations. This difference can be explained by considering the sharpness of the tips of the initial notches. The applied tensile stress required to propagate an atomically sharp crack has a magnitude predicted by the Griffith theory. However, if the notch is blunt, a

stress larger than the Griffith stress is required for fracture and thus the specimen acquires a greater amount of strain energy prior to crack propagation. This strain energy is released as surface and kinetic energies when fracture occurs in a brittle quartz crystal. Hence a crack, propagating from a blunt notch will have a greater acceleration than a crack propagating from a sharp notch and the terminal velocity will be approached within a shorter distance. Berry [20] formulated a theory which describes the velocity behaviour of a growing crack and also allows for the inclusion of an initial condition which describes the above effects when the fracture stress is greater than the Griffith stress σ_g. If we let

$$n = 2\sigma_g^2/\sigma_f^2$$

then Berry's equation is

$$V^2 = V_m^2(1 - c_0/c)\,(1 - \{n-1\}c_0/c).$$

This equation is plotted in Fig. 6 for the limiting values of n, namely $n = 0$ and $n = 2$, and the maximum crack velocity V_m is taken as that of Rayleigh surface waves V_R in the $[1\,\bar{1}\,0\,0]$ direction in the $(1\,1\,\bar{2}\,0)$ fracture plane for these specimens [21]. Various theories [22–24] for the propagation of high speed cracks in brittle solids predict an upper limit equal to the Rayleigh velocity but various experimental work suggests values of less than $0.7V_R$. The failure of the Berry equation to encompass our present experimental results may be due to an incorrect choice of V_m and to the assumptions inherent in the analysis. A more exact equation of motion of a semi-infinite crack under tensile loading is given by Freund [25] as

$$2\gamma = K_s^2(c)F(V)/E$$

where $K_s(c)$ is the static stress intensity factor for a crack of length c and $F(V)$ is a function of crack velocity V. Using the expression $\sigma_f\sqrt{(\pi c)}$ for the static stress intensity factor when an evenly distributed tensile stress σ_f is applied at $\pm\infty$ and the expression $(2E\gamma/\pi c_0)^{\frac{1}{2}}$ for the Griffith stress then Freund's equation becomes simply $c/c_0 = 1/F(V)$. For a blunt crack the fracture stress, σ_f is higher and letting $\alpha = \sigma_f^2/\sigma_g^2$, Freund's equation is $c/c_0 = 1/\alpha F(V)$. Our experimental values of fracture stress suggest that α is in the range 1 to 25 and the theoretical curves for $\alpha = 1$ and 16 are included in Fig. 4 for comparison with the experimental velocity curves.

4. Conclusions

(1) The stress required for the tensile fracture of quartz crystals is dependent upon the geometry of the initiating notch. Sharp notches introduced by thermal treatments give a value of approximately 2 J m^{-2} for the surface energy required for fracture at room temperature.

(2) The energy required for fracture shows a minimum at about 500 K.

(3) The presence of water reduces the stress required for fracture.

(4) Quartz shows a preference for cleavage along the rhombohedral planes. Fracture paths are influenced by static and dynamic stress fields.

(5) The velocity–distance curves show a form and a dependence upon fracture stress in the manner predicted by the theories of Berry [20] and Freund [25].

Acknowledgements

One of the authors (A. B.) is indebted to the Chamber of Mines of South Africa for the research award which enabled him to carry out this work at the Universities of the Witwatersrand and Cape Town. Mr R. Moir of The Standard Telephones and Cables Company is especially thanked for his kind co-operation with regard to the supply of the quartz crystals. Acknowledgements are also due to Mrs K. Peach and Mrs J.M. Rieder who assisted in the preparation of this paper. Professor F.R.N. Nabarro and Dr N.G.W. Cook have been responsible for the general guidance of the project and have constantly provided stimulating ideas and interpretations.

References

1. R. D. BAËTA and K. H. G. ASHBEE, *Phil. Mag.* 22 (1970) 601.
2. A. C. MCLAREN and J. A. RETCHFORD, *Phys. Stat. Sol.* 33 (1969) 657.
3. R. D. BAËTA, J. W. HEAVENS and K. H. G. ASHBEE, European Conference on Electron Microscopy (1968) p. 507.
4. N. E. W. HARTLEY and T. R. WILSHAW, *J. Mater. Sci.* 8 (1973) 265.
5. M. V. SWAIN, J. S. WILLIAMS, B. R. LAWN and J. J. H. BEEK, *ibid* 8 (1973) 1153.
6. F. D. BLOSS and G. V. GIBBS, *Amer. Minerol.* 48 (1963) 821.
7. R. J. CHARLES, *J. Appl. Phys.* 29 (1958) 1549.
8. F. R. L. SCHOENING, Thesis, University of the Witwatersrand, South Africa (1959).
9. B. W. PAYNE and A. BALL, to be published.
10. J. E. FIELD, *Contemp. Phys.* 12 (1971) 1.

11. L. PAULING, "The Nature of the Chemical Bond" (Cornell Press, New York, 1960).
12. R. B. SOSMAN, "The Properties of Silica" (Chemical Catalog. Co., New York, 1927).
13. N. H. PETCH, "Fracture", Vol. 1, edited by H. Liebowitz (Academic Press, New York, 1968).
14. B. SCHWARTZ, *J. Amer. Ceram. Soc.* 35 (1952) 325.
15. S. S. BRENNER, *J. Appl. Phys.* 33 (1962) 33.
16. J. CONGLETON, N. J. PETCH and S. A. SHIELS, *Phil. Mag.* 19 (1969) 795.
17. J. J. GILMAN, *J. Appl. Phys.* 42 (1971) 3479.
18. S. K. ICHIKAWA, *Amer. J. Sci.* 189 (1915) 455.
19. J. L. ANDERSON, *Geol. Soc. Amer. Bull.* 53 (1945) 409.
20. J. P. BERRY, *J. Mech. Phys. Solids* 8 (1960) 194.
21. F. W. VOLTMER, E. P. IPPEN, R. M. WHITE, T. C. LIM and G. W. FARNELL, *Proc. IEEE* 56 (1968) 1634.
22. E. H. YOFFE, *Phil. Mag.* 42 (1951) 739.
23. K. B. BROBERG, *Arkiv. Fysik.* 18 (1960) 159.
24. J. W. CRAGGS, *J. Mech. Phys. Solids* 8 (1960) 66.
25. L. B. FREUND, *ibid* 20 (1972) 141.

Received 31 July and accepted 14 October 1975.

front by waves continuously emitted by the growing crack, and subsequently reflected from the boundary at the initiation site. These markings should therefore give an approximation to the actual position of the crack front at an instant in time. At high magnification, it can be seen that near the origin, these fine lines are indeed perpendicular to the line drawn through the crack origin and parallel to the sides of the crystal. However, far from the origin (i.e. crack length $> 3\times$ the initial notch length) there is a small deviation and this will lead to an error of about 6% in the crack velocity.

Experimental measurements of crack velocities employing the successive breaking of a set of parallel resistors, vapour-deposited on the specimen surface, yield crack velocities close to those deduced by the anisotropic analysis and are included in fig. 4. The details of the extensive experiments which were designed to elucidate the behaviour of a growing crack are the subject of another publication (Ball and Payne 1976). It should be noted that if an attempt had been made to use the isotropic theory in the above case, eqn. (1) would be simplified by letting the shear wave front be perpendicular to its propagation direction (i.e. $\alpha = \pi/2$) and letting V_R be replaced by an average value. If an average of the ray velocities in the crack plane is taken to be 4 km sec^{-1}, then this leads to a calculated crack velocity approximately 50% lower than that derived by the above anisotropic theory.

References

Ball, A., and Payne, B. W., 1976, *J. mater. Sci.*, **11**, 731.

Cady, W. G., 1946, *Piezoelectricity* (McGraw-Hill).

Greenwood, J. H., 1971, *J. mater. Sci.*, **6**, 390.

Hull, D., and Beardmore, P., 1966, *Int. J. Fracture Mech.*, **2**, 468.

Love, A. E. H., 1892, *A Treatise on the Mathematical Theory of Elasticity* (Cambridge University Press).

Love, A. E. H., 1934, *A Treatise on the Mathematical Theory of Elasticity*, 4th ed. (Cambridge University Press).

Musgrave, M. J. P., 1970, *Crystal Acoustics* (Hold–Day).

Shand, E. B., 1954, *J. Am. Ceram. Soc.*, **37**, 559.

Smekal, A., 1950, *Glastech. Ber.*, **23**, 57.

Wallner, H., 1939, *Z. Phys.*, **114**, 368.

Fig. 3

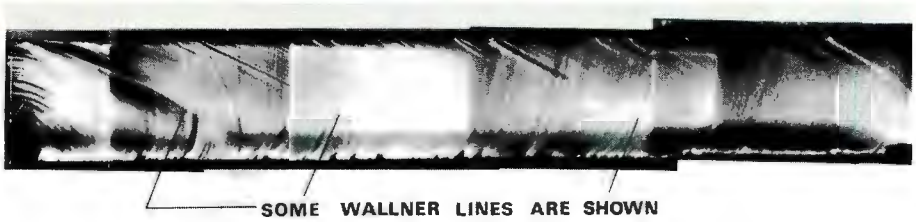

Photograph of fracture surface lying in YZ plane of α-quartz ($\times 15$).

The angles β and γ (see fig. 1) were obtained from the photograph of the fracture surface shown in fig. 3. The values of V_R and α were obtained from eqns. (6) and (7) and the crack velocity was then found from eqn. (1). The results are shown as a function of normalized crack length in fig. 4. The main sources of error introduced into the analysis are the measurements of angles from the photograph and the orientation of the crystal. These lead to a maximum error of about 10% in the crack velocity. Another possible error which could enter into the analysis is the deviation of the crack front from normality to its propagation direction. In this regard we make use of finely spaced surface markings which can be seen in addition to the Wallner lines in fig. 3. These are thought to be caused by a perturbation of the crack

Fig. 4

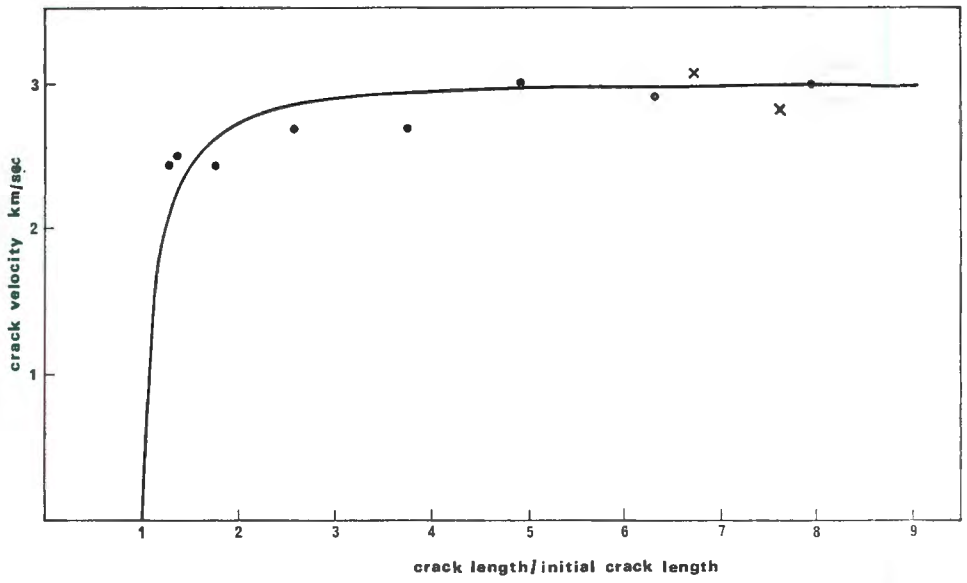

Crack velocity data obtained from Wallner lines (●) plotted against normalized crack length and compared with electrical resistance measurements (X).

Fig. 2

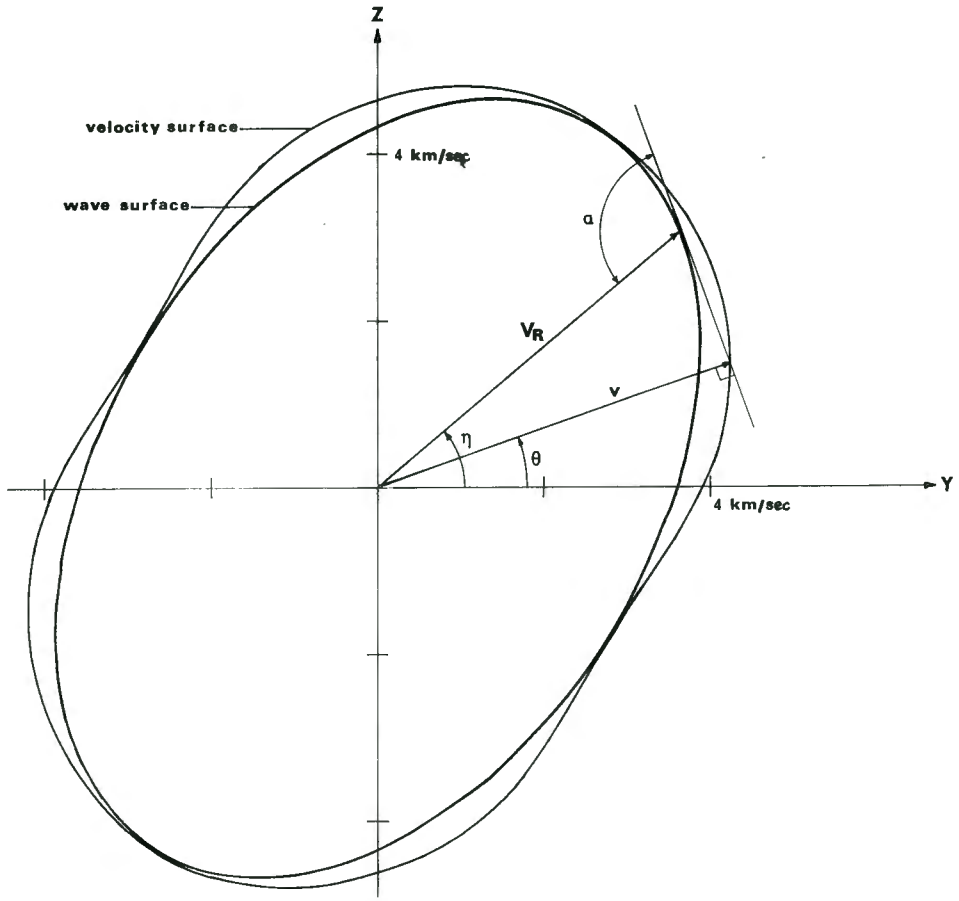

Velocity and wave surfaces for the X polarized shear wave in the YZ plane of α-quartz, showing the relationship between a tangent to the wave surface and a point on the velocity surface.

§ 2. Experimental

Single crystals of synthetic quartz with dimensions $60 \times 10 \times 1$ mm in the X, Y and Z directions, respectively, were orientated by the Laué back reflection X-ray technique and the positive crystal axes were found by the method of etch figures (Cady 1946). The specimens were tested by the application of a tensile stress along the X axis and fracture was initiated at a notch 1 mm long cut into the long edge of the crystal.

A typical fracture surface is shown in fig. 3. It should be noticed that far from the origin the Wallner lines become straight and parallel, indicating that the velocity of the crack is changing very slowly and that the crack front is straight.

where ρ is the density of the material and the Γ_{ij} are quadratic functions of the direction cosines ν_i and depend on the elastic stiffness constants c_{ij}. In the case of the YZ plane in α-quartz, the above equations become

$$\left.\begin{aligned} p_1\Gamma_{11} &= p_1\rho v^2, \\ p_2\Gamma_{22}+p_3\Gamma_{23} &= p_2\rho v^2, \\ p_2\Gamma_{23}+p_3\Gamma_{33} &= p_3\rho v^2, \end{aligned}\right\} \tag{3}$$

where

$$\Gamma_{11} = c_{66}\nu_2{}^2 + c_{44}\nu_3{}^2 + 2c_{14}\nu_2\nu_3.$$

If

$$v^2 = \Gamma_{11}/\rho \tag{4}$$

is taken as a solution to eqn. (3), then the plane wave is polarized in the X direction and is therefore the one of interest. (Since the particle displacement vectors are orthogonal, the other two waves are polarized in the fracture plane and hence do not interfere with the fracture front.) The ray velocities also lie in the plane and therefore the one corresponding to the pure shear wave can be obtained from eqn. (4) as

$$\partial v/\partial \nu_2 = (c_{66}\nu_2 + c_{14}\nu_3)/\rho v,$$
$$\partial v/\partial \nu_3 = (c_{44}\nu_3 + c_{14}\nu_2)/\rho v.$$

Let θ be the anticlockwise angle from the Y axis to the Z axis, then $\nu_1 = 0$, $\nu_2 = \cos\theta$ and $\nu_3 = \sin\theta$. If we write $\mathbf{V}_R$ in polar form $\mathbf{V}_R = (V_R, \eta)$ and set the sense of η the same as that of θ, then

$$\tan\eta = \frac{\partial v/\partial \nu_3}{\partial v/\partial \nu_2} = \frac{c_{44}\tan\theta + c_{14}}{c_{66} + c_{14}\tan\theta},$$

hence

$$\tan\theta = \frac{c_{14} - c_{66}\tan\eta}{c_{14}\tan\eta - c_{44}}. \tag{5}$$

V_R can then be found as a function of η from eqn. (5) and

$$V_R{}^2 = \frac{1}{\rho^2 v^2}\{\cos^2\theta(c_{66}{}^2 + c_{14}{}^2) + \sin^2\theta(c_{14}{}^2 + c_{44}{}^2) + 2\sin\theta\cos\theta(c_{66}c_{14} + c_{14}c_{44})\}. \tag{6}$$

Figure 2 shows the velocity and wave surfaces of the shear wave polarized in the X direction and the relation between the tangent to the wave surface and the direction of the ray and plane wave velocities. Hence α is given by

$$\alpha = \eta + \pi/2 - \theta. \tag{7}$$

Fig. 1

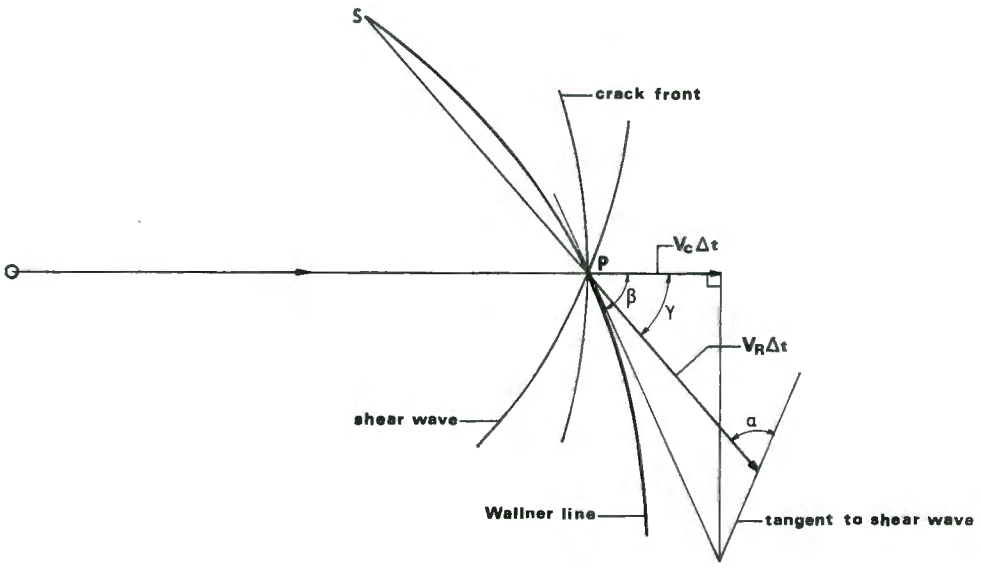

Geometrical construction for the determination of crack velocity from measurements of the angles designated β and α.

where v is the magnitude of the velocity of a plane wave propagating in a direction defined by the direction cosines ν_1, ν_2, ν_3. Geometrically (Musgrave 1970), the ray velocity surface (called the wave surface) is the envelope of plane wave fronts with respect to the plane wave velocity surface (called the velocity surface).

The only tractable case occurs when :

(i) one of the plane waves on the fracture surface is pure shear and has a particle displacement normal to the fracture surface ; and

(ii) the ray velocity corresponding to this pure shear wave also lies in the fracture plane. These two conditions will both occur if the plane is one of elastic symmetry (i.e. normal to a two-fold rotation axis). The YZ plane in α-quartz is one of elastic symmetry, although the crystal structure is not mirrored across this plane. (The contribution of the piezoelectric effect to the determination of ray velocities in α-quartz is small and will therefore be ignored.)

The direction cosines p_i for plane wave particle displacements are given by Love (1934) as

$$p_1(\Gamma_{11}-\rho v^2)+p_2\Gamma_{12}+p_3\Gamma_{13}=0,$$
$$p_1\Gamma_{12}+p_2(\Gamma_{22}-\rho v^2)+p_3\Gamma_{23}=0,$$
$$p_1\Gamma_{13}+p_2\Gamma_{23}+p_3(\Gamma_{33}-\rho v^2)=0,$$

PHILOSOPHICAL MAGAZINE, 1976, VOL. 34, NO. 5, 917–922

The determination of crack velocities in anisotropic materials by the analysis of Wallner lines

By B. W. PAYNE and A. BALL
Department of Metallurgy and Materials Science, University of Cape Town, Cape Town, South Africa

[Received 30 January 1976 and in present form 31 May 1976]

ABSTRACT

A general theory is developed for the determination of crack velocities in anisotropic materials by the analysis of Wallner lines on fracture surfaces. An application is given for fracture along a plane of elastic symmetry in α-quartz.

§ 1. THEORY

Since Wallner (1939) first explained the existence of certain markings on the facture surfaces of glass, attempts have been made to determine the velocity of cracks from an examination of these lines (Smekal 1950, Shand 1954). Workers who have used Wallner lines to determine crack velocities in crystalline materials have had to select planes of high symmetry in which the velocity of shear waves is isotropic (Greenwood 1971, Hull and Beardmore 1966). In order to include cases where the velocity of shear waves is anisotropic in the fracture plane, the analysis of Shand (1954) will be generalized.

Figure 1 shows a crack initiated at 0 and propagating from left to right in the plane of the paper. The state of stress responsible for the fracture is assumed to be uniform tension perpendicular to the fracture plane. This will allow the fracture front to diverge uniformly. When the crack front reaches a defect at S, the rapid change in stress at the point will result in the generation of an elastic disturbance. In general, three sheets of elastic waves will propagate from S. Consider one of them, travelling with velocity $\mathbf{V_R}$ which has associated with it a component of particle displacement perpendicular to the fracture surface. This wave will modulate the crack front and a Wallner line will result. In general, the tangent to the wave front and the wave propagation direction will not be perpendicular : let the angle between the two be α as shown in fig. 1. The velocity of the crack deduced from the geometrical construction shown in fig. 1 is given by

$$V_c = V_R \cos\beta \sin\alpha / \sin(\alpha - \beta + \gamma). \tag{1}$$

1.1. *Fracture along the YZ plane in α-quartz*

The velocity of a sheet of elastic waves propagating from a point source (called the ray velocity $\mathbf{V_R}$) is given by Love (1892) and Musgrave (1970) as

$$\mathbf{V_R} = (\partial v/\partial \nu_1,\ \partial v/\partial \nu_2,\ \partial v/\partial \nu_3), \tag{2}$$

Plate 1

Electronically enhanced image of an open crack on a glass surface

Plate 2

Open crack in quartz showing zig-zag along cleavage planes.

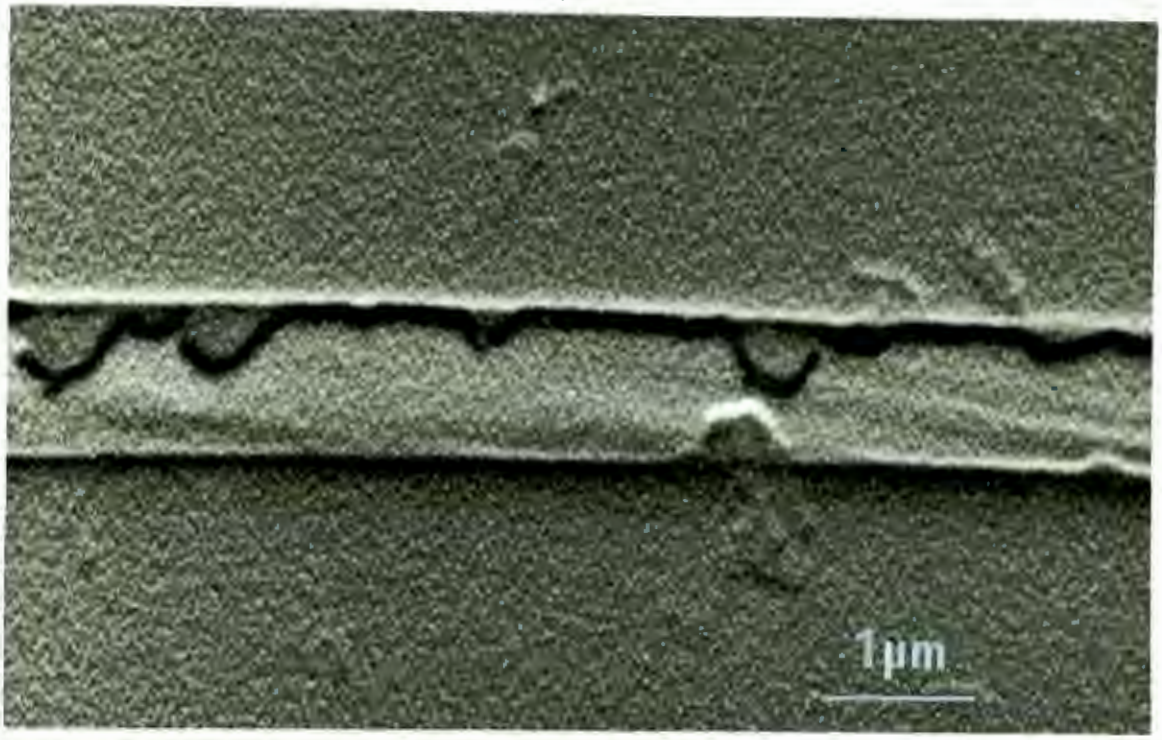
1µm

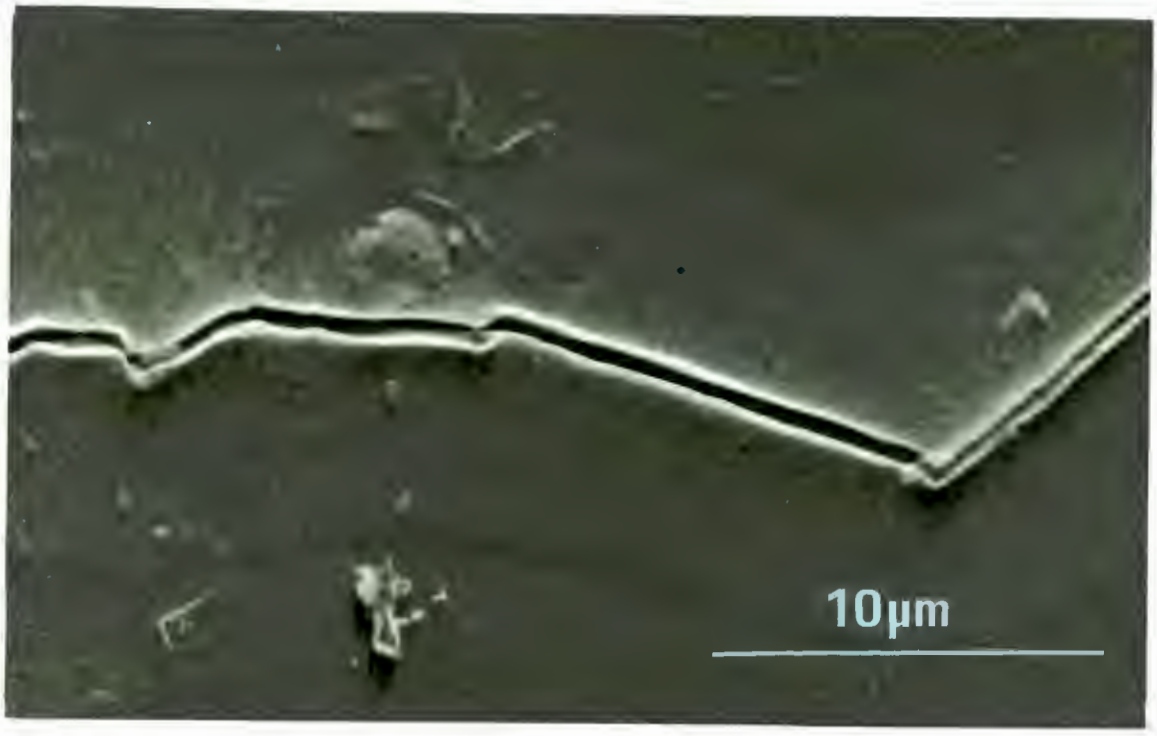
10µm

Plate 3

Resistance grid on fractured quartz crystal.

Plate 5

Photograph of oscilloscope screen of second crack velocity measuring circuit (see text). Each vertical scale division is 0.01V, and each horizontal scale division is 0.5μs.

Plate 4

Photograph of oscilloscope screen of first crack velocity measuring circuit (see text). Each vertical scale division is 0.3V, and each horizontal scale division is 0.5μs.

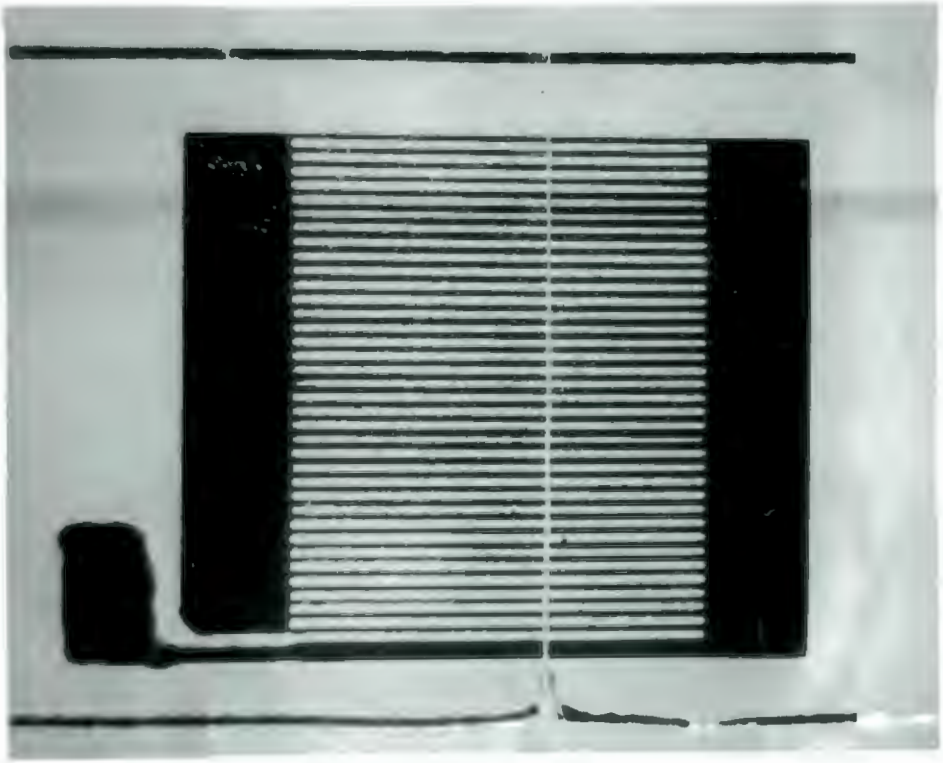

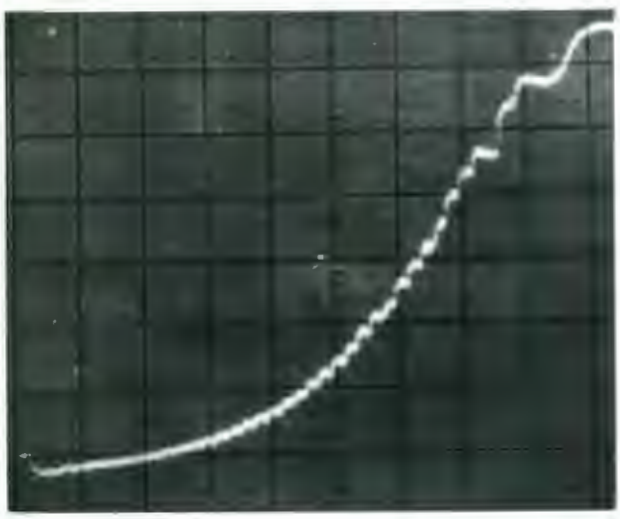

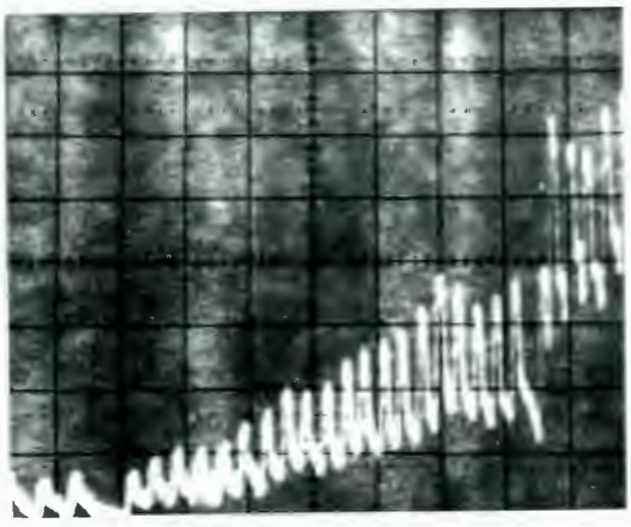

Plate 6

Smooth $(11\bar{2}0)$ fracture surface of quartz. A typical Wallner line is shown at A.

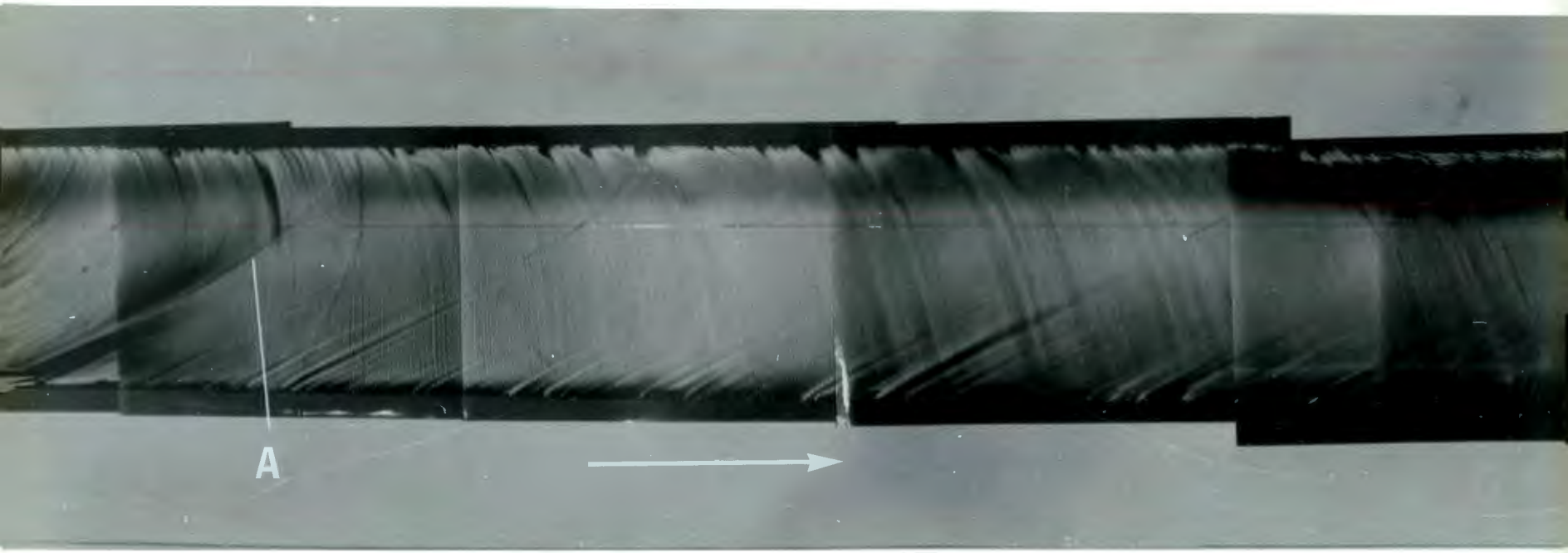
A

Plate 7

Fracture surface of quartz showing onset of surface roughening at high crack velocities.


300µm

Plates 8

Fracture surface of quartz of Orientation C (see section 5.3).

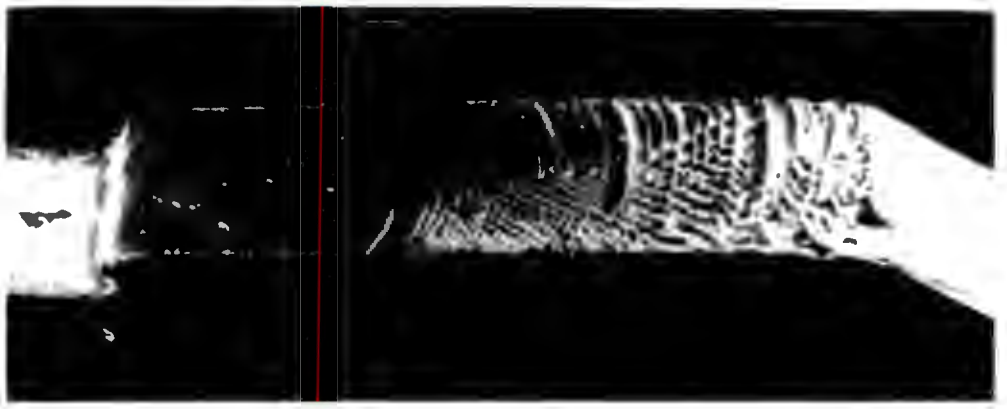

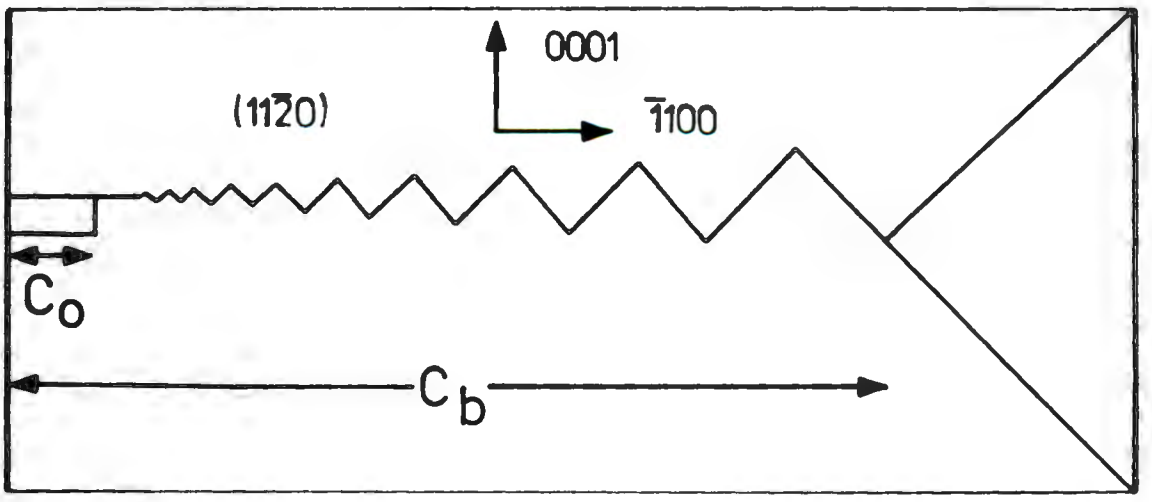
0001
(11$\bar{2}$0)
$\bar{1}$100
c_o
c_b

Plate 9

Vickers hardness indentation on the $(10\bar{1}0)$ surface of quartz showing fracturing at the sharp corners.

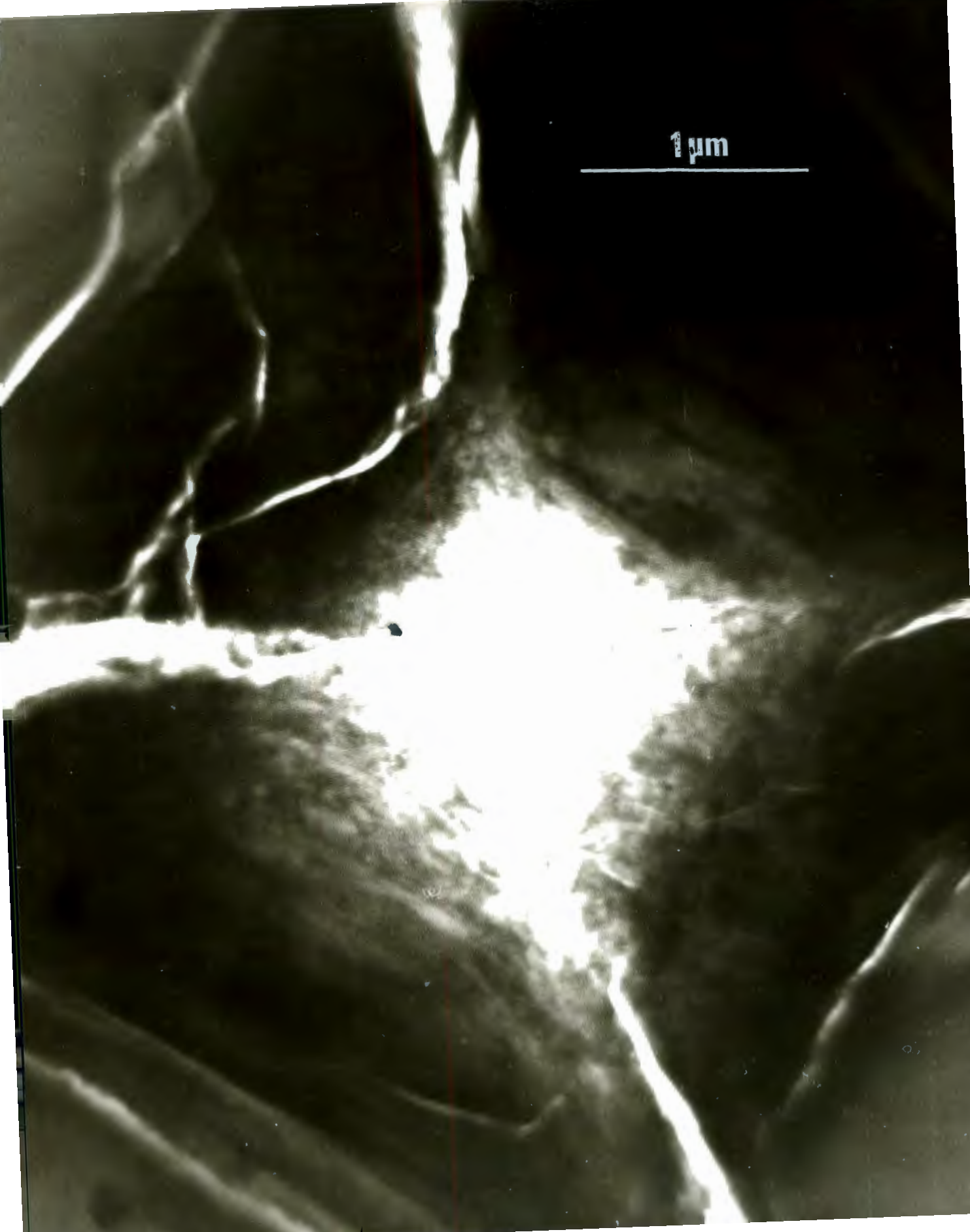
1 µm

Plate 10

Diffraction pattern taken at centre of indentation shown in plate 9.

Plate 11

View of an area around a Vickers hardness indentation on the $(10\bar{1}0)$ surface of quartz.


1µm
A
B

Plate 12

Higher magnification of region A on plate 11.


1 µm
C

Plate 13

Higher magnification of region B on plate 11.


1μm
Y
X

Plate 14

Defect similar to that shown at B in plate 11, but around another indentation.

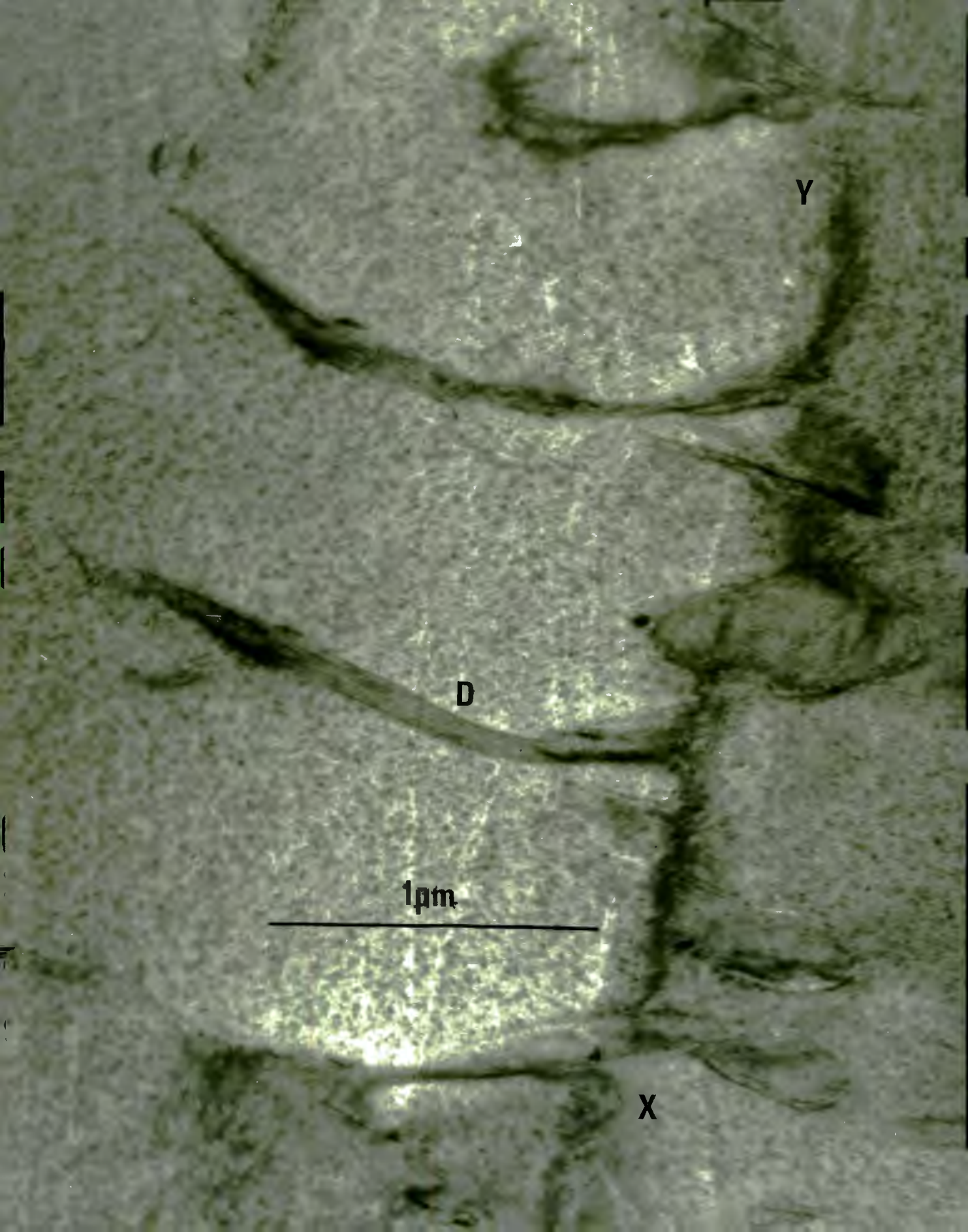
Y
D
1μm
X

Plate 15

Area near centre of indentation after specimen had been annealed for 12h at $800^{0}C$.


1µm

Plate 16

Dislocations generated along a scratch on the $(11\bar{2}0)$ surface of quartz by diamond polishing particles.

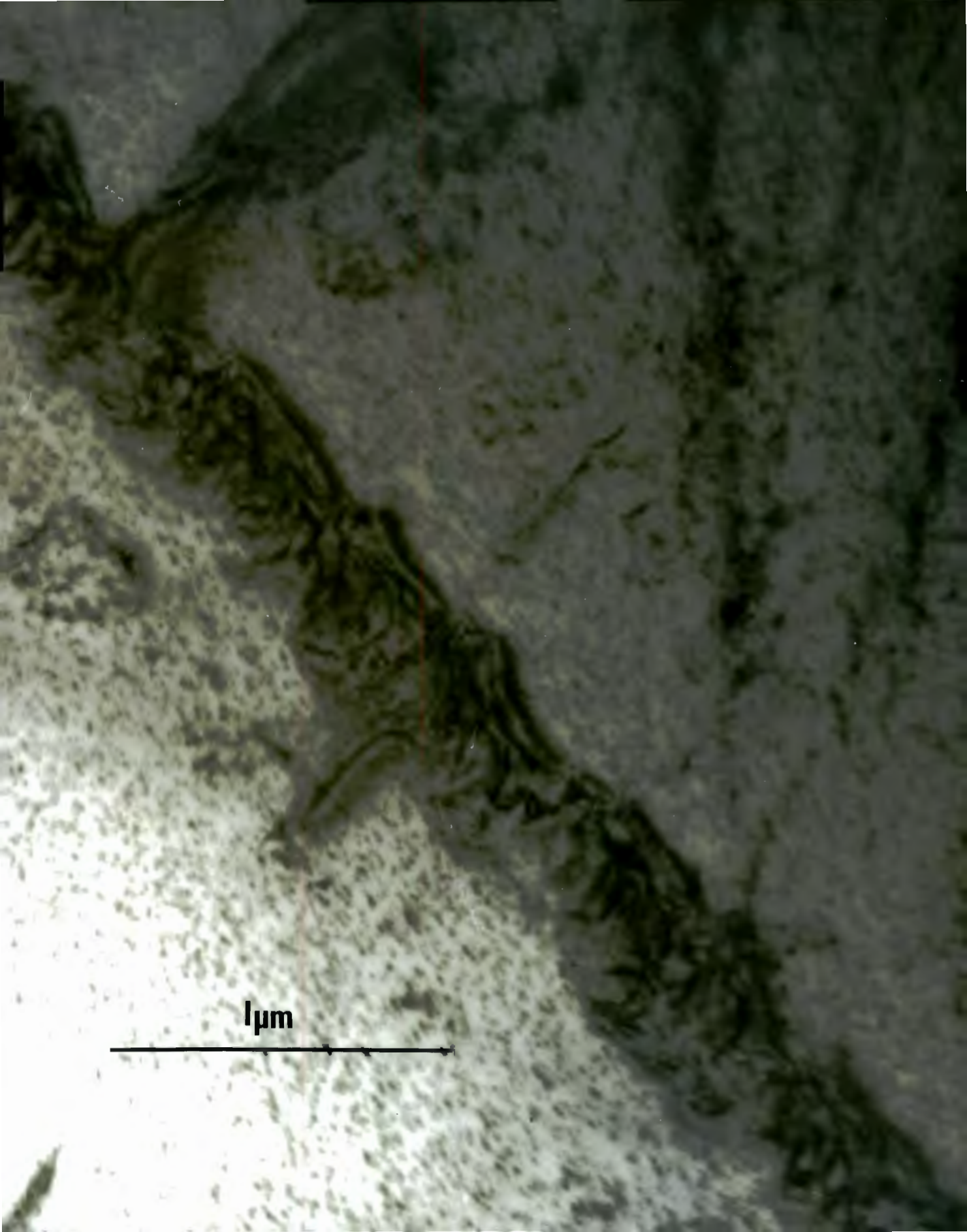
1μm

Plate 17

Scratches on quartz surface showing dislocation patterns as in plate 15.


0,5 µm

Plate 18

Etched $(11\bar{2}0)$ surface of scratched quartz showing absorption contrast at previous dislocation sites.

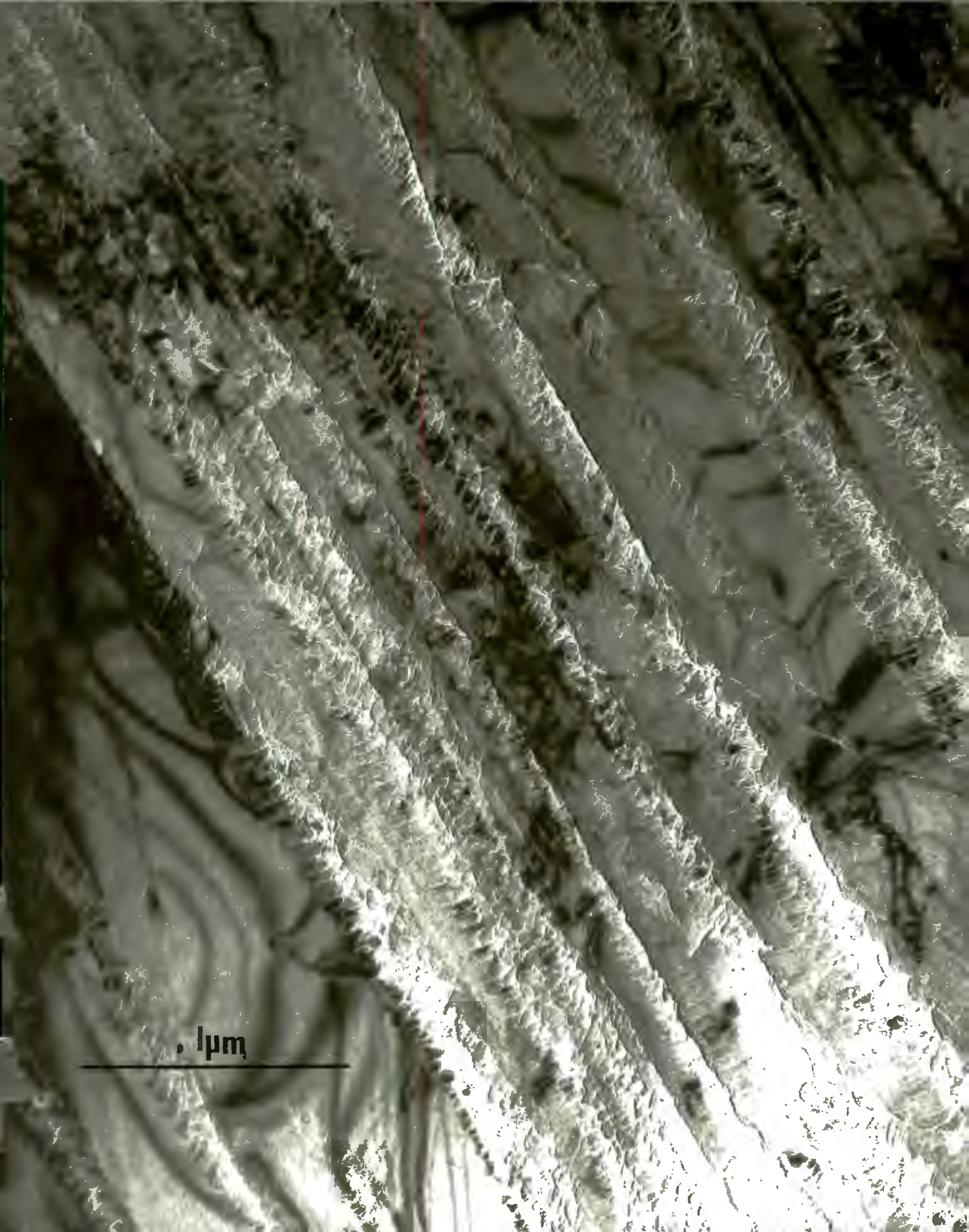
1μm

Plate 19

Incompletely closed Hertzian cracks in quartz.

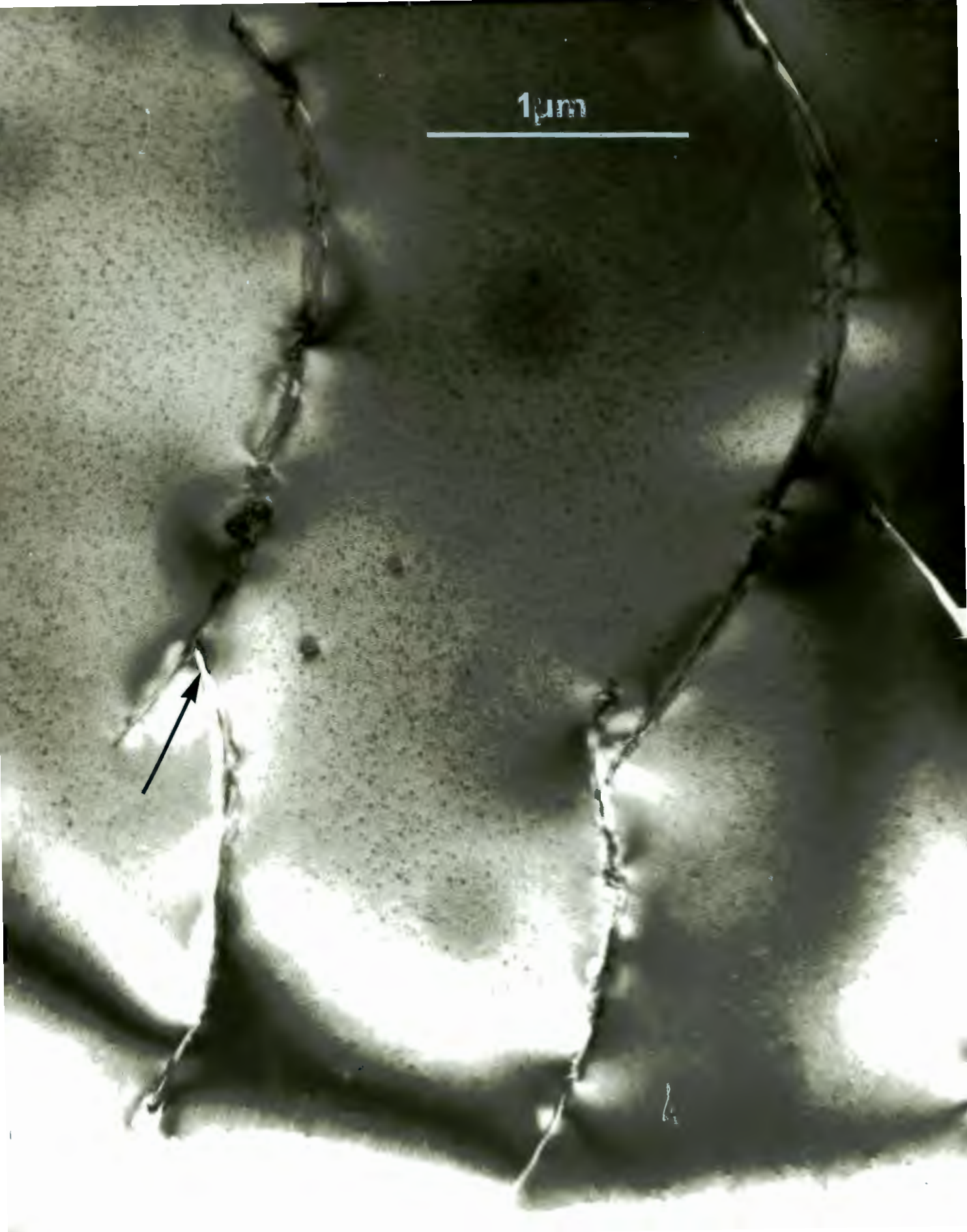
1μm

Plate 20

Scratch on quartz : applied load - 9.8N, speed - 8.5×10^{-2}mm s^{-1}, surface plane - $(11\bar{2}0)$ in direction of Y axis, polished surface, tested in air. Arrow indicates direction of scratching.

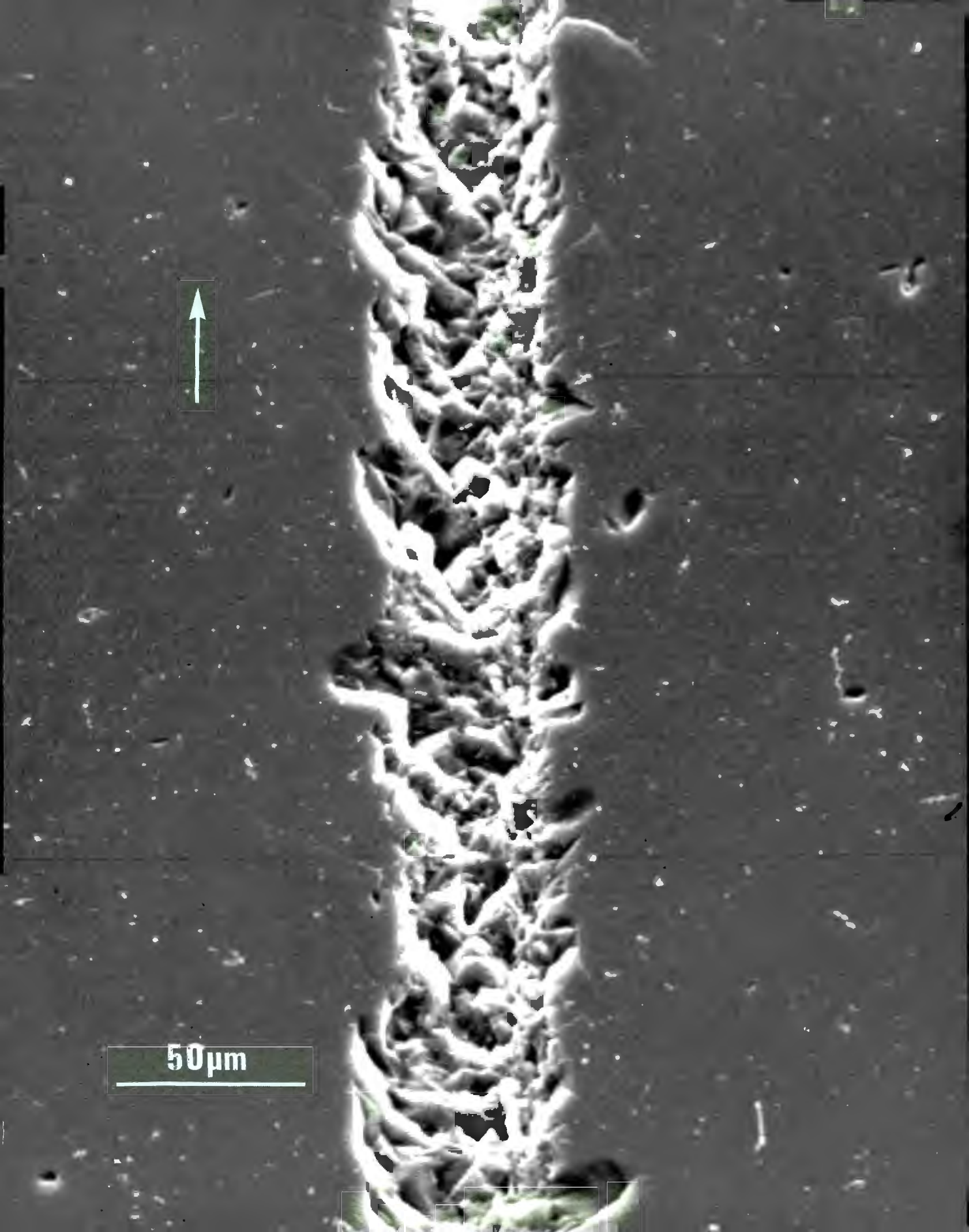
50µm

Plate 21

Scratch on quartz : applied load - 2.9N, speed - 8.5×10^{-2} mm s^{-1}, surface plane - $(11\bar{2}0)$ in direction of Y axis, polished surface, tested in air. Arrow indicates direction of scratching.

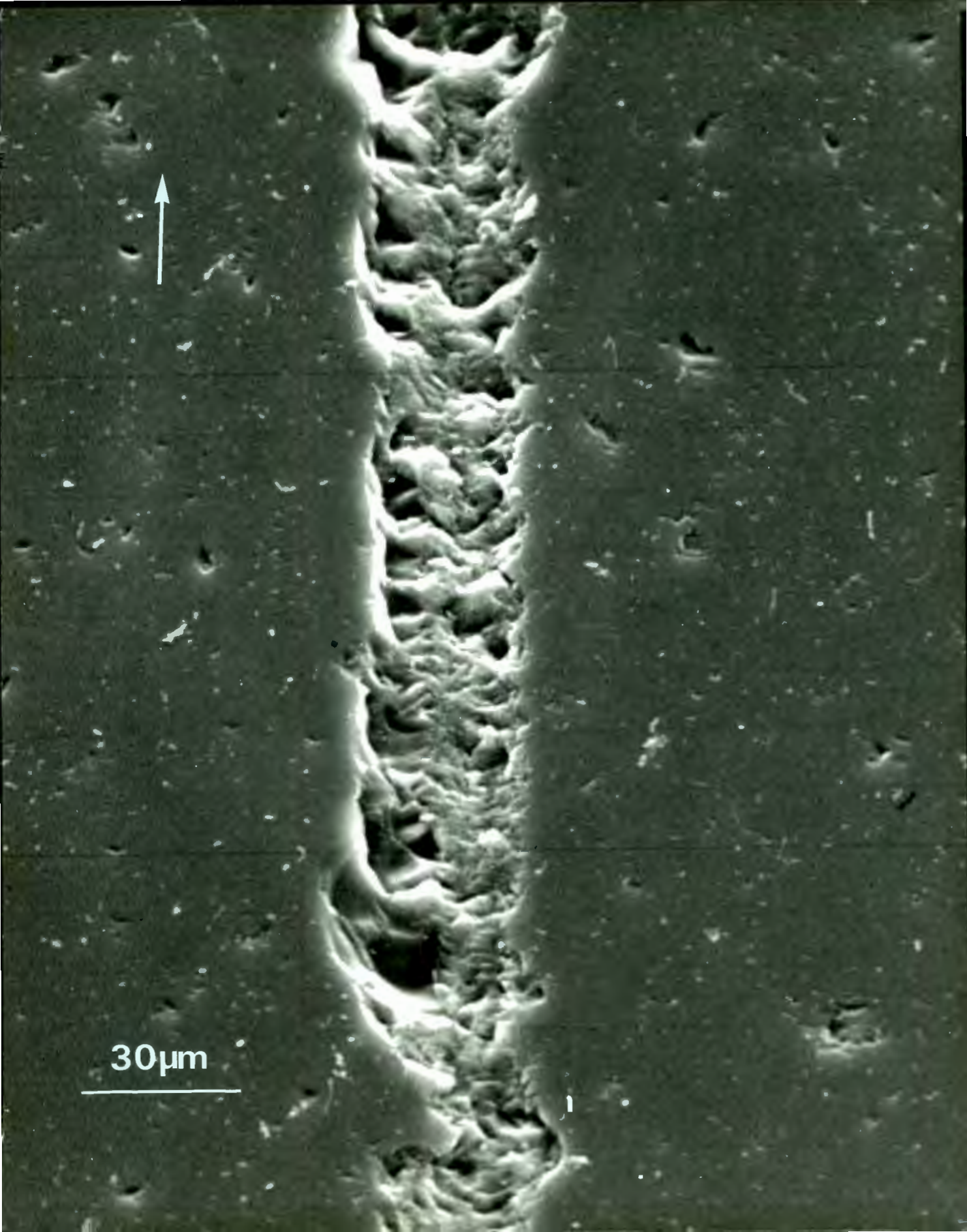
30µm

Plate 22

Scratch on quartz : applied load - 0.78N, speed - 8.5×10^{-2} mm s^{-1}, surface plane - $(11\bar{2}0)$ in direction of Y axis, polished surface, tested in air. Arrow indicates direction of scratching.

Plate 23

Scratch on quartz after etching : applied load - 0.78N, speed - 8.5×10^{-2} mm $^{-1}$, surface plane - $(11\bar{2}0)$ in direction of Y axis, polished surface, tested in air. Arrow indicates direction of scratching.

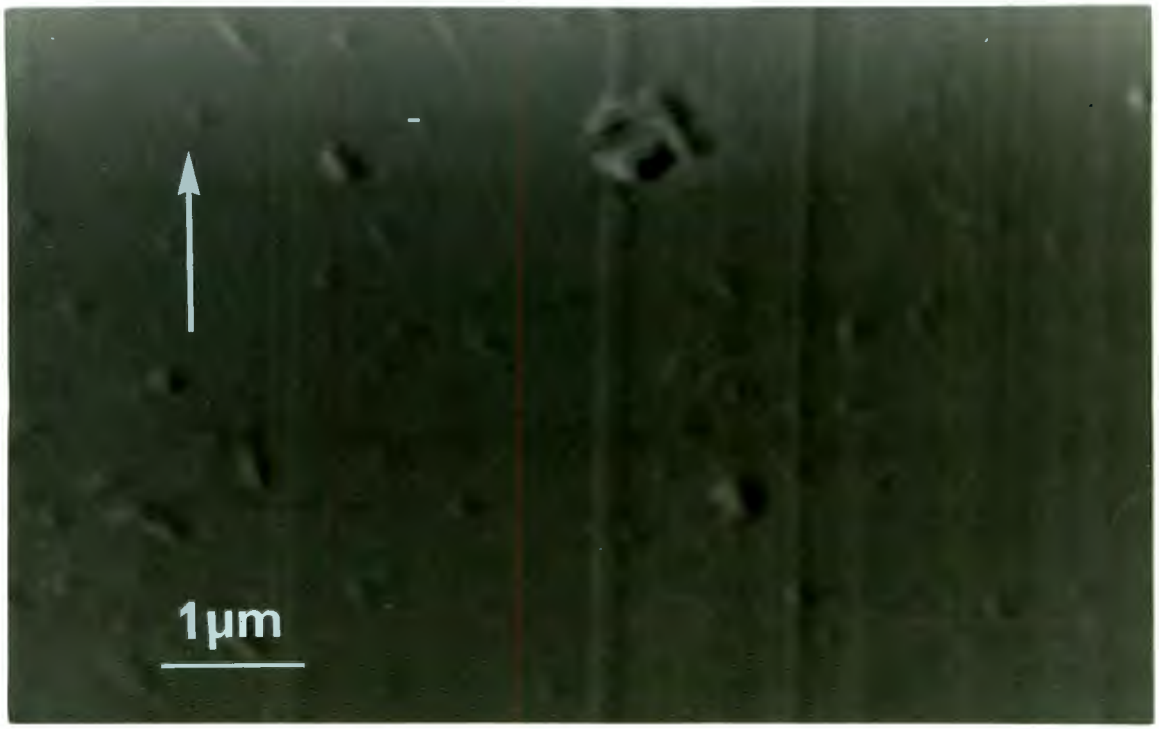
1µm

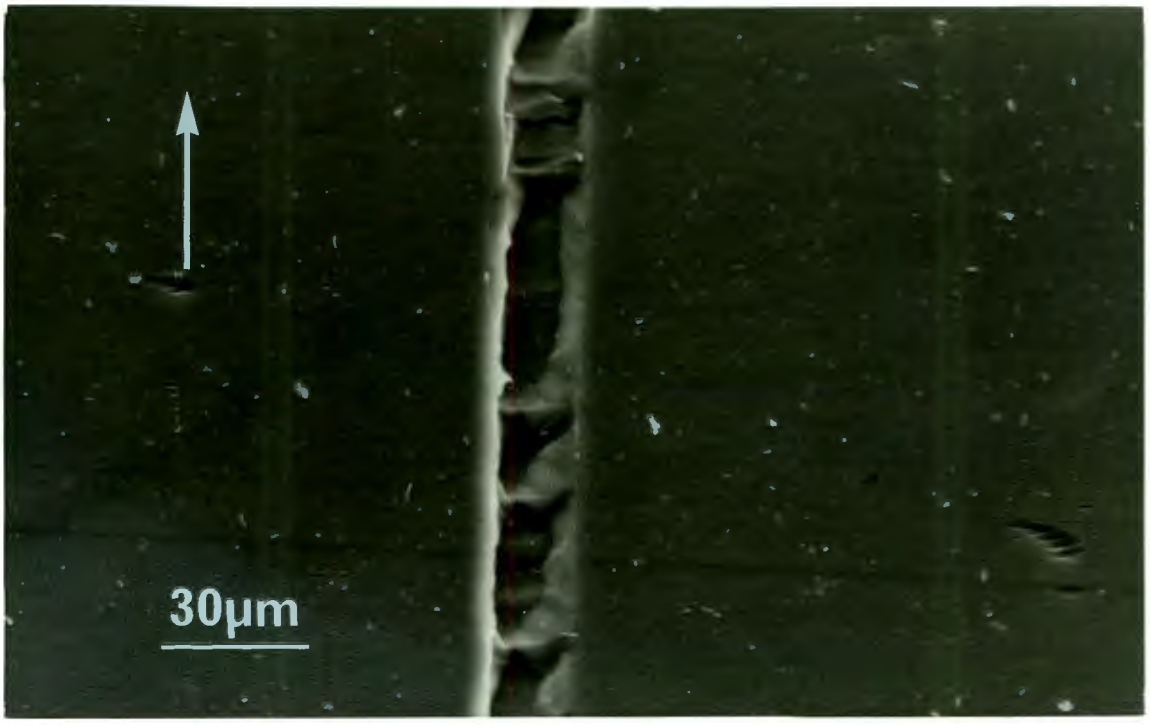
30µm

Plate 24

Scratch on quartz : applied load - 9.8N, speed - 8.5×10^{-2}mm s^{-1}, surface plane - $(11\bar{2}0)$ in direction of Y axis, polished surface, tested in air. Arrow indicates direction of scratching.

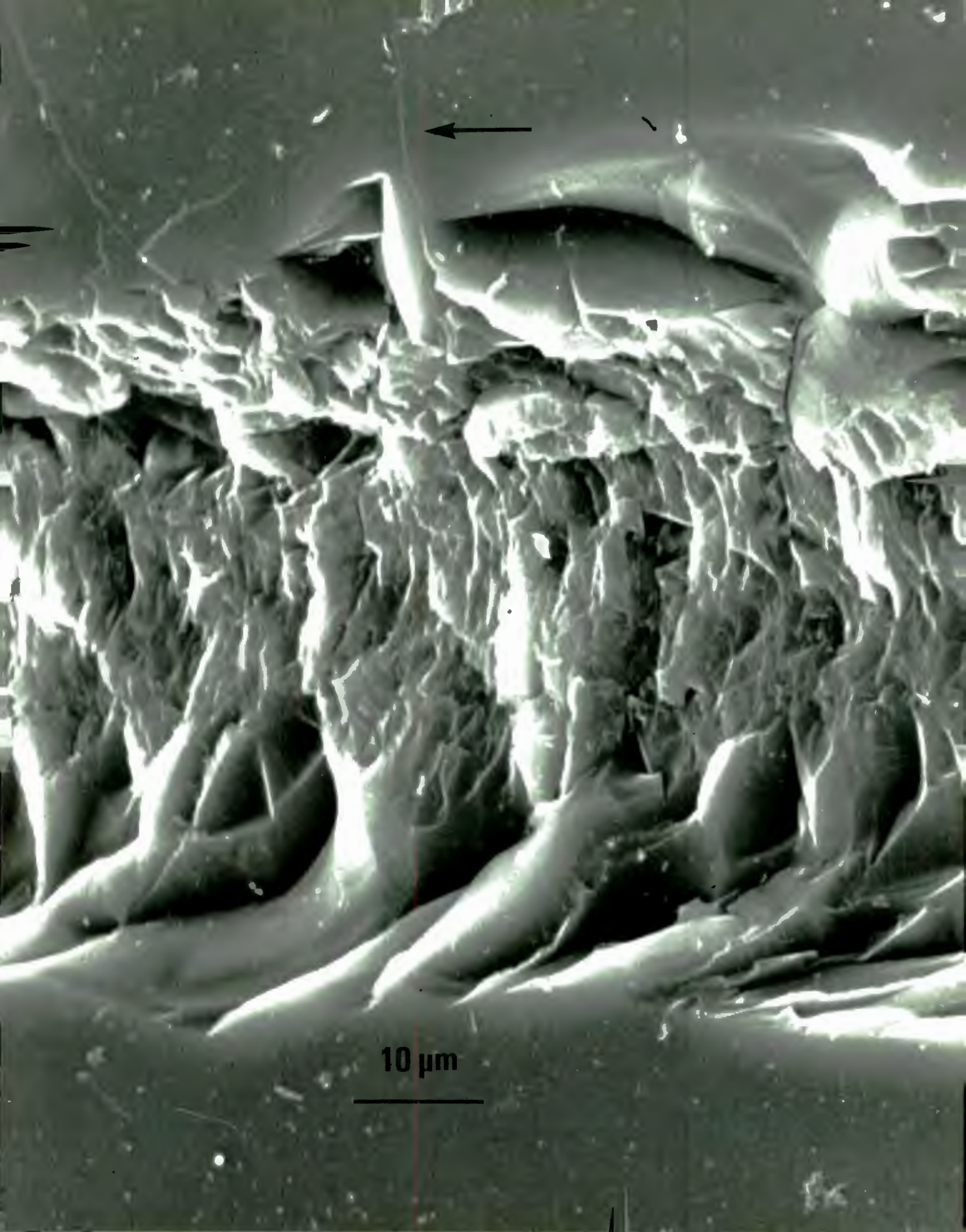
10 µm

Plate 25

Scratch on quartz after etching : applied load - 9.8N, speed - 8.5×10^{-2} mm s^{-1}, surface plane - $(11\bar{2}0)$ in direction of Y axis, polished surface, tested in air. Arrow indicates direction of scratching.

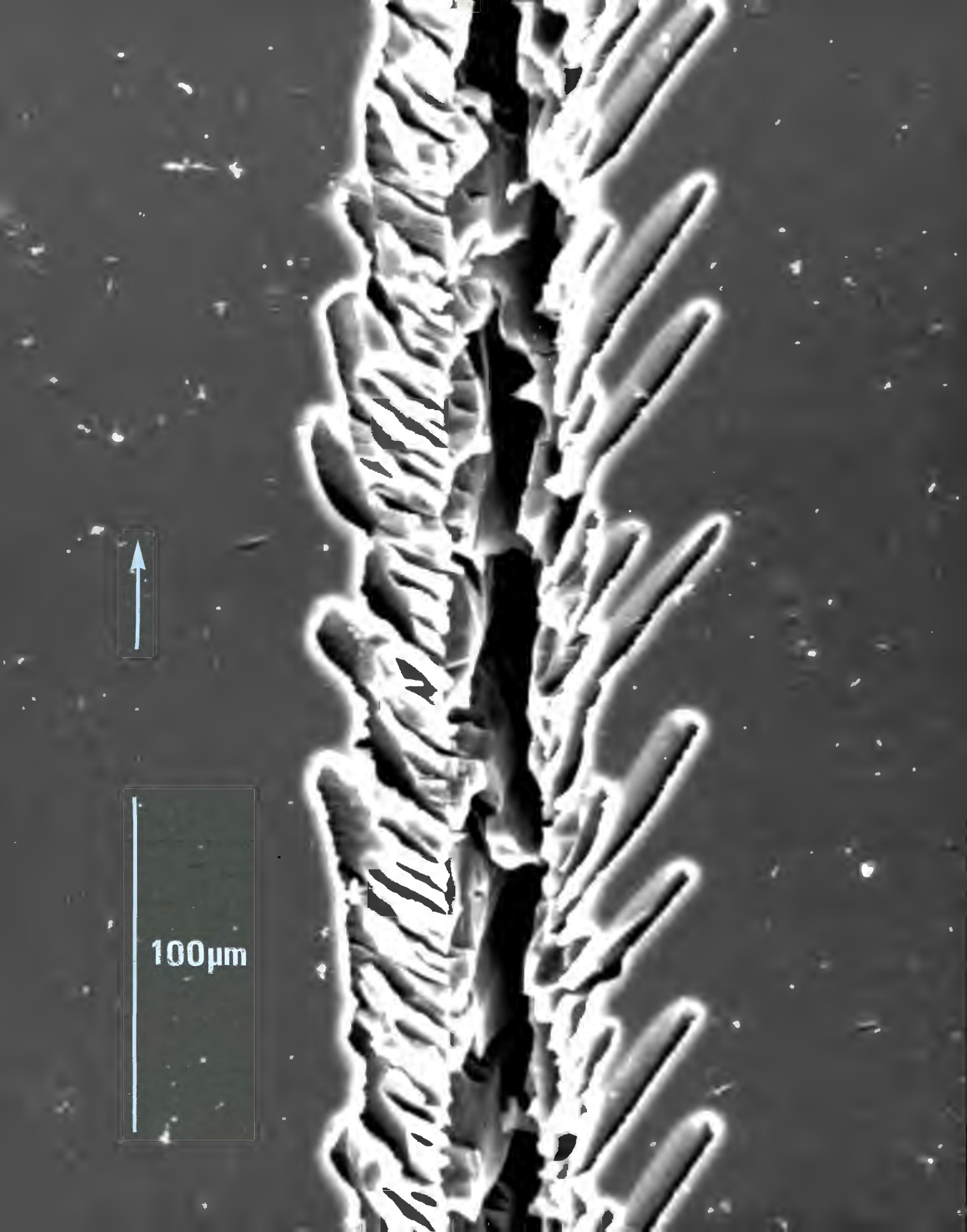
100µm

Plate 26

Scratch on quartz after etching _ applied load - 2.9N, speed - 8.5×10^{-2} mm s^{-1}, surface plane - $(11\bar{2}0)$ in direction of Y axis, polished surface, tested in air. Arrow indicates direction of scratching.

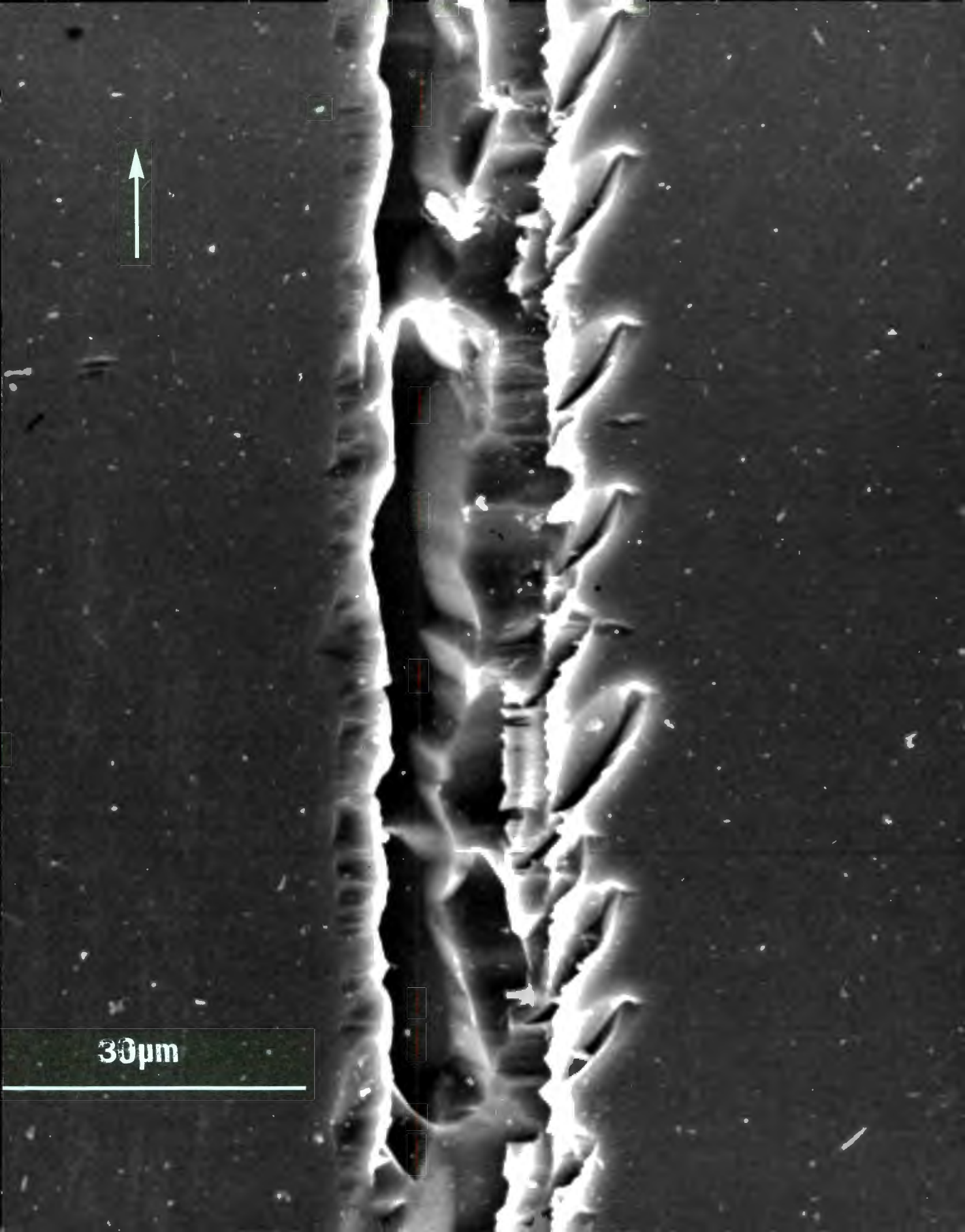
30µm

Plate 27

Scratch on quartz after etching : applied load - 0.2N, speed - 8.5×10^{-2}mm s^{-1}, surface plane - $(11\bar{2}0)$ in direction of Y axis, polished surface, tested in air. Arrow indicates direction of scratching.

Plate 28

Scratch on quartz after etching : applied load - 4.9×10^{-2}N, speed - 8.5×10^{-2}mm s^{-1}, surface plane - $(11\bar{2}0)$ in direction of Y axis, polished surface, tested in air. Arrow indicates direction of scratching.

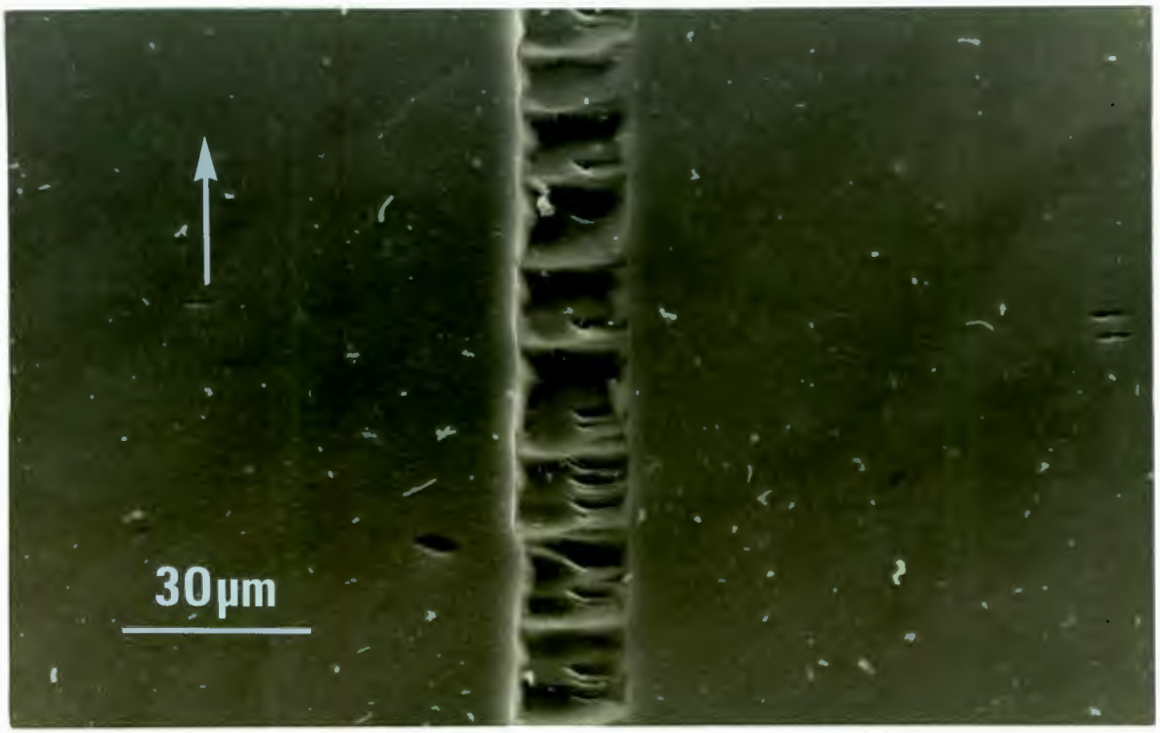
30µm

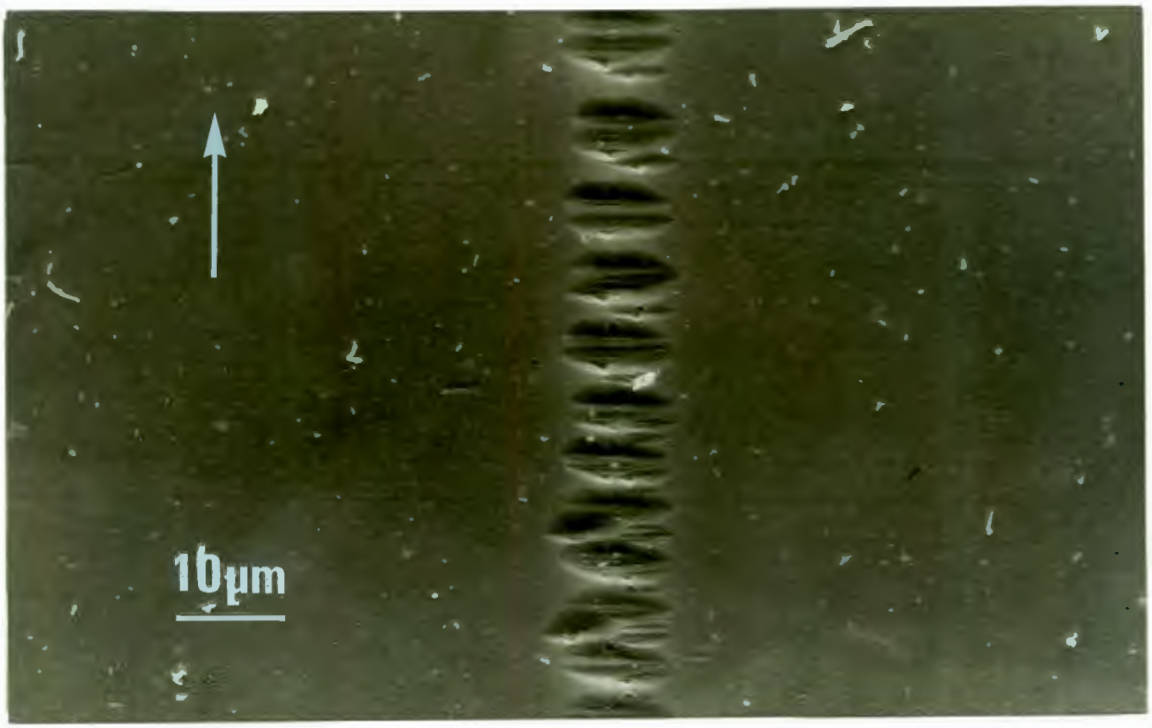
10µm

Plate 29

Score lines on debris material in scratch on quartz : applied load - 9.8N, speed - 8.5×10^{-2}mm s^{-1}, surface plane - $(11\bar{2}0)$ in direction of Y axis, polished surface, tested in air. Arrow indicates direction of scratching.

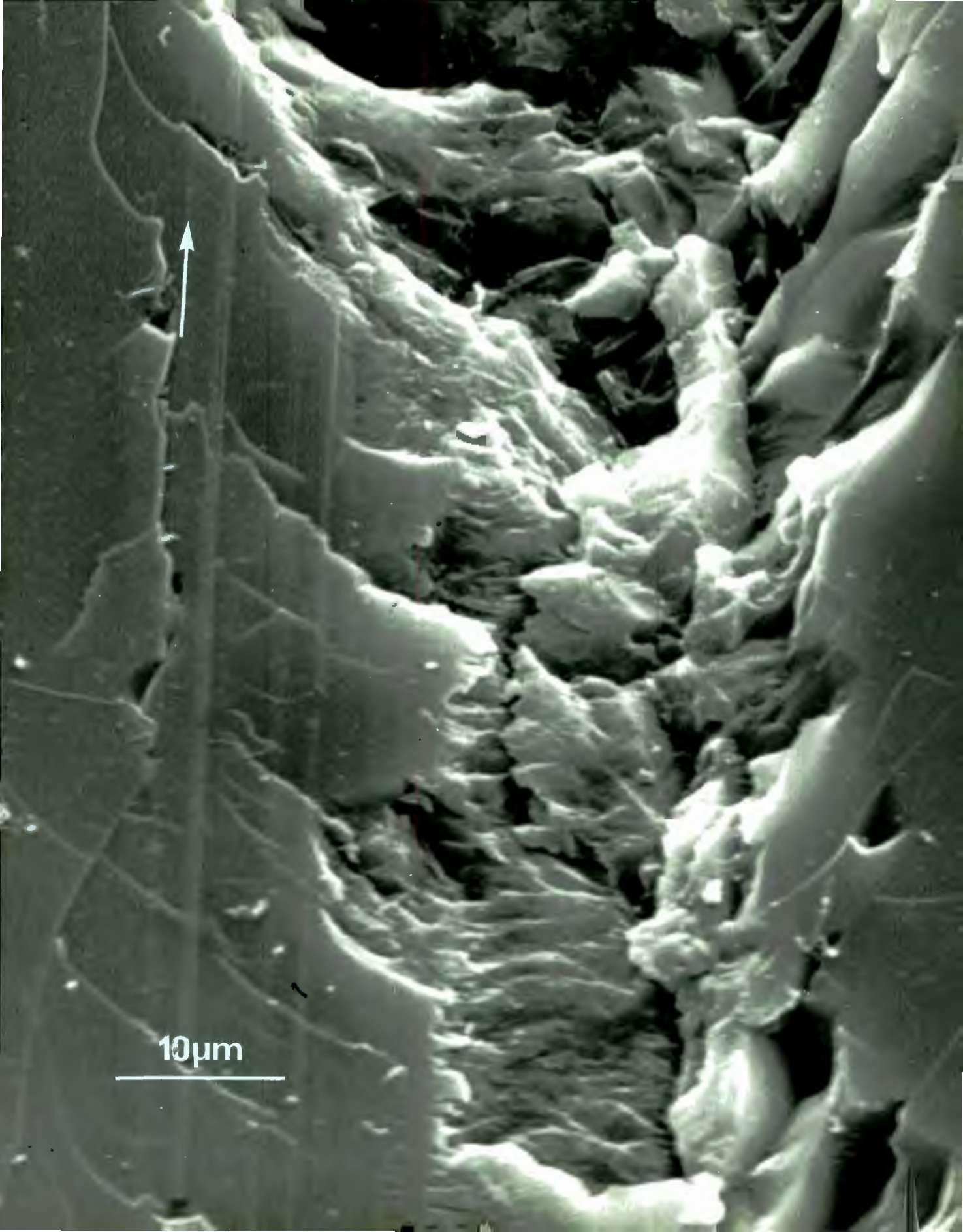
10µm

Plate 30

Section through scratch on quartz : applied load - 9.8N, speed - 8.5×10^{-2} mm s^{-1}, surface plane - $(11\bar{2}0)$ in direction of Y axis, polished surface, tested in air.

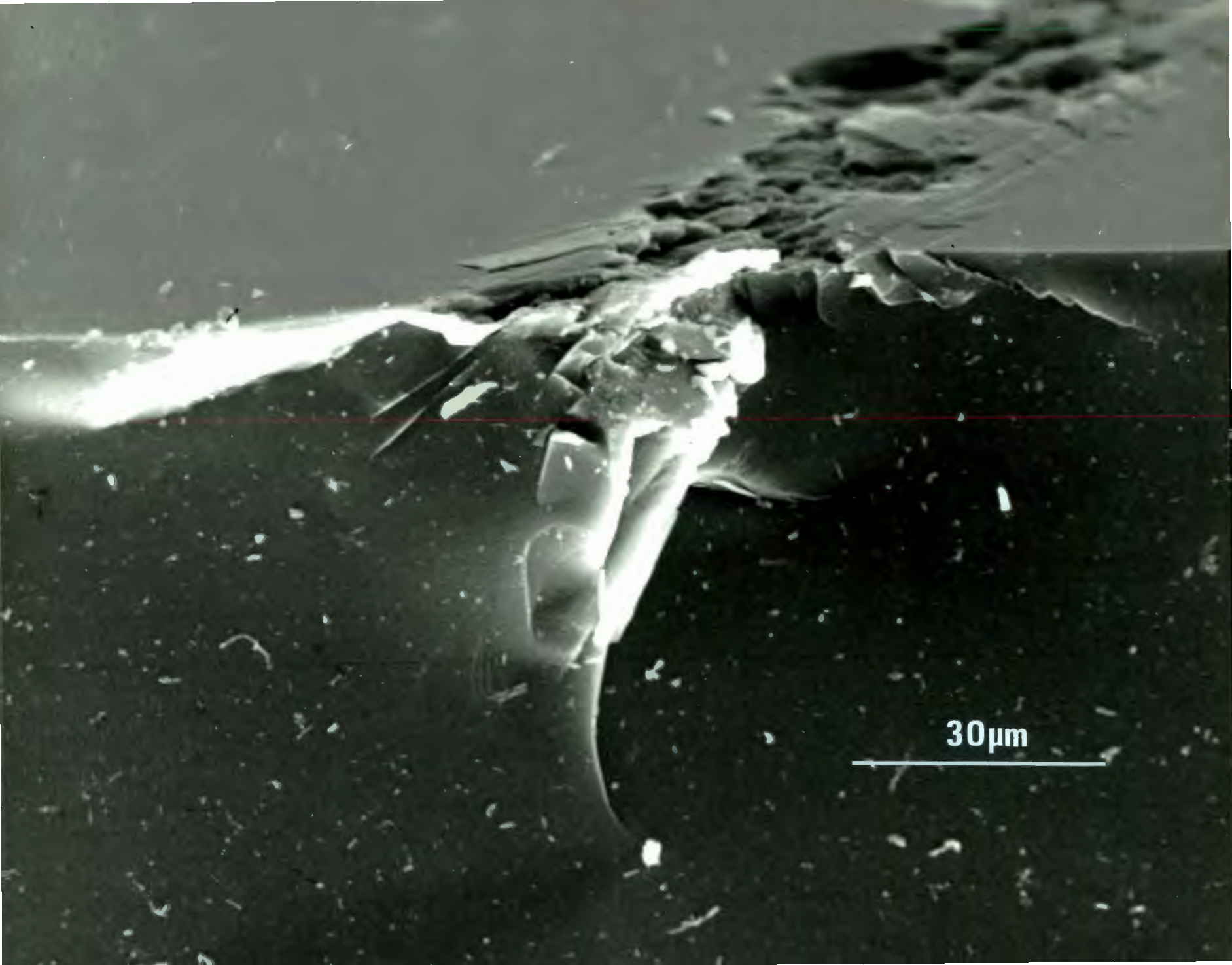
30µm

Plate 31

Section through scratch on quartz : applied load - 0.78N, speed - 8.5×10^{-2} mm s^{-1}, surface plane - $(11\bar{2}0)$ in direction of Y axis, polished surface, tested in air.

Plate 32

Section through scratch on quartz : applied load - 4.9×10^{-2}N, speed - 8.5×10^{-2}mm s^{-1}, surface plane - $(11\bar{2}0)$ in direction of Y axis, polished surface, tested in air.

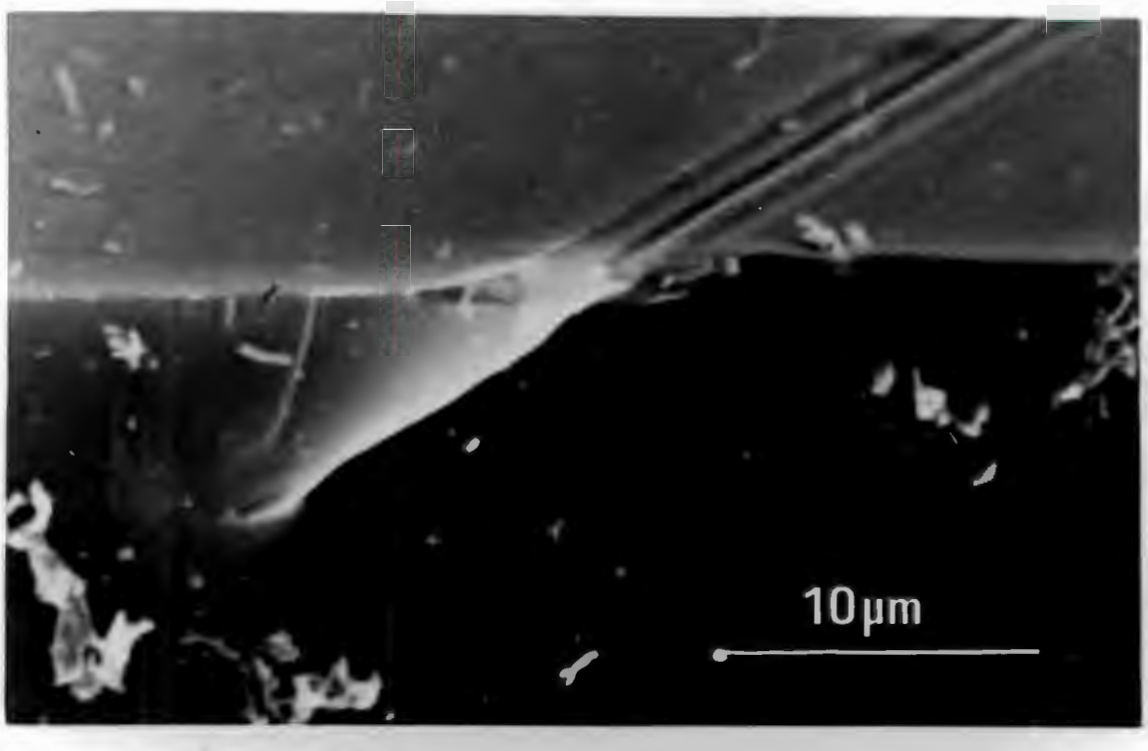
10µm

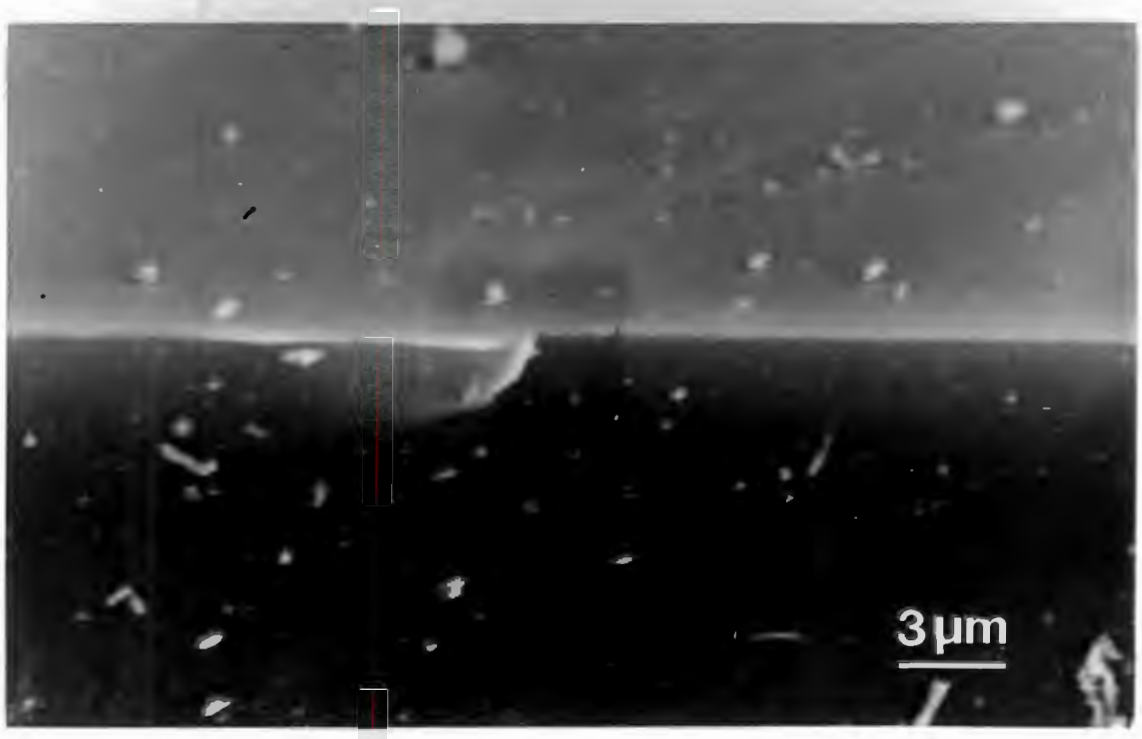
3µm

Plate 33

Scratch on quartz : applied load - 9.8N, speed - 8.5×10^{-2} mm s^{-1}, surface plane - $(11\bar{2}0)$ in direction of Y axis, polished surface, tested in air. Large arrow indicates direction of scratching and double arrowed line indicates the intersection of the rhombohedral planes with the surface.

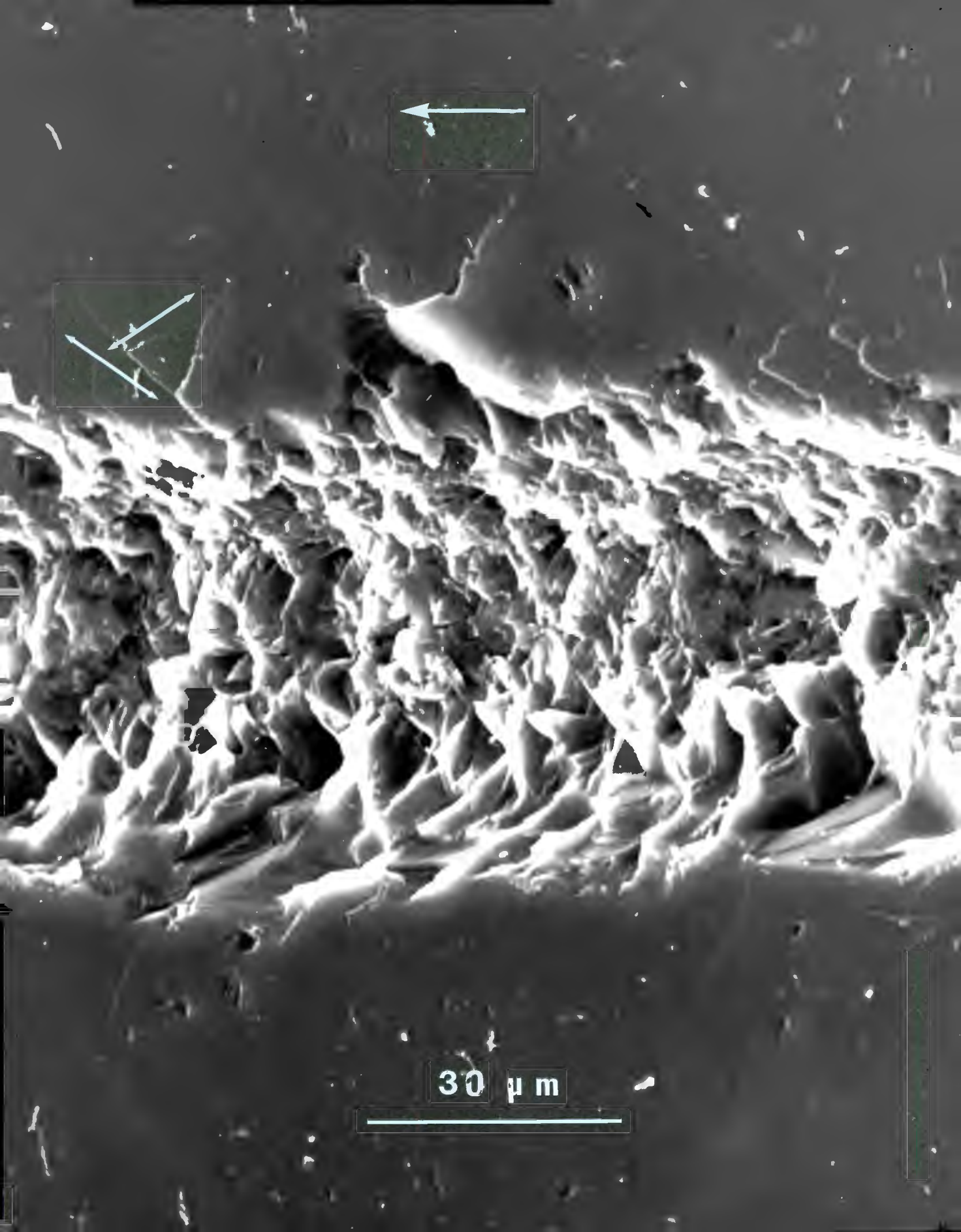
30 µm

Plate 34

Same specimen as in plate 33 but after etching.


30µm

Plate 35

Scratch on quartz : applied load - 9.8N, speed - 8.5×10^{-2} mm s^{-1}, surface plane (0001) in direction of Y axis, initial etched surface, tested in air. Arrow indicates direction of scratching.

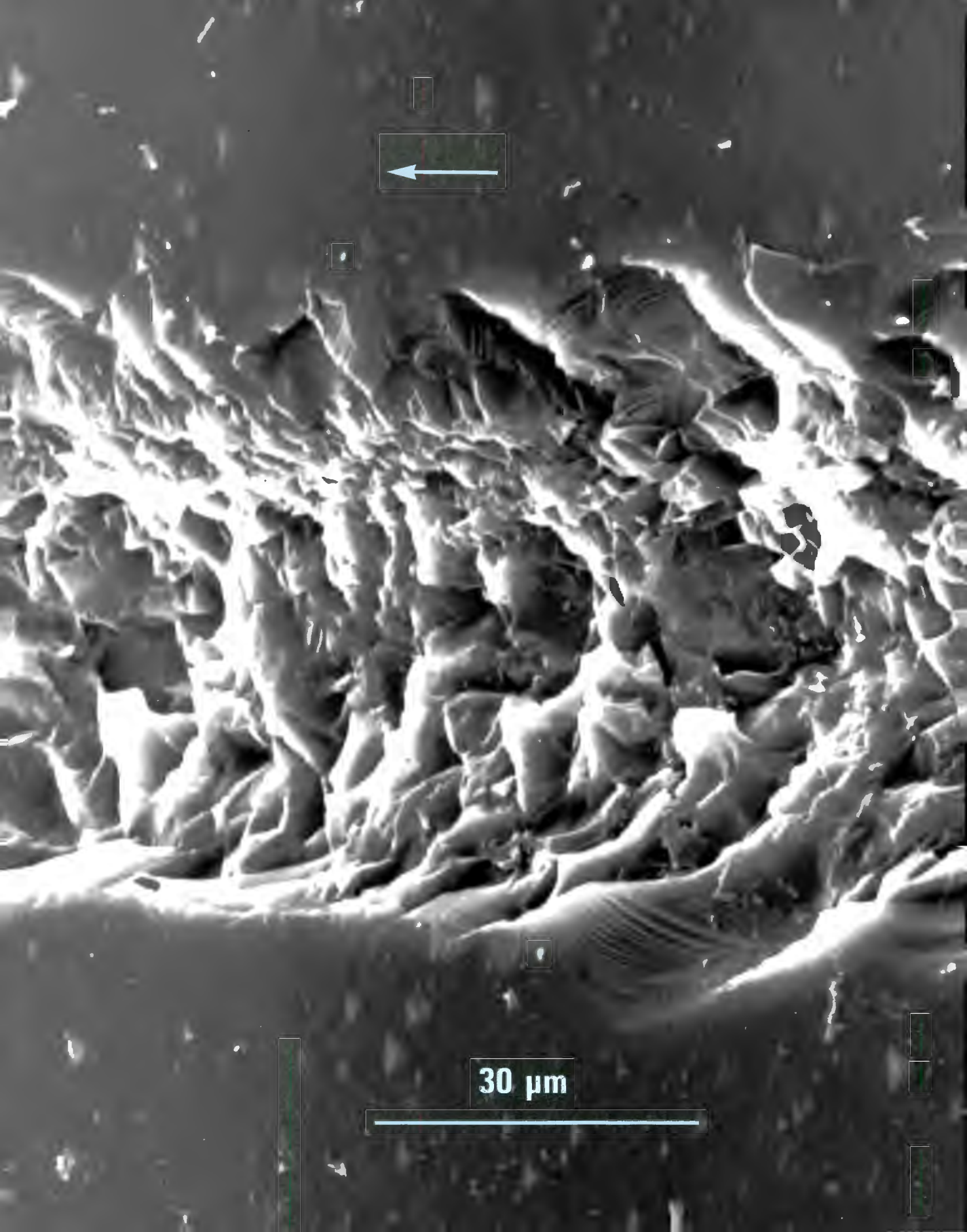
30 µm

Plate 36

Same specimen as in plate 35 but after etching.

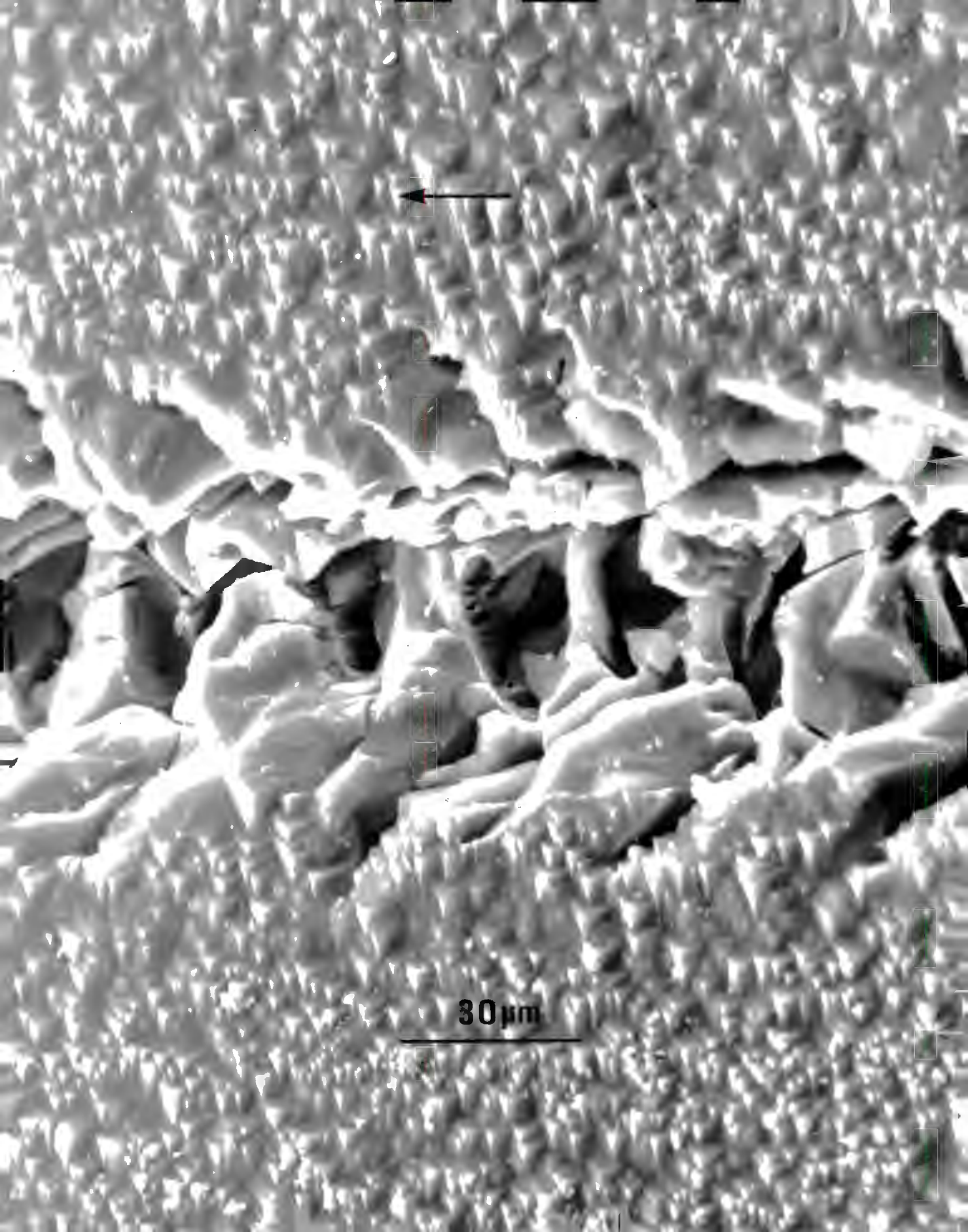
30 µm

Plate 37

Scratch on quartz after etching : applied load - 9.8N, speed - 8.5×10^{-2} mm s^{-1}, surface plane - $(1\bar{1}00)$ in X direction, polished surface, tested in air. Large arrow indicates direction of scratching and double arrowed line indicates the intersection of the rhombohedral planes with the surface.

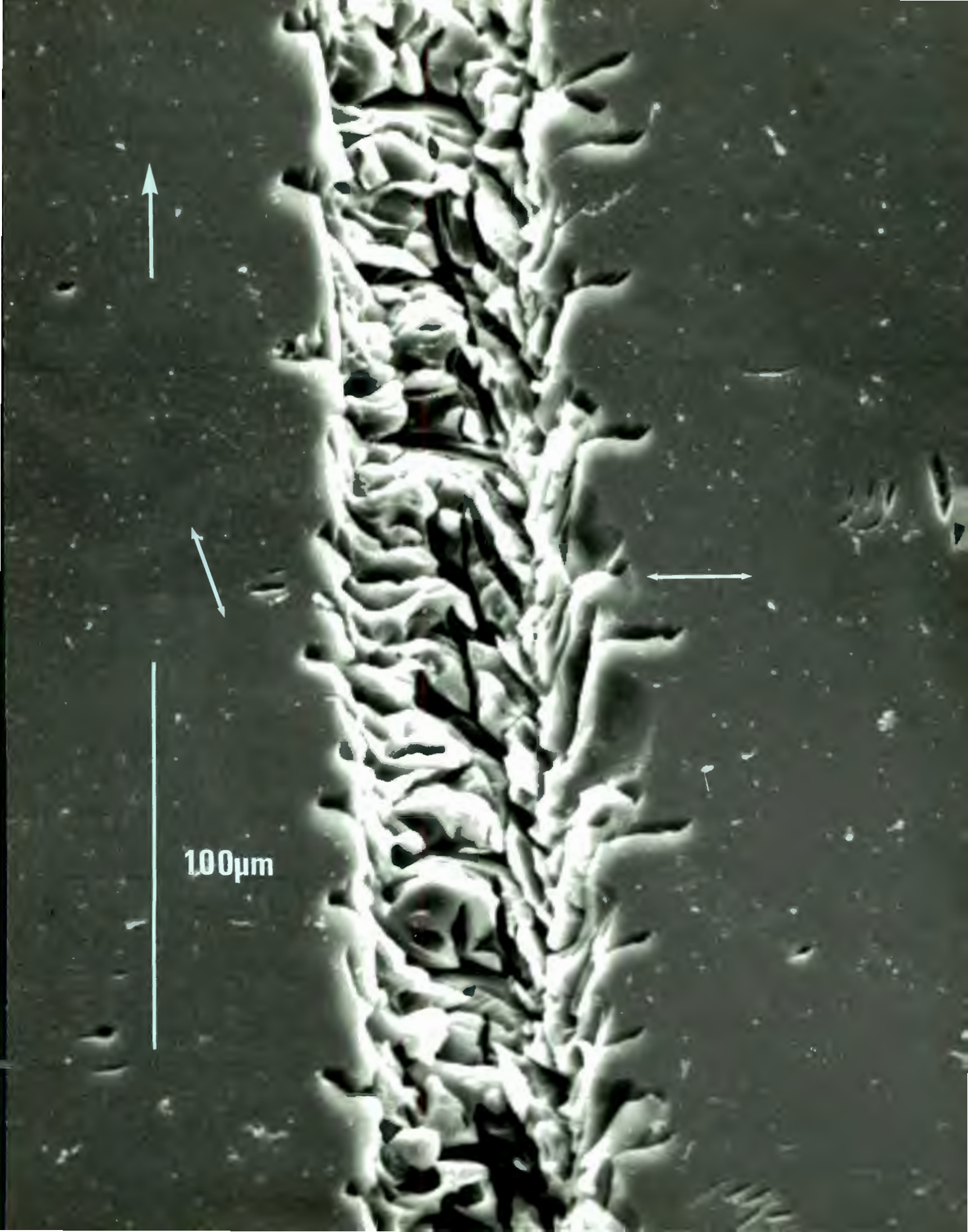
100µm

Plate 38

Scratch on quartz after etching : applied load - 9.8N, speed - 8.5×10^{-2} mm s^{-1}, surface plane - $(11\bar{2}0)$ 60^0 to the direction of the Y axis, polished surface, tested in air. Large arrow indicates direction of scratching and double arrowed line indicates the intersection of the rhombohedral planes with the surface.

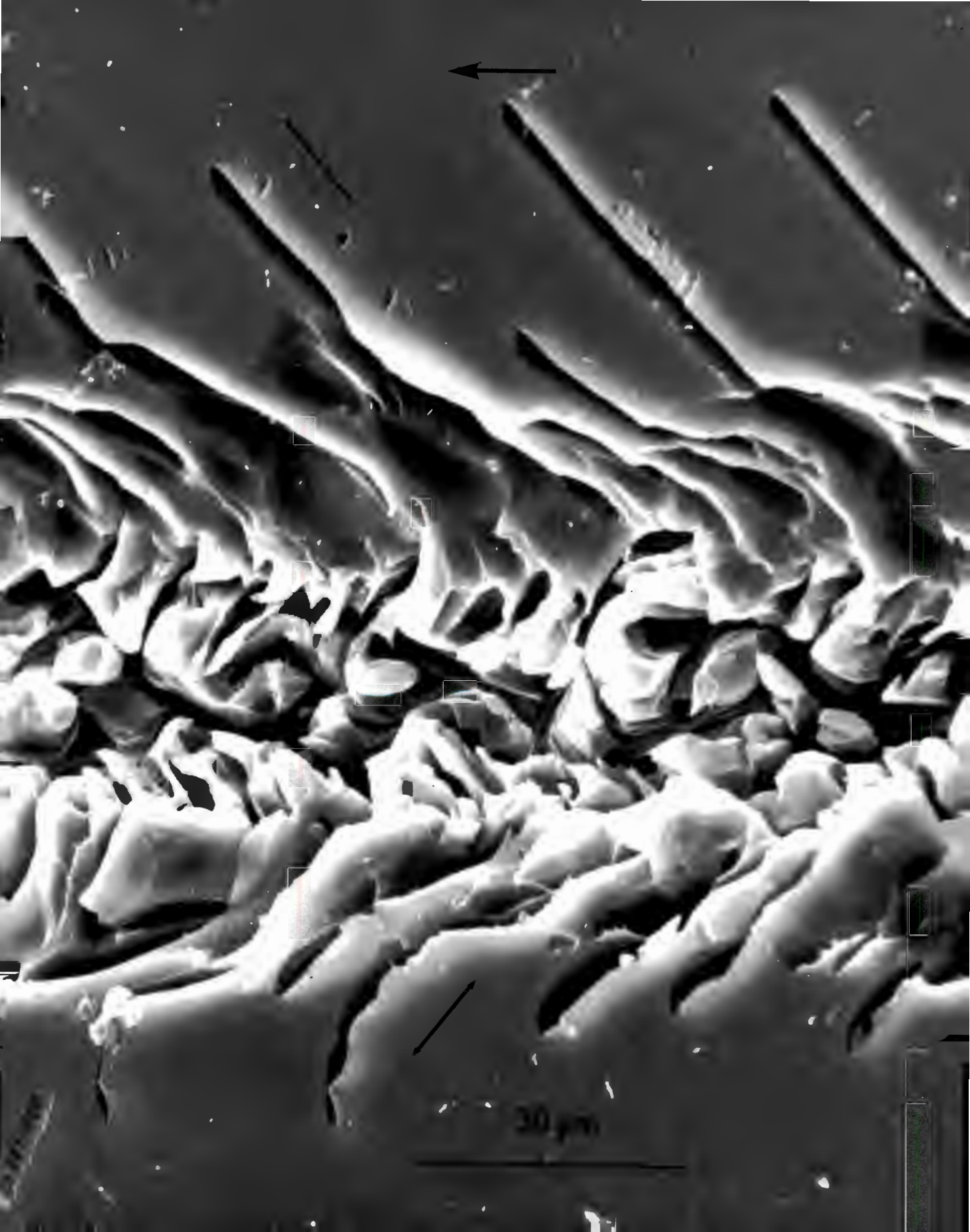
30 μm

Plate 39

Scratch on quartz after etching : applied load - 9.8N, speed - 8.5×10^{-2} mm s^{-1}, surface plane - $(11\bar{2}0)$ 105^{0} to the direction of the Y axis of the polished surface, tested in air. Large arrow indicates direction of scratching and double arrowed line indicates the intersection of the rhombohedral planes with the surface.

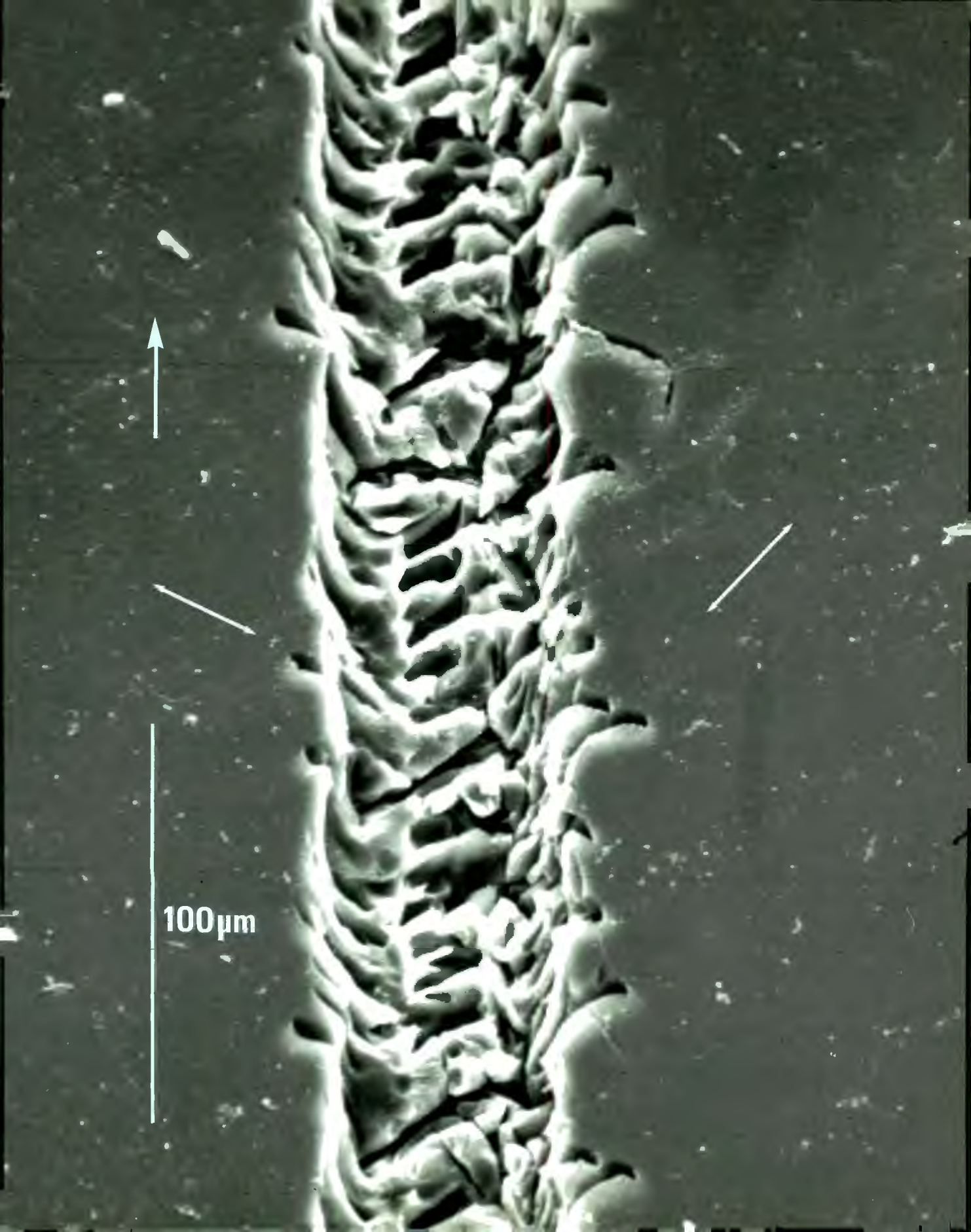
100µm

Plate 40

Section of scratch on quartz after etching : applied load - 2.9N, speed - 8.5×10^{-2} mm s^{-1}, surface plane - $(11\bar{2}0)$ in direction of Y axis, polished surface, tested in air.

10 µm

Plate 41

Same specimen as in plate 24 but after etching.

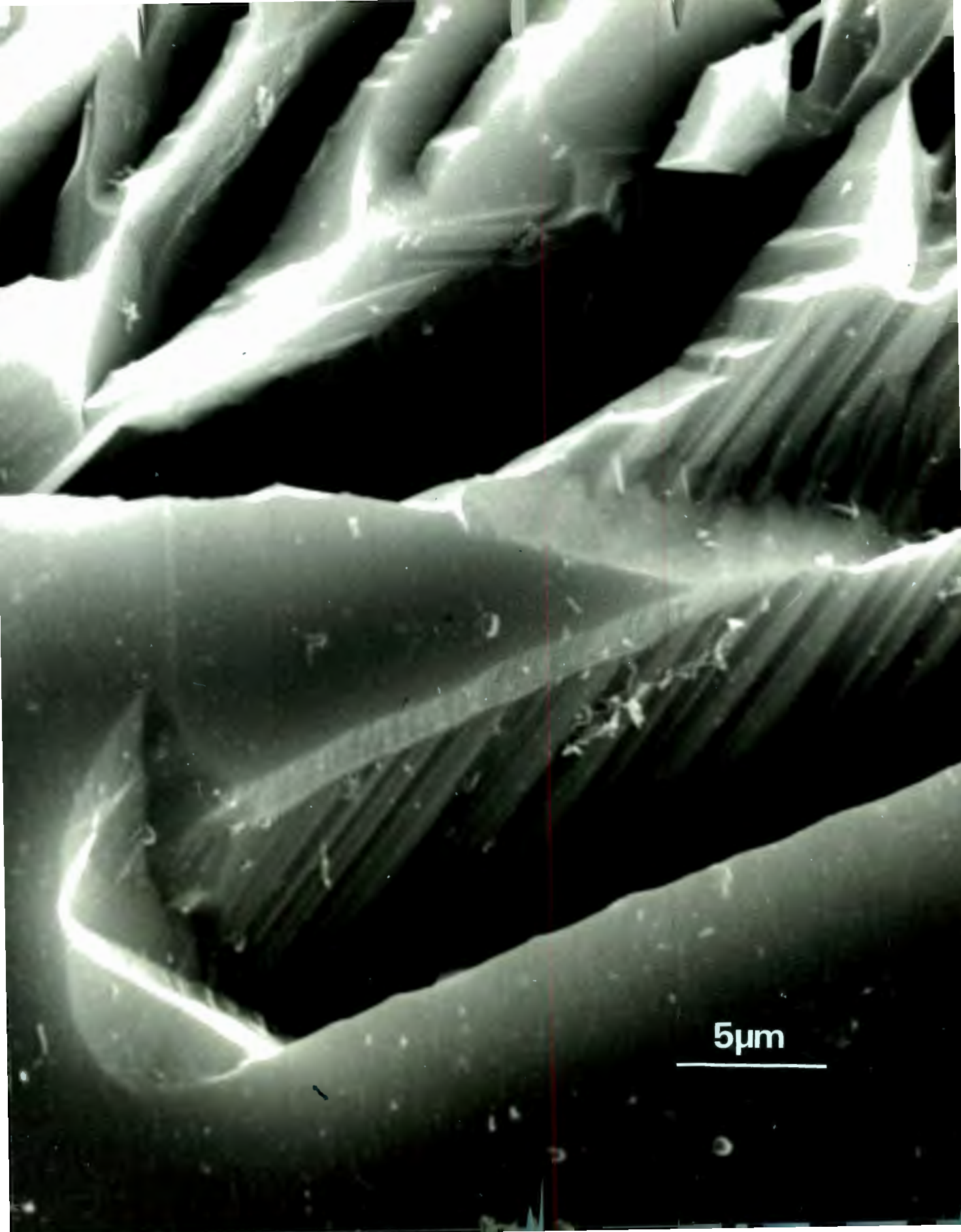
5µm

Plate 42

Scratch on quartz after etching : applied load - 9.8N, speed - 8.5×10^{-2} mm s^{-1}, surface plane - $(1\bar{1}00)$ in direction of X axis, polished surface, tested in distilled water. Arrow indicates direction of scratching.

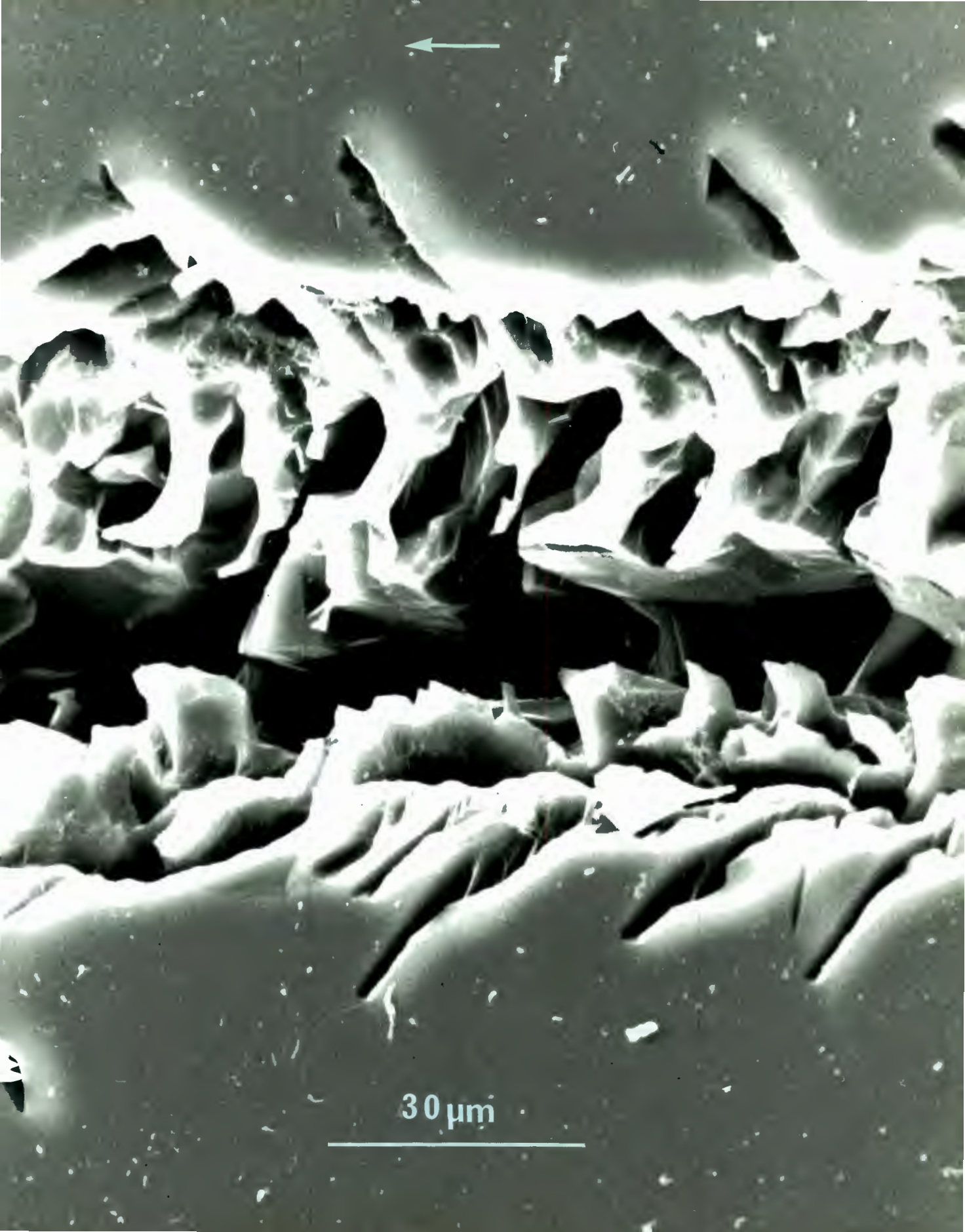
30 µm

Plate 43

Scratch on quartz after etching : applied load - 9.8N, speed - 8.5×10^{-2} mm s^{-1}, surface plane $(1\bar{1}00)$ in direction of X axis, polished surface, tested in heptyl alcohol. Arrow indicates direction of scratching.

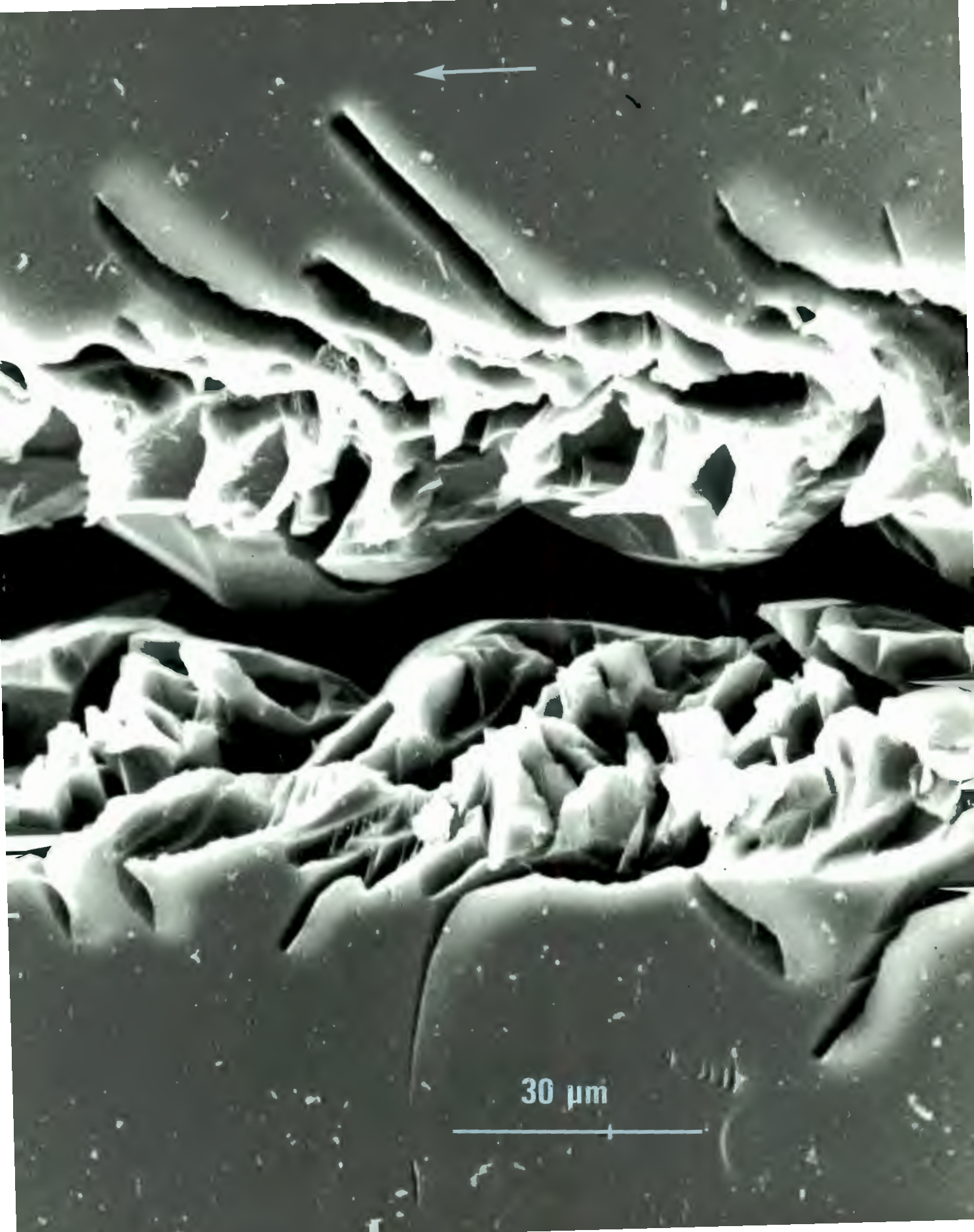
30 µm

Plate 44

Section of scratch on quartz : applied load - 9.8N, in direction of Y axis, polished surface, tested in air.

30μm

Plate 45

Friction machine.

Plate 46

Tensile testing rig.